# DEVELOPING A FUNDAMENTAL UNDERSTANDING OF HOW OIL IMPACTS DIAGENESIS AND THE EFFECT IN TRANSPORT PROPERTIES BY INVESTIGATING ROCK SAMPLES FROM CLOSE TO THE OIL-WATER CONTACT, BEN NEVIS FORMATION, HEBRON FIELD.

by © Francis Mujica

A thesis submitted to the School of Graduate Studies

in partial fulfilment of the requirements for the degree of

Master of Science (Geology)

Department of Earth Sciences

Memorial University of Newfoundland

August 2019

St. John's, Newfoundland and Labrador

# ABSTRACT

There is ongoing debate as to whether or not oil emplacement in a reservoir rock impedes or stops diagenetic process. The Ben Nevis reservoir in the Hebron Field, offshore Newfoundland has a short transition zone and a clearly identified oil-water contact (OWC). Rock samples from above and below the OWC were used to analyse the role of oil emplacement in the diagenetic processes, with the main focus on quartz overgrowth and its impact on transport properties. The main contributions of this work is that we challenge the debate on whether or not oil emplacement impacts diagenesis for the Hebron Field, a relatively shallow, low temperature reservoir (< 2 km depth, 50-70 °C) using pore size distribution instead of a singular porosity value, and digital rock analysis for the transport properties. Core analysis includes scanning electron microscopy, mineral liberation analysis, cathode-luminescence, mercury injection capillary pressure (MICP), micro-computed tomography scans, and digital rock analysis and simulations. Our results suggest that quartz cement tends to be more abundant towards the water leg. This observation is in agreement with the "oil emplacement retards diagenesis" theory discussed in the literature. Despite differences in quartz overgrowth, the pore size distributions (MICP results) and digital rock images do not reveal any significant differences in the pore structures above and below the OWC. This could indicate that the differences in quartz overgrowth is not substantial enough to cause a significant reduction of the pore size, and thereby impact transport properties.

# ACKNOWLEDGEMENTS

I would like to thank God for guiding me all along the way, and for giving me the necessary patience, perseverance, and strength to materialise this goal, infinite thanks.

To my parents, who taught me the values and ethics that have led me to achieve this goal. You both are my inspiration and the proof that working hard it is possible to achieve big things that at some point looked almost impossible. This achievement is yours.

To Larry, for always being there to encourage me to do my best, for his unconditional support, trust, love and respect. This is teamwork…!!!

To my supervisors for their constructive comments, suggestions, help and contributions. Their technical guidance and personal support were essential all the way long the research work. Special thanks to Dr Lesley James for believing on my ability to carry out this work. Dr Carl F. Berg for having me and provide me the opportunity to carry out all the digital rock analysis. Dr Derek Wilton for accepting me as his student in the Earth Sciences department.

To the Earth Sciences department and the Illustrious Memorial University, for opening their doors to me and allow me to grow personally and academically.

I thank the Natural Sciences and Engineering Research Council of Canada (NSERC), Research and Development Corporation of Newfoundland and Labrador (RDC) (now TCII), Hibernia Management and development Company (HMDC), Chevron Canada Limited, and the Hibernia EOR Research group for technical and financial support. I also thank the Research Council of Norway through its Centres of Excellence funding scheme,

project number 262644 for supporting Dr Berg's work. Tank you MITACS for providing the additional financial support to conduct the international research exchange in Norway. I would like to acknowledge the Canada-Newfoundland and Labrador Offshore Petroleum Board (C-NLOPB) for providing the rock samples and Hebron Field information. TechCore for providing the service of cutting the core plugs with their equipment and facilities. PetriCore for allowing using their equipment to carry out the μ-CT scans. PoreLab at NTNU for the technical support. The CREAIT network at MUN team, for their support during the SEM-MLA-CL and sample preparation. IHS Markit for providing the well-logs.

# TABLE OF CONTENTS

# LIST OF TABLES

# LIST OF FIGURES

# LIST OF EQUATIONS

# LIST OF ABBREVIATIONS AND SYMBOLS

| | | |
|---|---|---|
| °C | → | Celsius degree |
| °F | → | Fahrenheit degree |
| μ | → | Displacing Fluid Viscosity |
| μ-CT | → | Micro-computed tomography |
| μm | → | Micrometres |
| *a* | → | Tortuosity factor |
| A | → | Area |
| BNA | → | Ben Nevis-Avalon |
| BSE | → | Backscattered electrons |
| CL | → | Cathodoluminescence |
| C-NLOPB | → | Canada Newfoundland & Labrador Offshore Petroleum Board |
| CREAIT | → | Core Research Equipment & Instrument Training |
| CT | → | Computed tomography |
| D | → | Pore throat diameter |
| DENS | → | Density well-log |
| DRA | → | Digital rock analysis |
| EOD | → | Environment of deposition |
| EOR | → | Enhanced oil recovery |
| F | → | Formation resistivity factor |
| GR | → | Gamma Ray well-log |
| HCl | → | Hydrochloric Acid |
| HMDC | → | Hibernia Management and Development Company |
| *i* | → | Electrical current |
| k | → | Permeability |
| km | → | Kilometres |
| L | → | Length |
| *m* | → | Archie Cementation exponent |
| m | → | Metres |
| Ma | → | Million years (mega-annum) |
| MMbbls | → | Million barrels |
| MD | → | Measured depth |
| mD | → | Millidarcy |
| MICP | → | Mercury injection capillary pressure |
| MLA | → | Mineral Liberation Analyser |

| | | |
|---|---|---|
| MPa | → | Megapascal |
| MUN | → | Memorial University of Newfoundland |
| *n* | → | Archie Water saturation exponent |
| NEUT | → | Neutron well-log |
| nm | → | Nanometre |
| NSERC | → | Natural Sciences and Engineering Research Council of Canada |
| NTNU | → | Norwegian University of Science and Technology |
| OWC | → | Oil-water contact |
| P | → | Pressure |
| Pc | → | Capillary pressure |
| PLSF | → | Proximal lower shoreface |
| q | → | Flow rate |
| qo | → | Quartz overgrowth |
| R | → | Electrical resistivity |
| r | → | Pore throat radiou |
| RDC | → | Research and Development Corporation of Newfoundland and Labrador |
| Ro | → | Electrical resistivity of a rock @ Sw=100% |
| Rw | → | Brine water electrical resistivity |
| SED | → | Secondary electrons |
| SEM | → | Scanning Electron Microscope |
| TVDSS | → | True Vertical Depth sub-sea |
| TWS | → | Trainable Weka Segmentation |
| *v* | → | Darcy velocity |
| V | → | Voltage |
| γ | → | Interfacial Tension |
| θ | → | Contact angle |
| φ | → | Porosity |
| ΔE | → | Potential difference |

# LIST OF APPENDICES

# CHAPTER 1. INTRODUCTION

Conventional oil reservoirs generally occur in sedimentary rocks such as sandstone, limestone, and dolomite. Quartz is considered the main mineral in sandstones, however, sandstones also contain a variety of mineral types. Diagenesis is the process that includes all the changes undergone by the sediments to become a rock. They take place after deposition and before the metamorphism (Choquette & Pray, 1970; Pettijohn, Potter, & Siever, 1987; Tarbuck & Lutgens, 2005). During diagenesis, the cementation process is an essential aspect due to it plays a vital role in preserving, destroying or creating porosity (Worden & Burley, 2003).

Quartz cementation is of importance in petroleum geosciences since quartz cement can reduce porosity and permeability (Figure 1); thereby reducing the reservoir storage capacity and the rate at which the hydrocarbon can be produced (Choquette & Pray, 1970). The diagenetic reactions undergone by the rock, including quartz cementation, are strongly influenced by the original composition of the mineral framework, the chemistry of the surrounding fluids, the temperature, and pressure in the medium (Morad, Ketzer, & De Ros, 2000; Pettijohn et al., 1987; Worden & Burley, 2003).

The effect of oil emplacement in the quartz cementation has been debated in the literature. Some claim that diagenetic processes are stopped or retarded when pore water is displaced by hydrocarbons (Dixon, Summers, & Surdam, 1989; Gluyas, Robinson, Emery, Grant, & Oxtoby, 1993; Marchand, Haszeldine, Macaulay, Swennen, & Fallick, 2002; Marchand, Haszeldine, Smalley, Macaulay, & Fallick, 2001; Saigal, Bjørlykke, & Larter, 1992;

Worden, Bukar, & Shell, 2018; Worden, Oxtoby, & Smalley, 1998). However, another school believes that pore water displacement by oil does not stop the diagenetic process. This assumption is based on similar petrophysical properties in the water and oil leg, petrographic analysis, oil inclusions in authigenic minerals and models used to simulate the quartz precipitation rate using kinetic (time-temperature) calculations (Barclay & Worden, 2000; Midtbø, Rykkje, & Ramm, 2000; Molenaar, Cyziene, Sliaupa, & Craven, 2008; Walderhaug, 1990, 1996). These two opposing views consider diagenesis to have a direct impact on the distribution of petrophysical properties.

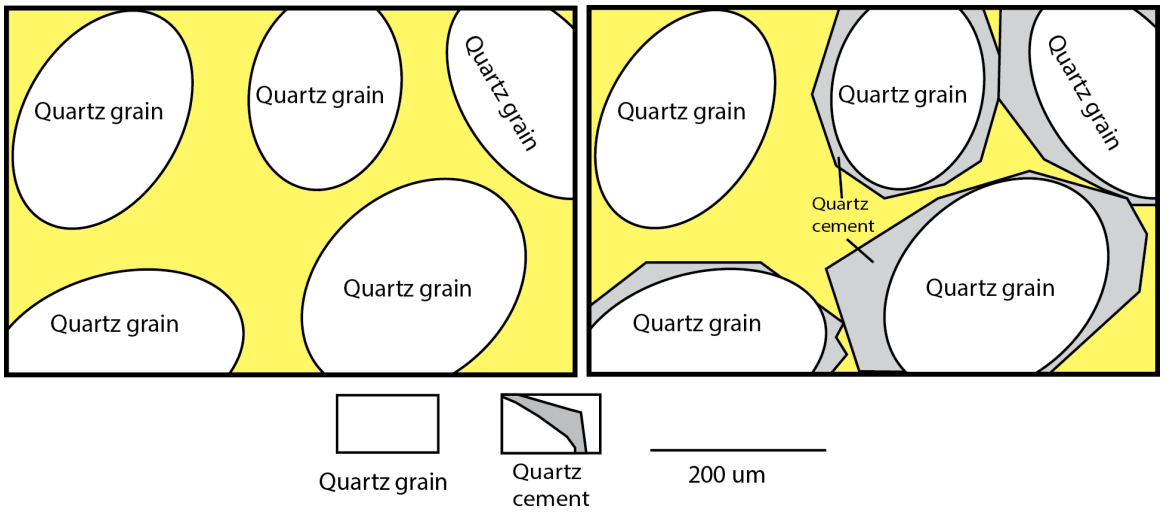


*Figure 1 Schematic picture of clean quartz grains (left) vs cemented quartz grains (right); adapted from Worden & Burley (2003)*

The effect of oil emplacement in the quartz cementation has been debated in the literature. Some claim that diagenetic processes are stopped or retarded when pore water is displaced by hydrocarbons (Dixon et al., 1989; Gluyas et al., 1993; Marchand, Haszeldine, et al., 2002; Marchand et al., 2001; Saigal et al., 1992; Worden et al., 2018, 1998). However, another school believes that pore water displacement by oil does not stop the diagenetic process. This assumption is based on similar petrophysical properties in the water and oil

leg, petrographic analysis, oil inclusions in authigenic minerals and models used to simulate the quartz precipitation rate using kinetic (time-temperature) calculations (Barclay & Worden, 2000; Midtbø et al., 2000; Molenaar et al., 2008; Walderhaug, 1990, 1996). These two opposing views consider diagenesis to have a direct impact on the distribution of petrophysical properties.

The Hebron Field is located offshore Newfoundland, Canada in the Jeanne d'Arc Basin. Hydrocarbon resources have been found in three different formation i.e the late Jurasic Jeanne d'Arc, and the early Cretaceous Hibernia and Ben Nevis formations. The study area corresponds to the early Cretaceous Ben Nevis reservoir. It is located at less than 2 km depth and temperatures around 50 - 70 °C (120-160°F).

In the Hebron Field, the Ben Nevis reservoir exhibits a short transition zone and a very distinctive OWC. The oil and water zones have been contacted by the I-13, M-04 and D-94 wells. In well D-94 both zones were cored. As will be presented later, the core samples on both sides of the OWC have similar properties. They therefore represent an excellent opportunity to evaluate how the presence of oil affect the diagenetic process.

We conducted scanning electron microscopy (SEM), mineral liberation analysis (MLA), cathodoluminescence (CL) for the rock characterisation and the diagenetic impact analysis. The mercury intrusion capillary pressure (MICP) was carried out to experimentally obtain a detailed description of the pore structure of the rock, and the micro computed tomography imaging (μ-CT) was performed for the digital rock construction and later transport properties simulations.

The final goal of analysing the quartz overgrowth in the reservoir zone is to evaluate its impact on the transport properties and reservoir performance.

## 1.1 Overview

The research project is divided into two main research questions:

1. Is quartz cementation affected by the presence of oil in the Ben Nevis reservoir, Herbon Field?

2. Do the diagenetic changes affect the transport properties?

Analysis carried out to describe the rock mineralogy and pore structure will help to answer if there is a relation between oil saturation and inhibition of quartz cement. On the other hand, the results obtained from the experimental and digital investigation of the pore structure will help to understand the impact of diagenetic differences on transport properties that are dependent on the pore structure.

In this research work, we analyse the impact of the oil presence on the quartz overgrowth and its effect on the transport properties. We consider porosity and pore size distribution using the MICP test instead of singular value porosity measurements. We use digital rock analysis to investigate the effect of differences in quartz overgrowth on transport properties from rock samples above and below the OWC. To the best knowledge of the authors, there are currently no publications on 3D rock representation from μ-CT scans and digital rock analysis (DRA) in the study area. This provides potential industrial and academic interest to this research.

## 1.2 Background

### 1.2.1 Geological framework

*1.2.1.1 Project area*

The Jeanne d'Arc Basin, offshore Newfoundland, is a significant oil producing region in Canada. World class producing fields in the basin include Hibernia, Terra Nova, White Rose, and the most recently developed field, Hebron. The Hebron Field is an offshore oil and gas accumulation located in the centre of this highly prospective basin, southern North Atlantic Ocean. Hebron Field is located 340 km South-east of St. John's, Newfoundland, Canada (Figure 2).

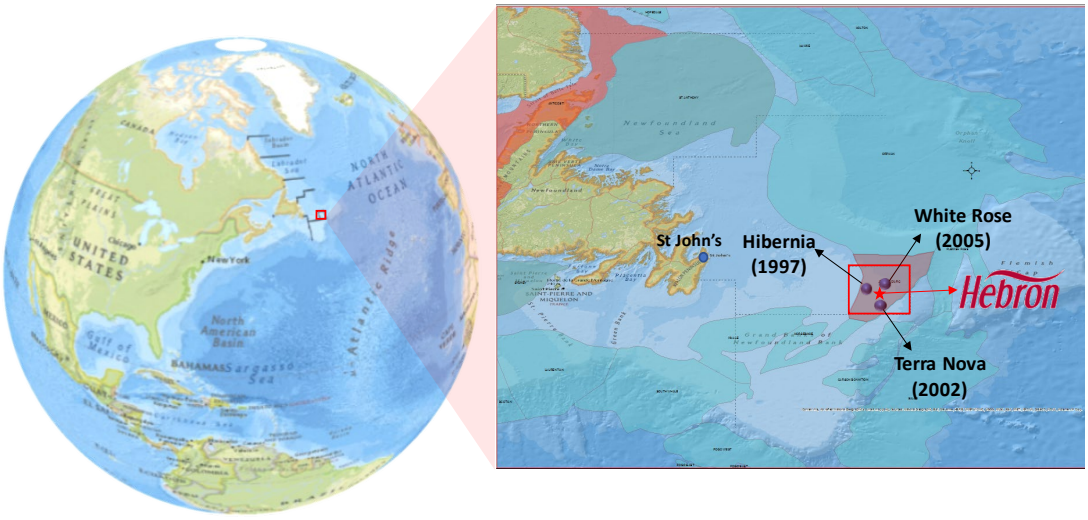


*Figure 2 Project Area (Land tenure Shapefiles from C-NLOPB, 2017)*

Over 900 million barrels have been estimated to be recoverable in the Hebron Field, as proven, probable, and possible original oil reserves (C-NLOPB, 2019a). All of these resources are also distributed in three formations; Ben Nevis/Avalon, Hibernia and Jeanne d`Arc formations. Several normal faults divide the Hebron-Ben Nevis complex into different fields (Hebron, West Ben Nevis and the Ben Nevis) and reservoirs (ExxonMobil

Canada, 2011). The Hebron Field is the newest offshore field in Newfoundland, Canada. It started production in November 2017.

As shown in Figure 3; Pool 1, Pool 2, and Pool 3 are all located in the Ben Nevis Formation across the Hebron-Ben Nevis complex. Pool 1 is in the highest part of the horst structure in the Hebron Field. Pool 2 is found in the West Ben Nevis Field down-dropped fault block. The third reservoir associated with Ben Nevis Formation in the Hebron complex is in the Ben Nevis Field (Pool 3). The late Jurassic Jeanne d'Arc Formation located in the Hebron Field is named Pool 4, and finally, the early Cretaceous Hibernia Formation in the same field is known as Pool 5.

This research focuses on the Ben Nevis Formation in the Hebron Field (Pool 1). The reservoir interval is located at 1808 m (True Vertical Depth sub-sea – TVDSS) with a gross thickness of 129 m and an OWC at 1900 m (TVDSS) in well D-94. The reservoir pressure range from 2600 to 2750 psi (180 to 190 bars) and temperatures between 50 and 70 °C (120-160°F) (Petro-Canada, Chevron-Canada, Mobil Oil, & Hydro, 1999a). This is considered the main reservoir since it is expected to produce around 80% of the total volume estimated (ExxonMobil Canada, 2011).

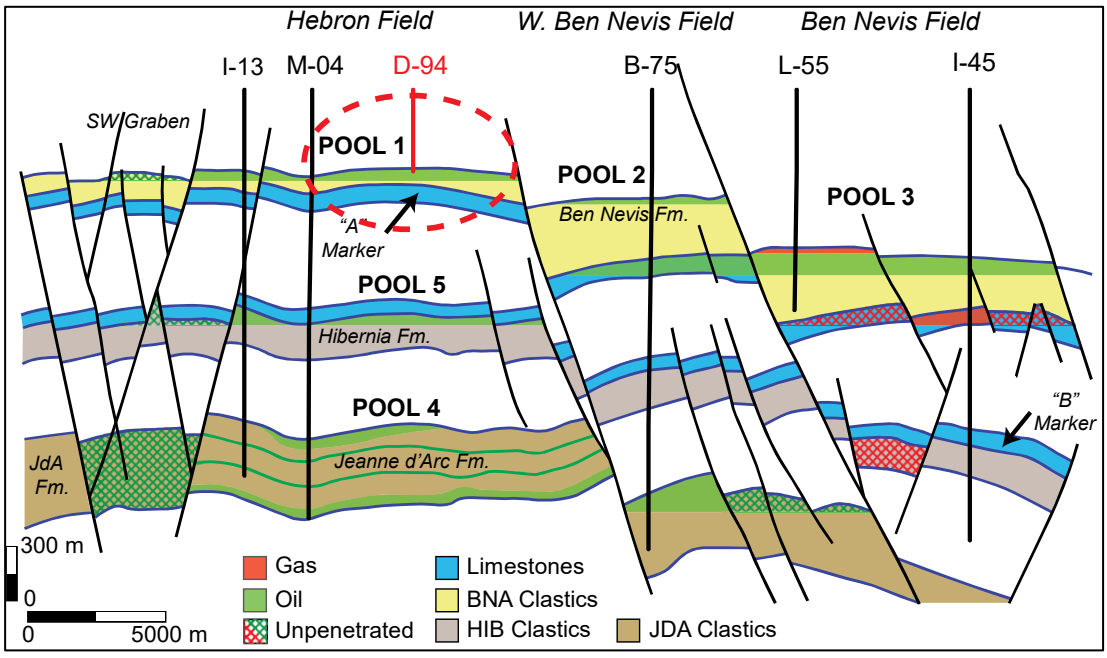


*Figure 3 Cross-section across the Hebron Project Area; adapted from (Cornaglia, 2018)*

*1.2.1.2 Structural eology*

The structure in the Hebron Field is a horst block with a graben to the southwest and to the northeast. The Hebron Field was formed by multiple rifting events during the late Triassic, late Jurassic-early Cretaceous, and early Cretaceous (Enachescu, 1987; Sinclair et al., 1992), producing several normal fault-bounded blocks that shaped the current geological configuration of the Hebron Field (Figure 4). The faulting occurred when the formation was being deposited, having an important impact on the geometry and thickness of the present reservoir section. The faulting-depositation synchronism is evidenced by significant growth in the thickness of the Ben Nevis Formation across the faults. However, changes in the reservoir quality are attributed to the deposition of more distal facies on the downthrown side of the fault where thicker formation sections have lower reservoir quality (ExxonMobil Canada, 2011).

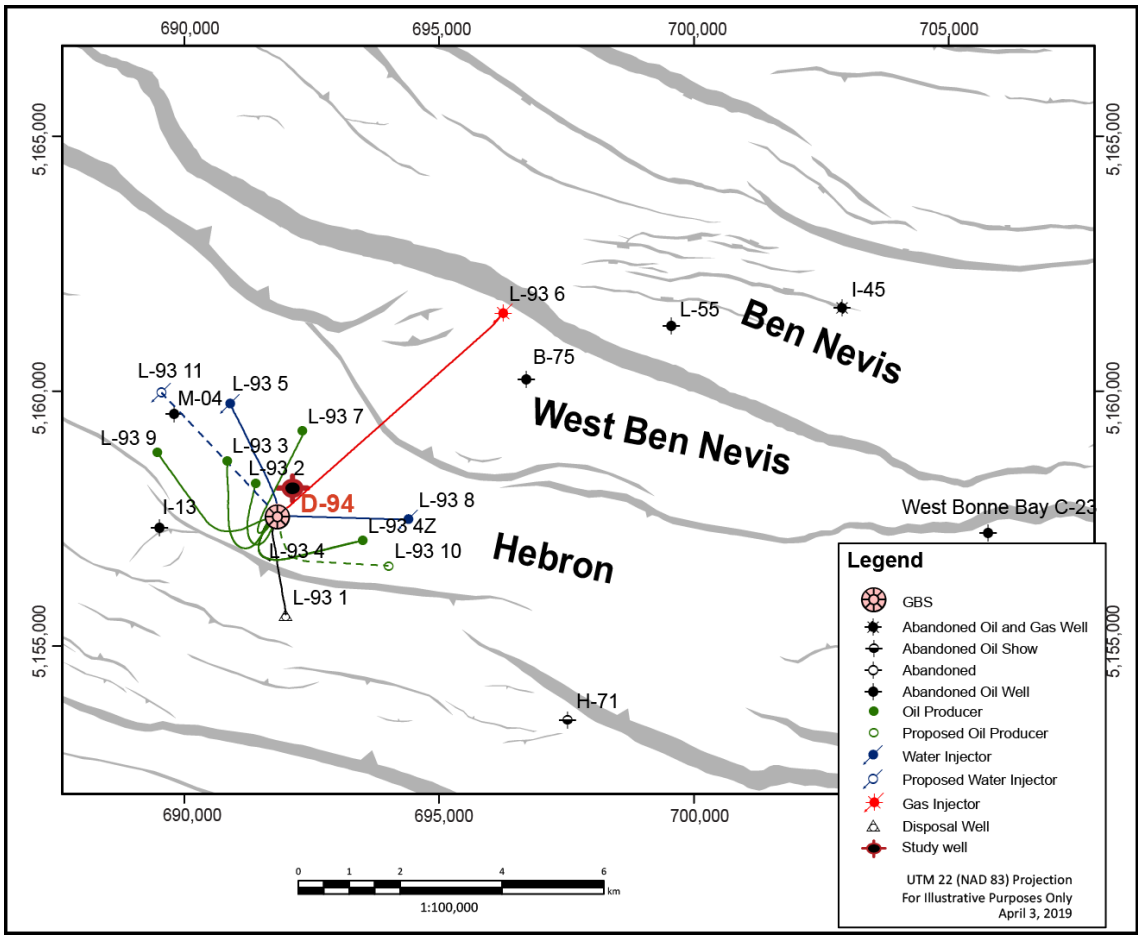


*Figure 4 Schematic map of faults and trapped hydrocarbons in the Hebron Field. Top of the Ben Nevis Formation. Adapted from C-NLOPB, (2019b)*

*1.2.1.3 Ben Nevis Formation*

The environment of deposition (EOD) in the Ben Nevis Formation at the Hebron Field is interpreted as a shallow marine, wave-dominated shoreface environment in open to restricted shelf (ExxonMobil Canada, 2011).

In the highest part of the horst block (Pool 1), the EOD is described as dominantly proximal lower shoreface, becoming a more distal and transitional environment in the northeastern fault blocks (Pool 3) since the main sediment sources are located to the south and west (Figure 5) (ExxonMobil Canada, 2011; McAlpine, 1990).

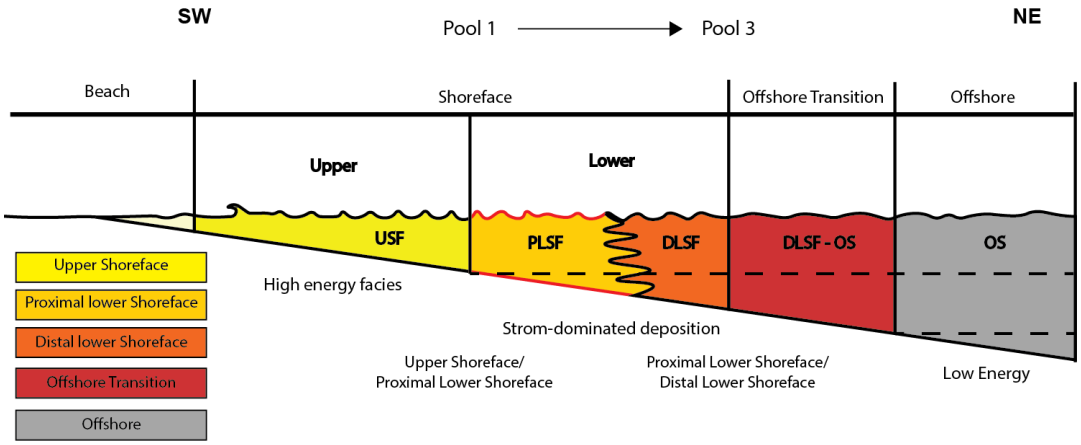


*Figure 5 Generalised cross-section showing the environment of deposition (EOD) for the Ben Nevis Formation in the Hebron Field. Adapted from Sam Boggs, (2006)*

The Ben Nevis Formation represents a marine transgression. It is a fining upward sandstone terrigenous sequence that unconformably lies upon the Avalon Formation (Figure 6) (Driscoll & Hogg, 1995; McAlpine, 1990). It is operationally named as Ben Nevis-Avalon (BNA) without differentiation.

The Age of Ben Nevis Formation is determined as early Cretaceous. From late Aptian to late Albian (McAlpine, 1990).

## 1.2.2 Rock properties

### *1.2.2.1 Porosity*

Porosity is the capacity of the rock to store fluids in the void spaces between the grains. It is calculated as the relationship between the volume of spaces (pore volume) and the bulk volume of the rock (Equation 1) (Glover, 2014; Jorden & Campbell, 1985; Schon, 2015; Tiab & Donaldson, 2016). Its units can be expressed either as a fraction or as a percentage of bulk volume.

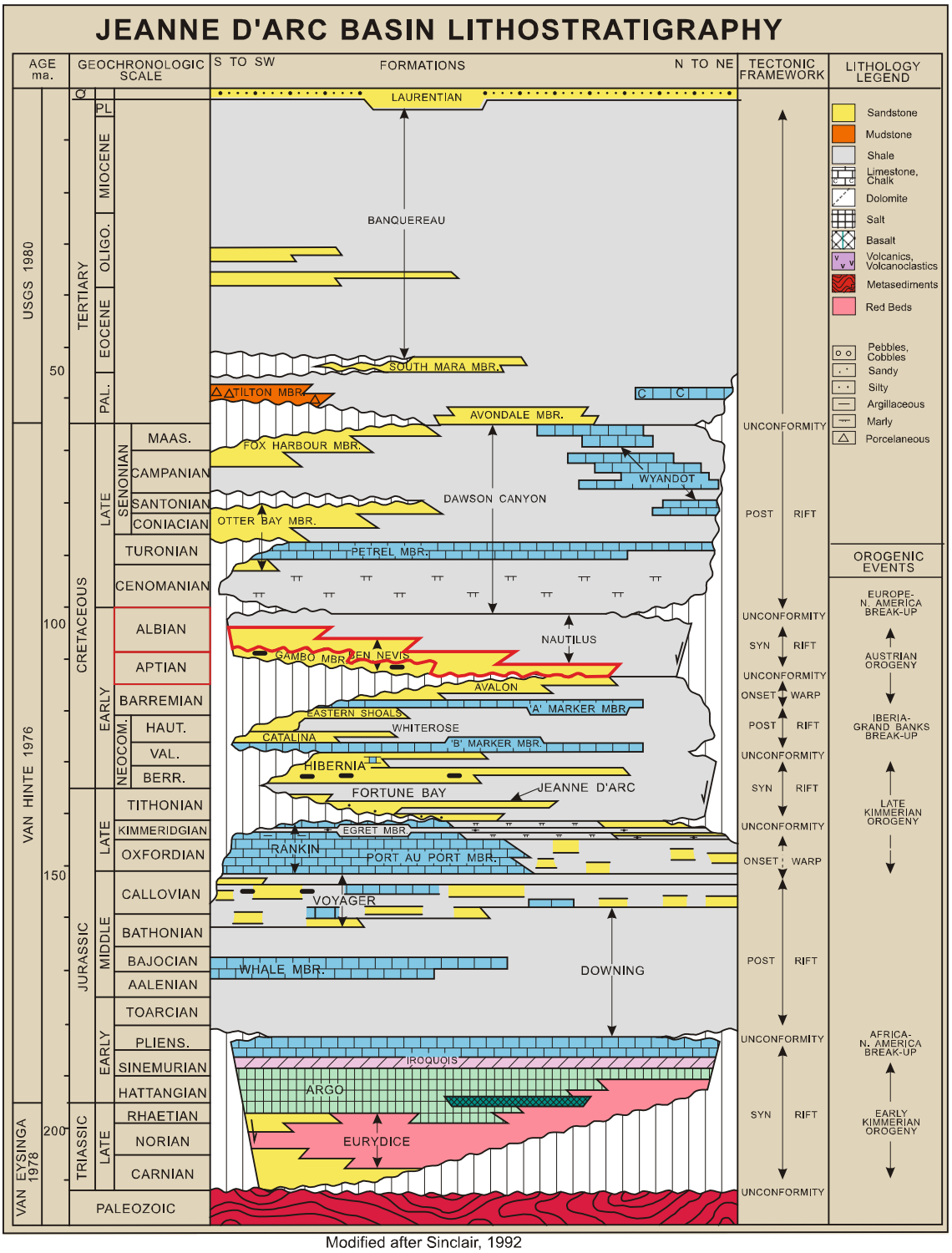


Modified after Sinclair, 1992

*Figure 6 Lithostratigraphy column of the Jeanne d'Arc basin (C-NLOPB, 2010)*

$$\varphi = \frac{Vpore}{Vbulk} = \frac{V_{bulk} - V_{Solid}}{V_{bulk}}$$

*Equation 1 General equation for porosity calculation*

To quantify and describe porosity, more than one method may be necessary. Porosity and its pore structure characterisation may need more than just one technique, since it includes a wide range of magnitude. The combination of different methods with different approaches helps to reduce the uncertainty, since each technique is based on different physical properties and assumptions (Anovitz & Cole, 2015).

Two types of porosity are commonly measured, total and effective (Torsæter & Abtahi, 2003). The former includes all void space in a volume rock, whereas the latter, also known as connected porosity, is the portion of pore space that is interconnected and able to contribute in the production of fluids (Amyx, Bass, & Whiting, 1960).

Direct experimental measurements and indirect methods have been generally applied to estimate the reservoir porosity (Anovitz & Cole, 2015). Buoyancy, helium porosimetry, fluid saturation and mercury porosimetry are the most common methods for core-porosity measurement (Glover, 2014). Indirect methods such as well-logs are most commonly applied in formation evaluation assessments to estimate porosity in longer reservoir intervals.

Digital rock representation provides an additional alternative for porosity evaluation. In this case, the porosity is estimated through the image analysis and segmentation to separate pores and grains. It is a volumetric estimation made on stitched 2D images usually acquired using CT scanning (Dvorkin, Gutierrez, & Grana, 2014). When working with digital rocks

and pore structure extracted from μ-CT scans, the unresolved porosity is defined as the porosity that is under the image resolution (C. F. Berg, Lopez, & Berland, 2017). The total porosity estimated using this technique represents the pore space that is bigger than the image resolution.

*1.2.2.2 Pore structure*

Mercury injection capillary pressure (MICP) test is a standard laboratory technique recommended to evaluate pore throat distribution.

The method is based on the physical principle that a non-reactive, non-wetting liquid does not enter a pore space until enough pressure is applied to overcome the capillary pressure of the pore throat (Giesche, 2006; Micromeritics Instrument, 2011; Van Brakel, Modrý, & Svatá, 1981). During the test, the pressure of mercury is progressively increased, helping the mercury to gradually reach smaller pores. It is used to evaluate pore sizes, ranging from the nano-scale to the micro-scale, 0.003 μm to 360μm (Webb, 2001).

The volume of mercury that is injected at each pressure is measured. The pore throat size (D) that is intruded at a certain pressure ($P_c$) is obtained by applying the Young-Laplace equation for cylindrical pores (Equation 2) assuming that mercury-air interfacial Tension ($\gamma$) and contact angle ($\theta$) are constant, during the drainage process (Giesche, 2006).

$$D = \frac{\gamma\ (-4\ \cos\theta)}{P_c}$$

*Equation 2 Young-Laplace equation for cylindrical pores*

Working with mercury-air systems, a surface tension value of 485 dynes/cm and a contact angle between 130° and 140° are commonly accepted and recommended (Giesche, 2006;

Micromeritics Instrument, 2011; Van Brakel et al., 1981). By using these values in Equation 2, a conversion factor is needed since the surface tension is expressed in dynes/cm, and the pore diameter is required in microns. Equation 3 shows a modified Young-Laplace equation accounting for unit conversion, where the capillary pressure (Pc) is expressed in psi, the surface tension (γ) in dynes/cm and the pore diameter (D) in microns. In this work surface tension of 485 dynes/cm and contact angle of 130 are used (Equation 3)

$$D = \frac{-0.58 * \ 485 \cos(130)}{P_c}$$

*Equation 3 Pore throat diameter estimation at different pressure*

Effective porosity, characteristic length, tortuosity, and a constriction factor are used as direct descriptors of the pore structure relative to the direction (C. F. Berg & Held, 2016). The effective porosity is the portion of the pore volume that is connected and able to conduct flow between two points. Characteristic (hydraulic) length represents the effective hydraulic pore radius of the porous medium. Tortuosity represents the path deviation of an actual flow to the straight path between inlet and outlet, and the constriction factor characterises the pore size variation along the flow line (Bear, 1988; C. F. Berg & Held, 2016).

*1.2.2.3 Permeability*

The generalised Darcy equation (Equation 4) is the most general method applied in the petroleum industry for permeability estimation. The theory assumes that the fluid does not interact with the medium, the flow regime is laminar, the medium is fully saturated by a

single-phase fluid, and it is a property of the medium that does not vary with the fluid, flow rate or pressure.

$$k = u\frac{\mu L}{\nabla p} \quad ; \quad u = \frac{q}{A}$$

*Equation 4 Darcy's equation*

The theory was proposed by Henry Darcy in the mid-1800s. Using laboratory experiments, Darcy flushed water through an unconsolidated sand pack in a cylinder under unequal pressure (Figure 7). In his experiments, Darcy did not investigate the effect of fluid properties such as fluid density and viscosity since just water was initially considered (Darcy, 1856). Darcy's experiment was subsequently replicated using different fluids and varying the inclination of the porous medium. By varying the orientation, it was corroborated that the pressure differences were the same for a particular flow rate (Cossé, 1993; Dake, 1997).

In the S.I and cgs systems, permeability is expressed as an area. The units used in Equation 4 correspond to a hybrid system of units where: the velocity (u) is given in cm/sec, viscosity (μ) in centipoise (cp), pressure (p) in atmospheres, and the length (L) in centimetre (cm) (Dake, 1997). The permeability result is then obtained in Darcy units.

The permeability previously described considers a medium fully saturated by a single-phase fluid; hence, it corresponds to the absolute permeability. It indicates the ability of the media to allow fluid flow. It is a rock property directly affected by the characteristic length, constriction factor, tortuosity and effective porosity as descriptos of the pore structure (C. F. Berg, 2014).

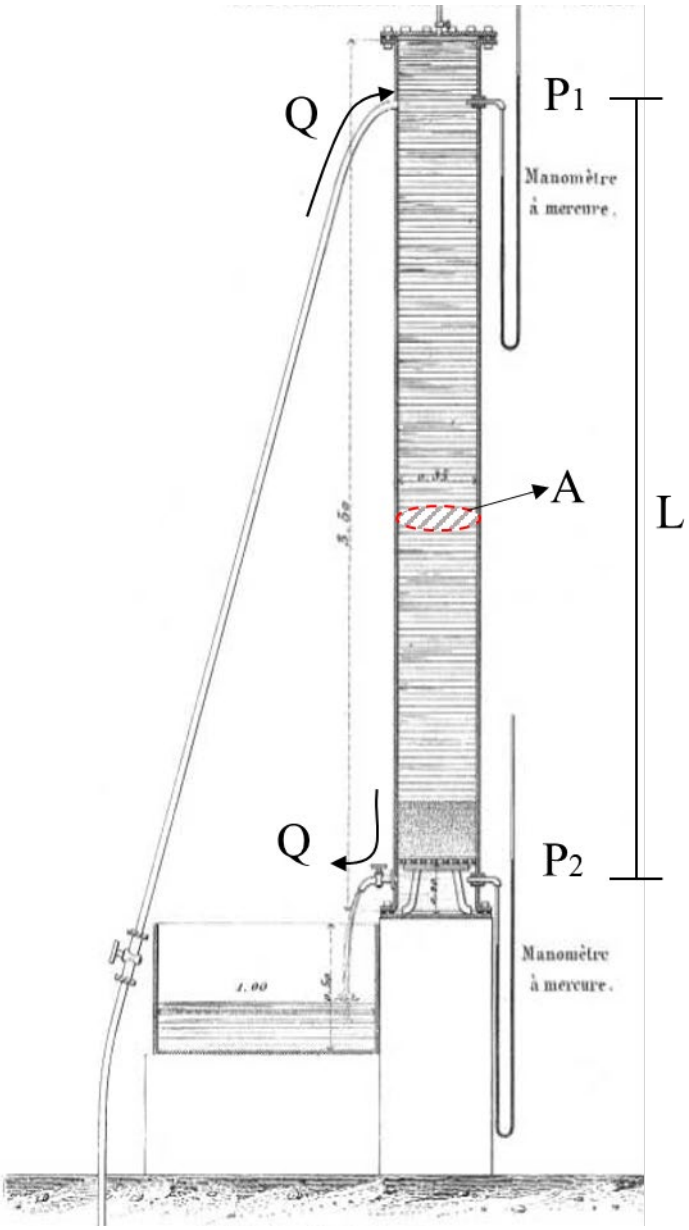


*Figure 7 Darcy's original experiment schematic design (Darcy, 1856)*

*1.2.2.4 Formation factor*

The electrical conductance is the capacity of the rock to transmit electrical current. Reciprocaly, the electrical resistivity is how hard the rock resists the electrical current to pass through.

The physical principle is based on Ohm s law. The electrical resistivity (R) is the specific resistance of a specific area and length (Figure 8). It is obtained from the ratio of the difference in voltage across the sample (ΔE) in the cross-sectional area perpendicular to the current flow (A) and the electrical current (*i*) in one unit length (L) (Equation 5) (Oldenburg & Jones, 2007).

$$R = \frac{\Delta E_{in-out}}{i_{in-out}} \frac{A}{L}$$

*Equation 5 Electrical resistant*

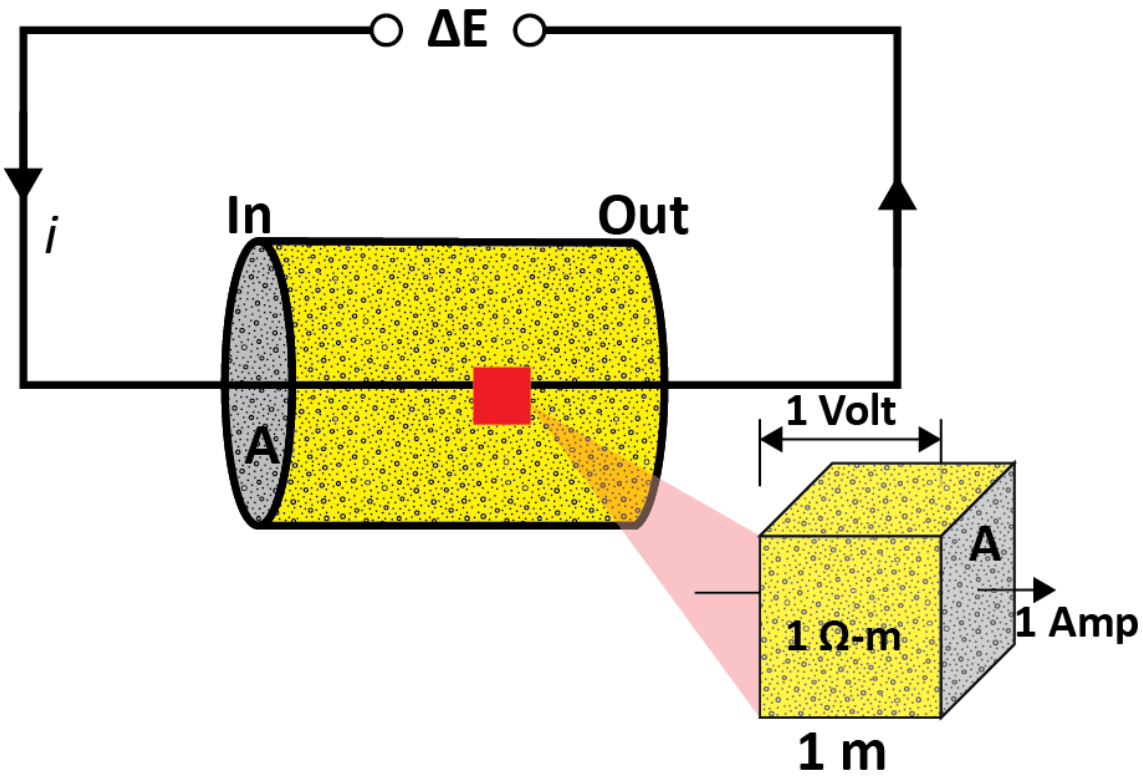


*Figure 8 Electrical resistivity definition*

The electrical resistivity of a rock sample is used to calculate the formation factor. Based on Archie (1942), in real reservoirs, the rock system is constituted by the rock framework minerals that are semiconductors or insulators, hydrocarbons that are also resistant to the electrical current, while the only component that is low resistant is the formation water. If the medium is fully saturated by brine, the electrical current can be assumed to be conducted by the pore fluids.

The formation factor is obtained by the ratio between the electrical resistivity of the bulk rock where the pore space is fully saturated by brine ($R_o$) and the electrical resistivity of the brine ($R_w$) (Archie, 1942). The formation factor can be related to porosity through the Archie law in a clean and brine-saturated rock (Equation 6). The Archie cementation exponent ($m$) can be describped by pore microstructure descriptors such as tortuosity and constriction factor (C. F. Berg, 2012).

$$\frac{R_o}{R_w} = F = a\,\frac{1}{\varphi^m}$$

*Equation 6 Formation factor as a function of bulk and brine resistivity and Archie's parameter*

### 1.2.3 Diagenesis

Diagenesis is the process including all the chemical, physical, and biological changes that affect the sediments after deposition, during and after lithification, but before achieving the metamorphism conditions (Pettijohn et al., 1987; Sam Boggs, 2006; Tarbuck & Lutgens, 2005). Changes in temperature and pressure conditions control the reaction and interaction between sediments and adjacent fluids which determine the porosity and permeability preservation, creation or destruction (Morad et al., 2000).

Choquette & Pray (1970) divided the diagenesis process in reservoir rocks into three regimes, namely eogenetic, mesogenetic, and telogenesis. These three stages are also recognized as early diagenesis, burial diagenesis and uplift-related diagenesis. The classification was initially applied to described limestone diagenetic processes; however, it is also used for sandstones since the fundamental processes and controls considered are basically the same (Worden & Burley, 2003).

The eogenetic regime (early diagenesis), commonly refers to all the processes taking place from deposition to shallow burial. During this stage, the chemical composition of the interstitial water is related to the sedimentary environment, and the space between the sediments is continually occupied by water. The alteration of the pore water geochemistry and/or the replacement by hydrocarbon fluids are considered essential factors during the mesogenesis (burial diagenesis) which comprises those processes affecting the sediments at deeper levels before the metamorphism. Finally, the telogenesis stage (uplift-related diagenesis) takes place in rocks that have been exposed and are in contact with fresh ground water not related to the depositional environment (Choquette & Pray, 1970; Morad et al., 2000; Worden & Burley, 2003).

#### *1.2.3.1 Sandstone Cementation*

When the rock is being lithified, two main basic processes are included in the porosity reduction; compaction and cementation. Compaction involves mechanical loading, producing a volume reduction and pore water expulsion, whereas cementation involves precipitation of minerals as a result of chemical diagenetic changes (Pettijohn et al., 1987; Tarbuck & Lutgens, 2005; Ulmer-Scholle, Scholle, Schieber, & Raine, 2014).

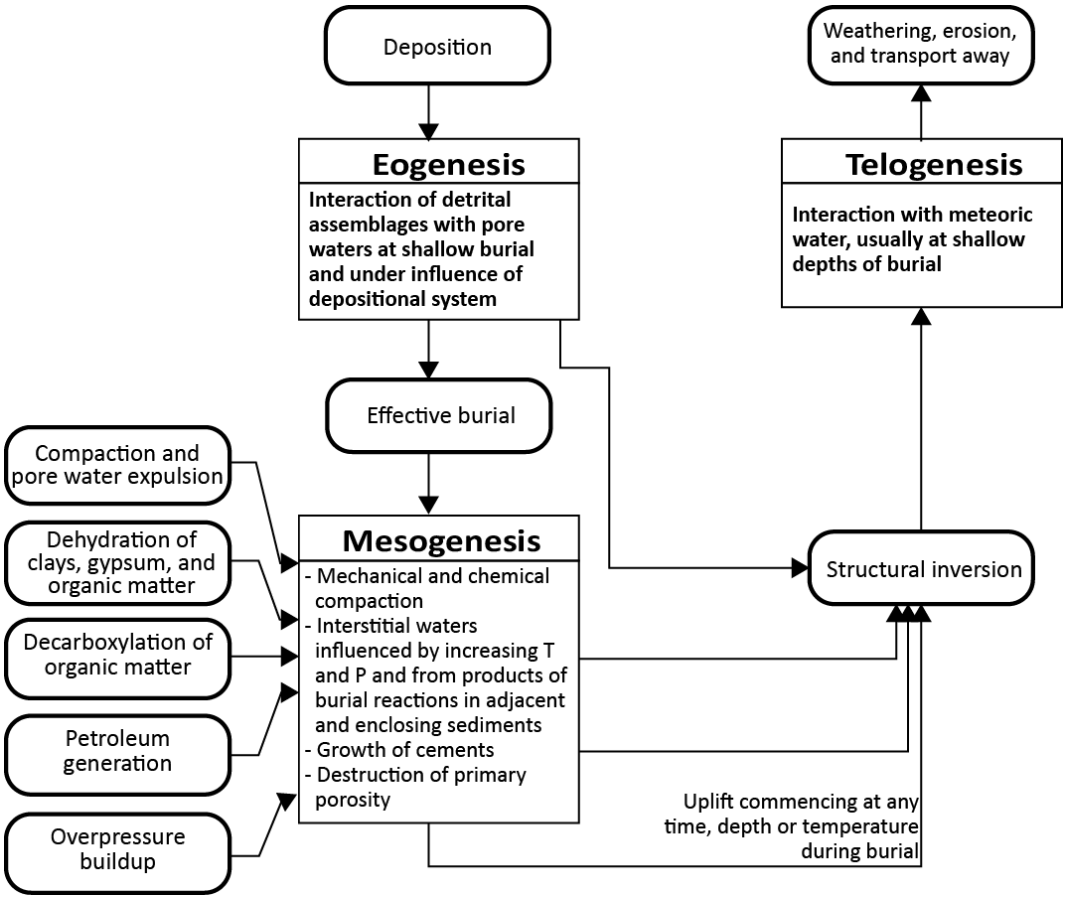


*Figure 9 Diagenetic process flow chart* (Stuart D. Burley, 1993; Worden & Burley, 2003)

In the case of sandstones, the main changes occur during the cementation process, which is controlled by chemical reactions between the sediments and the chemical composition of the fluids inside the pore system (Pettijohn et al., 1987; Sandoval, 2000; Southard, 2007). The most common types of cement in sandstones are quartz, calcite, clay minerals and iron oxide (Choquette & Pray, 1970; Southard, 2007; Tarbuck & Lutgens, 2005); however, dolomite, siderite, feldspar, anhydrite, pyrite, and zeolite cements have also been frequently found (Sandoval, 2000).

The formation temperature, pressure, and chemistry influence the mineral that is going to precipitate as cement (Ulmer-Scholle et al., 2014). Formation of quartz cement has been

reported at relatively low temperatures between 40-60 °C (McBride, 1989). However, it is commonly more abundant in deeply buried reservoir (3- 4.5 km) with temperatures higher than 60-80 °C (Bjørlykke & Egeberg, 1993; Ulmer-Scholle et al., 2014). Conditions that have not been reached in the study area, since the reservoir is at lower temperature (50-70°C) and shallower depths (< 2 km).

The temperature at which the quartz cement was formed can be different from the present-day temperature in the reservoir. The quartz-cementation paleo temperature is commonly estimated based on fluid inclusions, and depends on the basin subsidence history (Worden & Morad, 2000). Pressure has also been described to have a significant influence in quartz cement. In general trends, over-pressured sandstones have reported more quartz cementation than normally pressured sandstones (Osborne & Swarbrick, 1999). Regardless of the type of cement, the cementation process will finally result in porosity reduction.

#### *1.2.3.2 Sandstone cementation impact on rock properties*

As the cement content increases, it is expected to result in a general pore volume reduction when additional variables remain constant. Based on the pore structure, the electrical formation factor will tend to increase in a sample with higher cement content (Archie, 1942), and the permeability will tend to be reduced (Carman, 1937). The increase in the formation factor results from the reduction in the tortuosity value and the increase in the constriction factor of the pore structure (C. F. Berg, 2012); whereas the decrease in permeability is produced by the changes in characteristic hydraulic length, constriction factor, tortuosity, and effective porosity (C. F. Berg, 2014).

The way the cement placed in the pore structure could affect the transport properties differently. When the quartz cement grows in the pore throat, then pore throats are expected to be generally reduced requiring more pressure to be applied for the mercury to get into the pore space. The electrical formation factor will tend to rapidly increase (Schwartz & Kimminau, 1987), and the permeability will tend to be reduced since the pathways will be constrained or blocked increasing the tortuosity of the medium (C. F. Berg, 2014; Øren, Bakke, & Arntzen, 1998). By contrast, if the cement is mainly placed in the pore body, the formation factor will tend to increase slowly (Schwartz & Kimminau, 1987) and permeability will be less affected since the pore volume will tend to decrease, but the pores are still interconnected.

## 1.3 Thesis organisation

This manuscript compiles an introductory chapter and two linked papers, where the author of the manuscript is also the first author of the articles.

The introductory chapter includes an introduction to the topic, research objectives, purpose, and importance. This chapter also provides background information relevant to the research topic.

The first paper is titled *"Developing a fundamental understanding of how oil impacts diagenesis by investigating rock samples from close to the oil-water contact, Ben Nevis Formation, Hebron Field."*. The purpose of this paper is to investigate whether or not the presence of oil impacts the diagenetic process of the rock. It is focused on quantification of quartz overgrowth, and related pore structure differences. Petrographic results from SEM-

MLA on thin sections from samples above and below the OWC are presented. The amount of quartz overgrowth was quantified through SEM-CL image analysis. Finally, the internal pore structure of the samples was analysed from the MICP test results. This paper is going to be submitted to the Canadian Journal of Earth Sciences.

The paper in chapter 3 represents the second paper prepared during the research project. It is titled "*An experimental and digital investigation into the impact of diagenesis above and below the oil-water contact".* Based on the observed diagenetic differences in quartz overgrowth, the impact in the pore structure was investigated using MICP test and digital rock physics for simulation of transport properties depending on the pure structure. A poster of this paper was presented at the 33rd International Symposium of the Society of core analysts in August 2019 and will be submitted to the Bulletin of Canadian Petroleum Geology.

## 1.4 Co-authorship Statement

Francis Mujica, B.Eng., is the main practical and intellectual contributor to the thesis and the two papers. She performed the mineralogical and quartz overgrowth analysis. Additionally, she conducted the sample preparation, MICP test and data analysis for the experimental pore structure evaluation. She also performed the image processing, segmentation, 3D volume construction and simulations for the Digital Rock analysis of transport properties. Finally, the main author analysed the data and prepared the two articles and the present manuscript.

Lesley A. James, PhD., was the graduate supervisor. She was fully involved during all the stages in the project, from the project' structure to the data analysis, papers, and manuscript preparation. Her supervision was constant during the experimental phase and data analysis. Her technical expertise and editorial advice were present all along the project. She brought particular contributions during the experiments performance, data analysis, and results presentation.

Carl F. Berg, PhD., was a co-supervisor. He was fully involved since the beginning of the project. He provided important advice, guidelines, and supervision in the practical aspect of the thesis and data analysis. His mentorship was especially significant during the digital rock investigation. He was the author of the code used for the formation factor estimation in Chapter III. He also helped with the design and delineation of the research as well as providing constructive suggestions for papers and manuscript preparation.

Derek H.C Wilton, PhD., was also a co-supervisor. He provided important guidelines in the geological aspects. His contribution was more pronounced during the SEM-MLA, SEM-CL tests and data analysis. He also provided comments and suggestions to improve the quality of the papers and manuscript.

Salem Akarri, PhD candidate, joined the project at the beginning of the second article (Chapter III) conducting the μ-CT scans, image acquisition and reconstruction. He made an important contribution to the quality and resolution of the images acquisition and provided valuable guidance in the image processing step. He also reviewed the second article providing comments and suggestions for improvements.

# CHAPTER 2. DEVELOPING A FUNDAMENTAL UNDERSTANDING OF HOW OIL IMPACTS DIAGENESIS BY INVESTIGATING ROCK SAMPLES FROM CLOSE TO THE OIL-WATER CONTACT, BEN NEVIS FORMATION, HEBRON FIELD.

Francis Mujica[1], Lesley A. James[1], Carl F. Berg[2], Derek H.C Wilton[1]

[1] Memorial University of Newfoundland, St John's. NL, Canada
[2] Norwegian University of Science and Technology, Trondheim, Norway

## 2.1 Abstract

There is ongoing discussion as to whether pore water displacement by hydrocarbons can halt diagenetic chemical processes in sandstone reservoirs. Understanding the impact of oil presence on diagenesis can improve models for predicting porosity and permeability, and thus increases the accuracy in the reservoir performance. Most research on the impact of oil presence on diagenesis has been conducted on sandstone reservoirs in the North Sea and the Gulf Coast, where the reservoirs are at several kilometres depth and relatively high temperatures. In contrast, the Hebron Field sandstone reservoir is located at < 2 km depth with 50 to 70 °C (120-160°F) and 180 to 190 bars (2600 to 2750 psi).

The Ben Nevis reservoir in the Hebron Field exhibits a short transition zone with an abrupt oil-water contact (OWC) that was cored. Core samples collected close to this distinctive OWC were analysed to compare the characteristics of both water and oil-bearing rocks, as well as the transition zone between the two where mobile saturation of both fluids coexist. This research will ultimately result in a better understanding of the Ben Nevis reservoir,

Hebron Field, as well as provide new evidence about the impact of oil presence in diagenetic processes.

In this study, the core samples from above and below the OWC were petrographically examined using a combination of Scanning Electron Microscopy (SEM), Cathode-luminescence (CL), Mineral Liberation Analysis (MLA), and Mercury Injection Capillary Pressure (MICP). The purpose is to investigate whether the presence of oil impacts diagenesis, in particular whether it impacts cementation, and pore structure in the Ben Nevis reservoir, Hebron Field.

The results suggest that quartz cement content tends to increase towards the water leg. From 3 to 4% in the oil-leg to 4 to 6% in the water-leg. Quartz overgrowths in the Ben Nevis Formation, Hebron Field, are not very well developed and even when quartz is the main cement, the percentage is not representative enough to impact the porosity, pore structure and the transport properties.

## 2.2 Introduction

Most oil reservoirs occur in sedimentary rocks such as sandstone, limestone, dolomite, and shale (unconventional resources). These lithologies are predominantly composed of quartz, calcite, dolomite, and clay minerals. Quartz is considered the main mineral in sandstones, but sandstones also contain a variety of other minerals depending on the source of detritus.

Diagenesis includes all changes that sediments may undergo following deposition but prior to metamorphism. It is an important aspect of hydrocarbon exploration as it plays a vital role in either preserving, destroying, or creating porosity (Worden & Burley, 2003).

Diagenetic processes can be subdivided into three major stages, i.e. early, burial, and uplift-related. During the early diagenetic stage, pore spaces are continually occupied by interstitial water where the chemical composition of the water is controlled by the environment of deposition (EOD). Changes in pore water geochemistry and/or the replacement by hydrocarbons fluids are considered to be the main factors controlling diagenesis during the burial stage (Choquette & Pray, 1970; Worden & Burley, 2003).

It is still a matter of discussion as to whether diagenetic chemical processes are stopped, or retarded, after the pore water is displaced by hydrocarbons. It has been suggested that when oil enters a system, the diagenetic evolution of sandstone can be suspended (placed on hold) or retarded, thus preserving porosity and mineralogy in the now oil-bearing rock (Dixon et al., 1989; Gluyas et al., 1993; Marchand, Haszeldine, et al., 2002; Marchand et al., 2001; Saigal et al., 1992; Worden et al., 2018, 1998). Conversely, it has been argued that diagenetic processes continue after oil emplacement in the pore system, as indicated by the presence of oil inclusions in authigenic minerals, quartz cementation models based on time and temperature regardless of the oil presence, and the fact that there are no significant differences in porosity and quartz cement volume between the water and oil legs (Barclay & Worden, 2000; Midtbø et al., 2000; Molenaar et al., 2008; Walderhaug, 1990, 1996).

Understanding if/how oil presence in the reservoir affects quartz cementation, and consequently its impact on porosity and permeability distribution in a geological model is important for reservoir characterization and enginering. A change in reservoir characterization may impact well planning strategy, e.g. the number and position of wells (injection and production), the reservoir performance based on the degree of pressure

support from the aquifer (Worden et al., 1998), and the production strategy including any enhanced oil recovery technique (Heaviside, Langley, & Pallatt. (1983) in Emery, Smalley, & Oxtoby, 1993).

The purpose of this research is to investigate the zones above and below the oil-water contact (OWC) in the Ben Nevis reservoir, Hebron Field, to evaluate diagenetic differences in quartz overgrowth. This study is based on petrographic examination and laboratory tests of core samples close to the OWC. The petrographic analyses include Scanning Electron Microscopy (SEM), Mineral Liberation Analysis (MLA), and Cathode-luminescence (CL). Mercury Injection Capillary Pressure (MICP) are used to evaluate the porosity and pore structure.

## 2.3 Background

The following section provides a brief overview of earlier efforts to determine if quartz cementation is affected by the presence of oil, based on rock properties from the oil and water legs.

Dixon et al. (1989) investigated porosity preservation in upper Jurassic sandstones from the Norphlet Formation in Alabama based on petrographic observation integrated with porosity and permeability to the air analysis from conventional core analysis. They found that porosity preservation was the product of a series of time overlapping diagenetic events. They considered that migration of hydrocarbons and geopressuring inhibited cementation to help preserve porosity. The Norphlet reservoir is located at depths of more than 6 km with a high pressure gradient.

Based on petrographic (point counts and cathodoluminescent microscopy) and fluid-inclusion microthermometry studies, Saigal et al. (1992) analysed thin sections from reservoir units saturated with oil and different reservoir units saturated with water. They suggested that quartz overgrowth continued in the oil-saturated units, but the rate was retarded compared to the water-saturated units. Their analyses were primarily based on paragenesis and mineral reactions rather than petrophysical properties.

Barclay & Worden (2000) combined petrophysical and petrographical analyses above and below the OWC from three different wells in the upper Jurassic Magnus sandstone member, Magnus Field, northern North Sea. For the well logs porosity estimation, they used sonic, neutron and density logs, while for the petrographic analysis, they applied traditional point-counting. They found little or no variation in quartz cement contents above and below. Based on these results, they suggested that oil emplacement did not affect the quartz cementation. Marchand et al. (2001) investigated the effect of oil on quartz cement based on petrographic data and quartz cementation modelling in the upper Jurassic Brae Formation, Miller Field, North Sea. They concluded that the porosity preservation in these deeply buried sandstones was caused by the early emplacement of oil that slowed down and even stopped quartz cement precipitation. Similarly, Marchand, Smalley, Haszeldine, & Fallick (2002) found that early oil emplacement prevented the precipitation of quartz cement and preserved porosity. The Brae Formation Unit 2 in the Miller Field and Unit 1 in the Kingfisher Field were oil-charged in an early stage of the diagenetic process. The Brae Formation in both fields was buried to depths of about 4 km under temperatures around 120 °C. Worden et al. (2018) investigated whether the presence of oil had a

significant effect in quartz cementation by comparing mineralogically and texturally similar samples grouped in three different facies subdivided by water saturation. The petrographic analysis was carried out by point-counting on polished thin sections. Quartz cement was quantified using point counting and validated for three control samples using SEM-CL. Geothermometric analyses were conducted on fluid-inclusions to define homogenization temperatures for both aqueous and petroleum inclusions. Core and well-log porosities were also compared. Based on the results obtained from the analyses and different model scenarios, they concluded that oil emplacement appears to have inhibited quartz cementation. The analyses were conducted for this considerably deeper reservoir at 3-4 km. Quartz overgrowth was interpreted to have formed at temperatures as low as 103 °C but mainly at 120 °C.

Unlike most of the previous work mentioned, the reservoir conditions for this work were on shallower depths and lower temperature and pressure conditions using a combination of different techniques. Porosity and pore size distributions were considered using the MICP test instead of singular value porosity measurements. Additionally, the present approach is more focused on core samples specifically above and below a very well defined OWC .

In the Hebron Field, there are very limited data on oil-bearing fluid inclusions, especially in the Ben Nevis Formation, to provide insight into the P-T conditions extant when quartz overgrowth developed. According to Stasiuk (2001), however, the first episode of oil migration into the Ben Nevis Formation occurred when the formation was still shallowly buried. This interpretation is based on petrographic and geochemical analysis used to model the subsidence and paleotemperature history.

Stasiuk (2001) investigated the organic petrology and fluid inclusions in the Ben Nevis Formation using data from the West Ben Nevis B-75 well (neighbour field), Hebron I-13, and North Trinity H-71 (located to the south-east of the D-94 well). Based on the lack of aqueous fluid inclusions in quartz cement and lack of consolidation in the Ben Nevis Formation, it was inferred that the oil charging occurred at an early diagenetic stage shortly after quartz cementation began. The process is similar to the charging history described for fields in the North Sea; for instance, the Miller and Kingfisher fields (Marchand et al., 2001; Marchand, Smalley, et al., 2002).

Shimeld, MacRae, Moir, Fowler, & Stasiuk (2005) integrated and analysed 1D basin modelling, using apatite fission track length, petrography, fluid inclusions primary in quartz cement, and geochemistry to reconstruct the subsidence and paleotemperature history of the Terra Nova, Hebron and Ben Nevis fields. They concluded that there were three peaks in hydrocarbon generation (early Cretaceous, late Cretaceous and mid-Cenozoic) and two main periods of hydrocarbon migration into the reservoir (early Cretaceous and post-Paleocene). Based on a one-dimensional forward paleotemperature model, the Ben Nevis reservoir at the Hebron Field was interpreted to be cooler than 60 °C at the mid-Turonian (~90.5 Ma), when the first pulse of oil migration into the Ben Nevis Formation and the initial subsidence happened (Figure 10). After the mid-Turonian, the Ben Nevis Formation is interpreted to be exposed at temperatures lower than 70 °C (Figure 11).

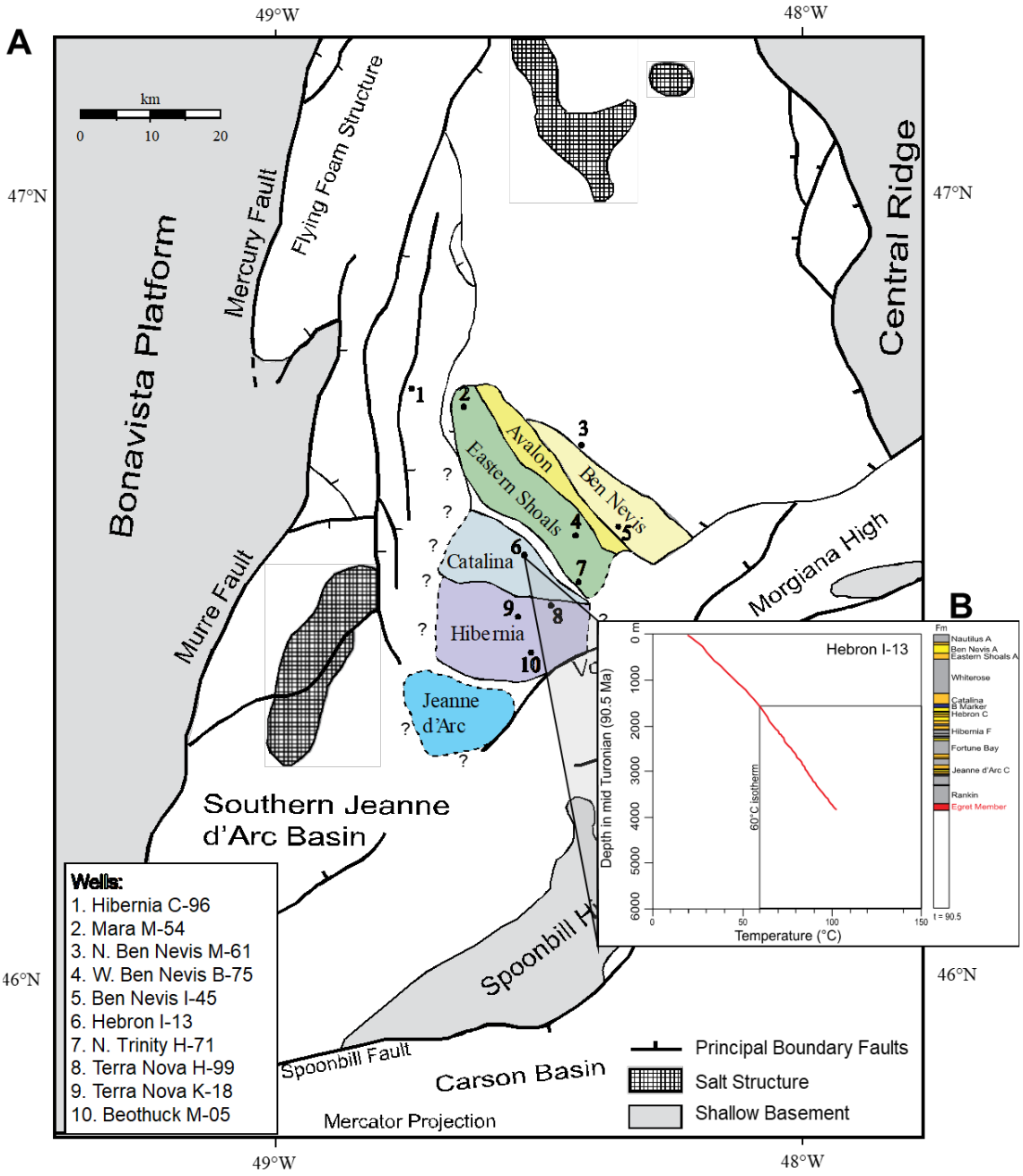


*Figure 10 (A)Forward modelling regional map showing the youngest formation at the paleo-isothermal of 60 °C at the Mid-Turonian (Shimeld et al., 2005). (B) Depth versus temperature plots at the mid-Turonian time (90:5 Ma) from 1-D forward models of the basin history using BasinMod™ (Shimeld, Altheim, MacRae, Grist, & Moir, 2001)*

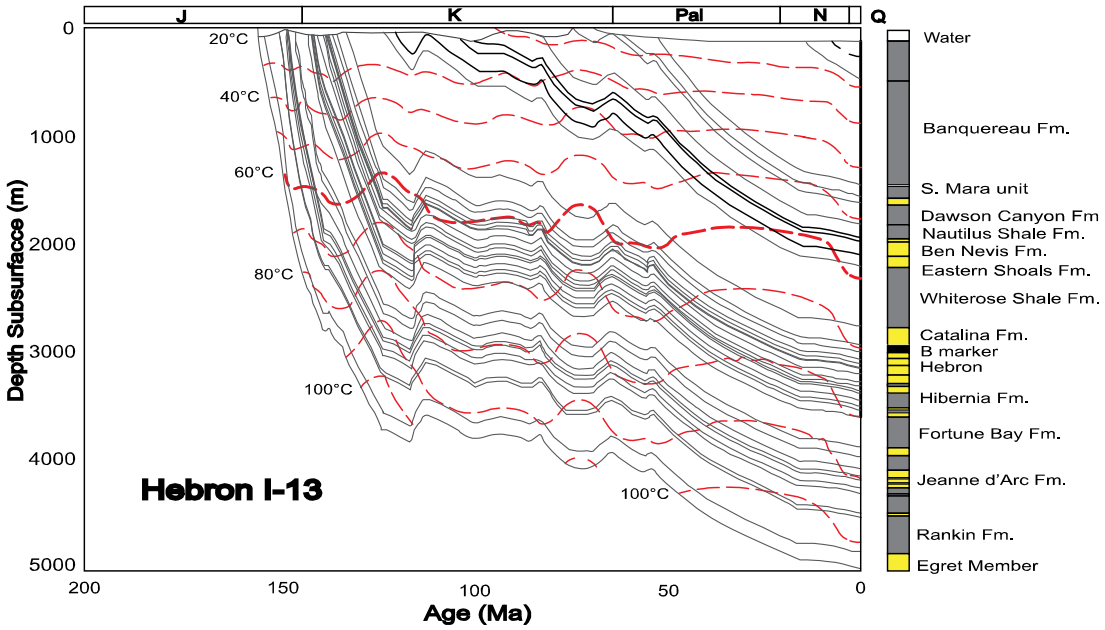


*Figure 11 Paleo-isotherms obtained from the 1D forward basin model in the Hebron I-13 well (Shimeld et al., 2005)*

## 2.4 Geological Setting

The Jeanne d'Arc Basin, offshore Newfoundland, is well-known for its strong economic potential. Currently, it is a significant region in Canada for light oil with producing fields such as Hibernia, Terra Nova, White Rose and the most recently developed Hebron Field.

The Hebron Field is located in the Southern North Atlantic ocean at the East-Central part of the basin. It is located 32 km southeast of Hibernia, 9 km north of the Terra Nova Field, and 46 km southwest of White Rose, all oil producing fields since 1997, 2002, and 2005 respectively (Figure 12).

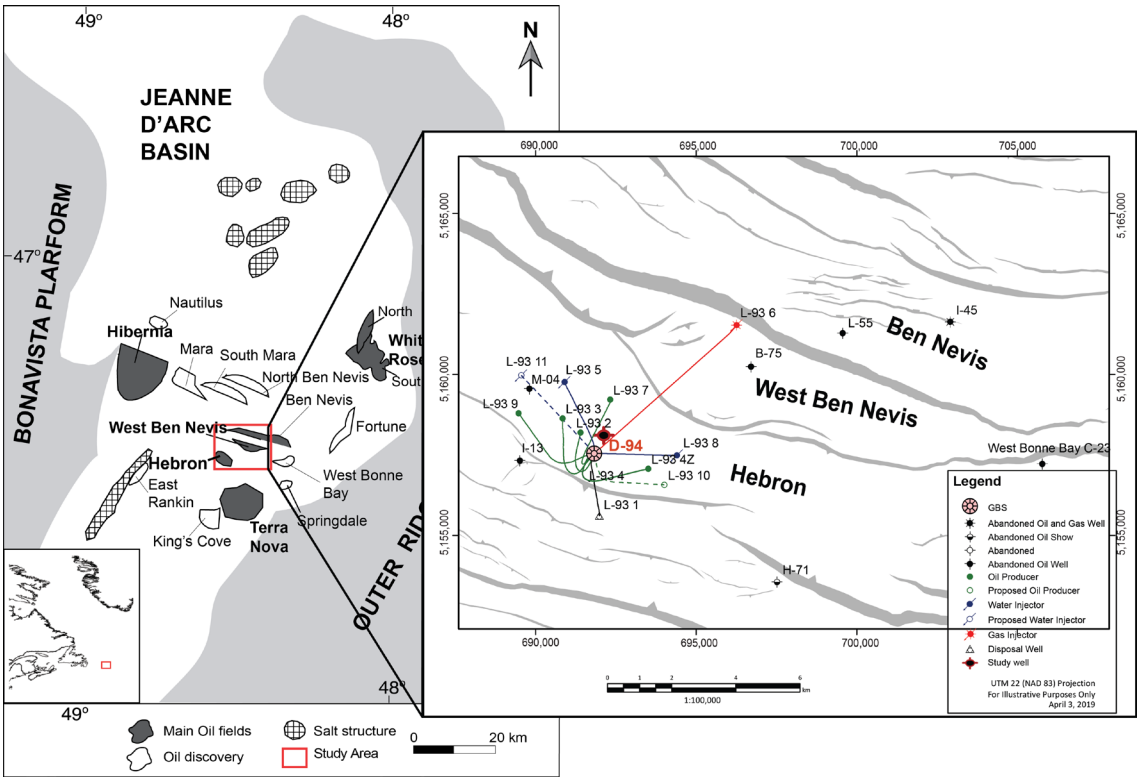


*Figure 12 Location map of the Jeanne d'Arc basin with inset map of a more general location (left). The red square contains the Hebron, West Ben Nevis and Ben Nevis Fields. Inset: The Hebron Field structural map and well location (right). Adapted from (C-NLOPB, 2019b; Magoon, Hudson, & Peters, 2005)*

The Hebron Field together with the West Ben Nevis and Ben Nevis fields comprise the Hebron-Ben Nevis complex in which resources are estimated to be greater than 3000 million bbl of oil (MMbbls) and the estimated ultimate recovery (EUR) more than 700 MMbbls (C-NLOPB, 2012). As shown in Figure 13, the total resources are located in different pools.

The resources in the Hebron Field occur in three different formations, namely Jeanne d'Arc (pool 4), Hibernia (pool 5), and Ben Nevis (pool 1). The Hebron Field was formed by multiple rifting events during the Late Triassic, Late Jurassic-Early Cretaceous, and Early Cretaceous (Enachescu, 1987; Sinclair et al., 1992), producing several normal fault-

bounded blocks that make up the current geological configuration of the Hebron Field (Figure 12 and Figure 13).

The Ben Nevis Formation (pool 1) is located in the highest part of the horst structure and it is separated from the same formation of the neighbour West Ben Nevis Field (pool 2) by normal faults (ExxonMobil Canada, 2011; Sinclair et al., 1992).

All the hydrocarbon resources discovered are contained in Mezosoic sediments (Jurassic and Cretaceous). The main reservoirs correspond to the Ben Nevis, Hibernia, and Jeanne d'Arc formations. The Late Jurassic Egret Member, Rankin Formation, is the main source rock (DeSilva, 1999). The age of the Ben Nevis Formation has been defined as early Cretaceous, ranging from late Aptian to late Albian (McAlpine, 1990).

Regionally, the Ben Nevis Formation is an upward fining sequence of sandstone, interbedded with sandy limestone, glauconitic siltstone, and shale representing a marine transgression (Driscoll & Hogg, 1995; McAlpine, 1990). In general, two subunits are defined: the lower subunit comprises interbedded shale and sandstone and local coal beds, and the upper subunit consists of quartzose, moderately to well sorted, fine to very fine-grained sandstone at the top (McAlpine, 1990). The unit unconformably overlies the Avalon Formation, however, operationally it is commonly termed Ben Nevis-Avalon (BNA) without differentiation.

The dominant depositional environment of the Ben Nevis Formation, Hebron Field, is interpreted as proximal lower shoreface, becoming a more distal and transitional

environment in the northeastern faulted blocks (Ben Nevis Field) (ExxonMobil Canada, 2011; McAlpine, 1990).

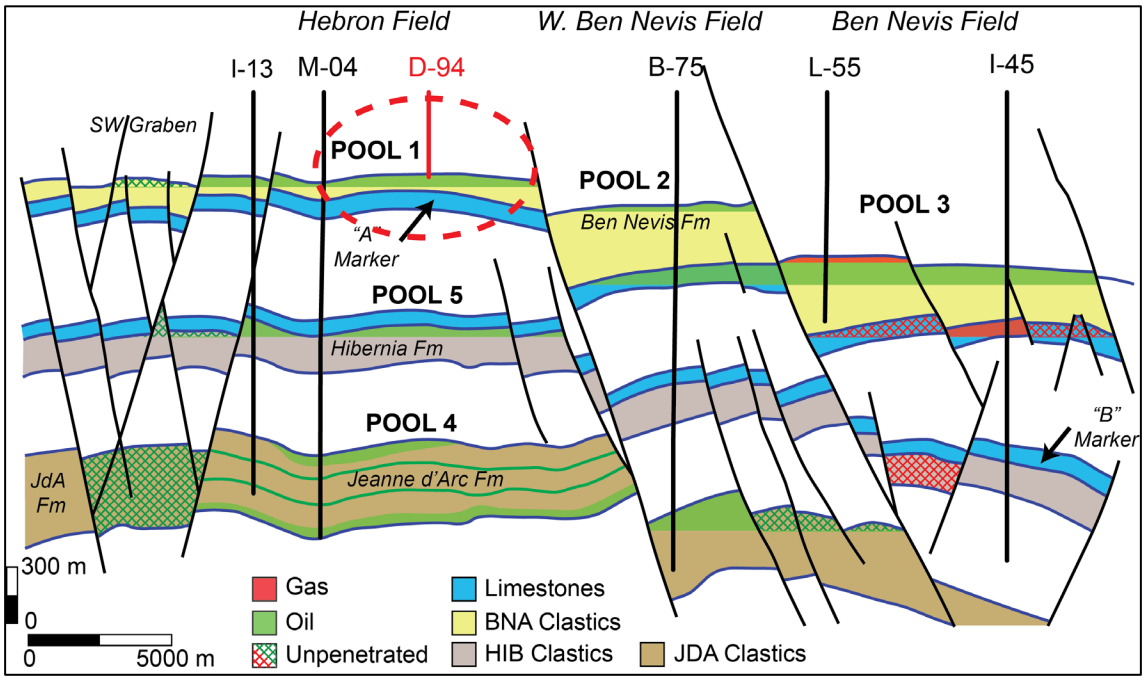


*Figure 13 Hebron Field schematic section. The red dotted ellipse shows the studied reservoir; adapted from Cornaglia (2018)*

The Ben Nevis Formation, Hebron Field (pool 1) is considered the main reservoir in the field, expected to produce around 80 % of the total recoverable oil from the Hebron-Ben Nevis complex (Cornaglia, 2018). Previous core analysis in pool 1 reported average porosity typically between 10 % and 30 % (Cornaglia, 2018) and average permeability ranging from 50 to 400 mD (ExxonMobil Canada, 2011); an average value of 1427 mD was reported after core analysis in the reservoir units (Nicoud, 2000). The reservoir was found at 1808 m (True Vertical Depth sub-sea – TVDSS) with a gross thickness in the well of 129 m. In overall, 89.5 m of core were acquired in the well, with an average recovery of 75% giving a total of 67.1 m of core recovered in six core intervals. The reservoir pressure

ranges from 2600 to 2750 psi (180 to 190 bars) and temperatures between 50 and 70 °C (120-160°F) (Petro-Canada, Chevron-Canada, Mobil Oil, & Hydro, 1999b)

## 2.5 Experimental Methodology

### 2.5.1 Materials

All core samples collected for this study belong to well D-94. The target for this well was the Ben Nevis Formation, and this well was considered to be the most reliable well during the Hebron Field delineation stage.

Core 6 was taken from 1905.2 m to 1928.2 m measured depth (MD) from which 21 m (91%) were successfully recovered (Petro-Canada et al., 1999b). This core contacted both oil and water zones, as well as the oil-water contact (OWC). Optical microscopy analyses carried out by Nicoud (2000) indicate that rock samples correspond to Subarkose to Sublitharenite (Folk, 1980; McBride, 1963; Pettijohn et al., 1987) in the clastic sedimentary rock classification scheme (Figure 14).

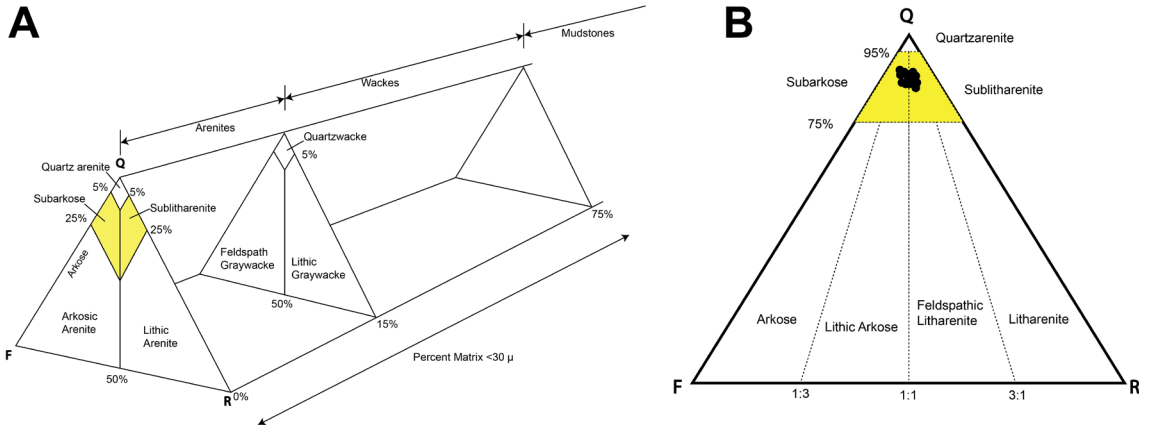


*Figure 14 Ben Nevis Formation clastic sedimentary rock classification from the reservoir section. Classification after (A) Pettijohn et al., (1987) (B) Folk, (1980). Adapted from Nicoud (2000). The highlighted areas show the subarkose and sublitharenite rock types*

Samples above and below the OWC were used in this work, as indicated in Figure 15. The samples were distinguished using a number and a letter. The number represents the relative distance of the sample from the OWC. The letter indicates if the sample came from above (A) or below (B) the OWC. “SP” is just an abbreviation for the word “sample”

Based on direct observations of the core, well log information, original pictures of the core, and lithological descriptions, a set of samples was defined above and below the oil-water contact for analysis. The sampling points were selected where the rock characteristics appear to be as similar as possible. The density and neutron log responses were very similar across the OWC. The most notable log change is related to the change in the fluid that is saturating the medium: the OWC is identified both in the resistivity log as well as visually in the core. Sample SP-6A is an exception, it is from a different facies of very tight carbonate-cemented interval with strong HCl reaction and a notable increase in the resistivity (RT) and density logs. This sample was included just for the petrographic description and excluded from CL and MICP analysis.

A subset of six samples (SP-7A, SP-4A, SP-1A, SP-1B, SP-3B, SP-5B) distributed through the oil and water zones was used for the petrographic analysis and quartz overgrowth comparison (see Figure 15).

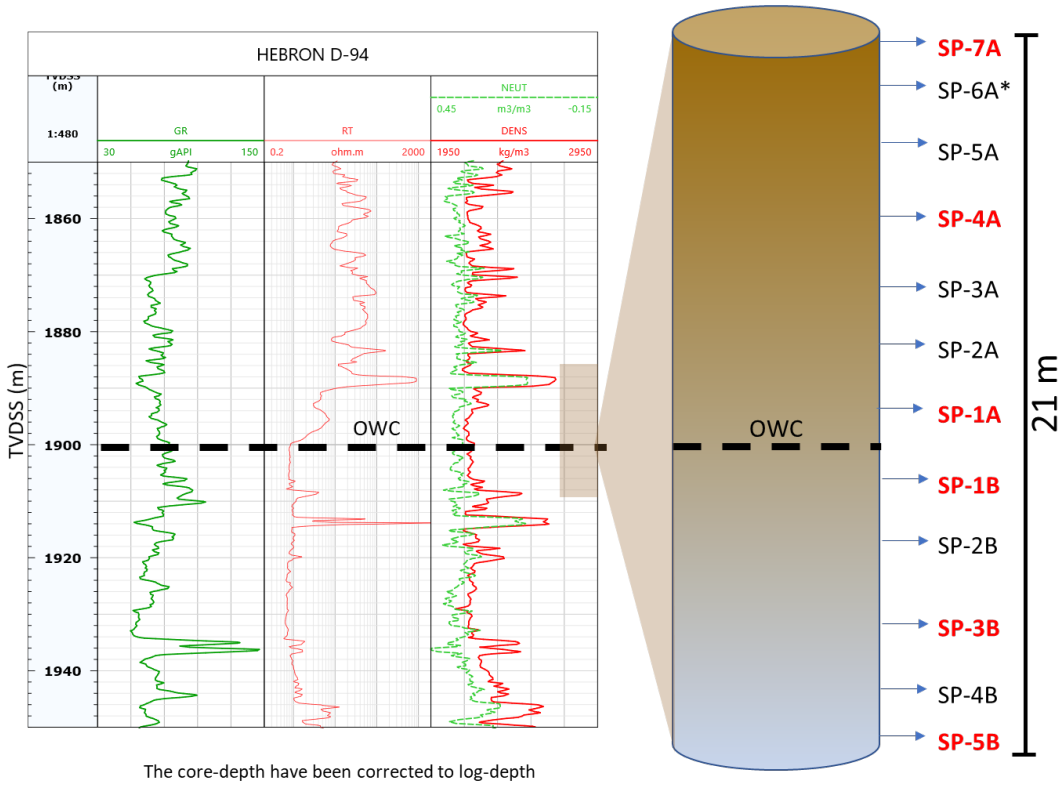


*Figure 15 Samples location versus depth. Samples in red correspond to the subset of samples used for petrographic analysis and quartz overgrowth comparison. *indicates the sample that was not included in further analysis*

### 2.5.2 Mineral Liberation Analysis (SEM-MLA)

The analysis consists of a scanning electron microscope (SEM) that generates a beam of electrons. Digital images are produced by recording the signals resulting from interactions between the focused beam of electrons and the sample. The backscattered electrons (BSE) are used to produce digital images based on the average atomic number (Nanakoudis, 2018; Zhou, Apkarian, Wang, & Joy, 2007).

The electrons interactions with the sample also produce X-ray signals. The energy spectrum of X-rays emitted is detected by the energy dispersive spectrometers (EDS) producing a characteristic pattern of the elements present. Based on the X-ray spectra and BSE images, the software for automated mineralogy (MLA) can identify the minerals from a database

allowing the quantitative analysis of mineral abundance (Gu, 2003; MUN CREAIT, 2012; Sylvester, 2012).

SEM acquisition and MLA classification were used to define the overall mineralogy of each sample from polished thin sections. These analyses were conducted using the FEI MLA 650F instrument in the CREAIT Network's Micro-Analysis facilities at Memorial University.

### 2.5.3 Cathodoluminescence (SEM-CL)

This technique uses energetic electrons that strike the rock sample, causing light emission. The CL responses in minerals is a function of the composition, lattice structure and structural damage of the mineral. It provides information about the origin, growth, replacement and deformation of the mineral (Darrell, 2016; Pagel, Barbin, Blanc, & Ohnenstetter, 2000). Characterization of grains using the SEM-CL is a powerful tool to identify and differentiate different generations of the same mineral, for example the detrital quartz grains and authigenic quartz overgrowth in sandstones (Evans, Hogg, Hopkins, & Howarth, 1994; SERC Carleton College, 2016).

The combination of SEM-CL and image analysis was used to quantify the quartz overgrowth, thereby quantifying possible diagenetic differences caused by the oil presence. For the quartz overgrowth interpretation, 10 points were defined in each sample for imaging at higher magnification. The most common magnification used for quartz cement quantification is between 100X and 200X (Evans, Hogg, Hopkins, & Howarth, 1994). In

this work, 150x of magnification in the field emission JEOL JSM7100F SEM equipped with a Deben Centaurus CL receptor was used.

The images were analysed using the Image J software (Schindelin et al., 2012). The criteria used to define quartz overgrowths was mainly based on CL responses and grain morphology. On the SEM-CL images, detrital and authigenic quartz generally display different luminescent responses, as seen in Figure 16. Both detrital and authigenic quartz may display different intensities under CL. However, detrital quartz generally looks brighter, and the authigenic quartz, darker (Evans et al., 1994). Quartz overgrowth can exhibit euhedral outlines such corner forming, sharp edges produced by a well-defined face (Ulmer-Scholle et al., 2014). The observation of this morphology around the grains, pointing out pore space, suggest in-situ growth of the mineral phase. Possible euhedral shapes of the quartz grains were also used as interpretation criteria. See Figure 16.

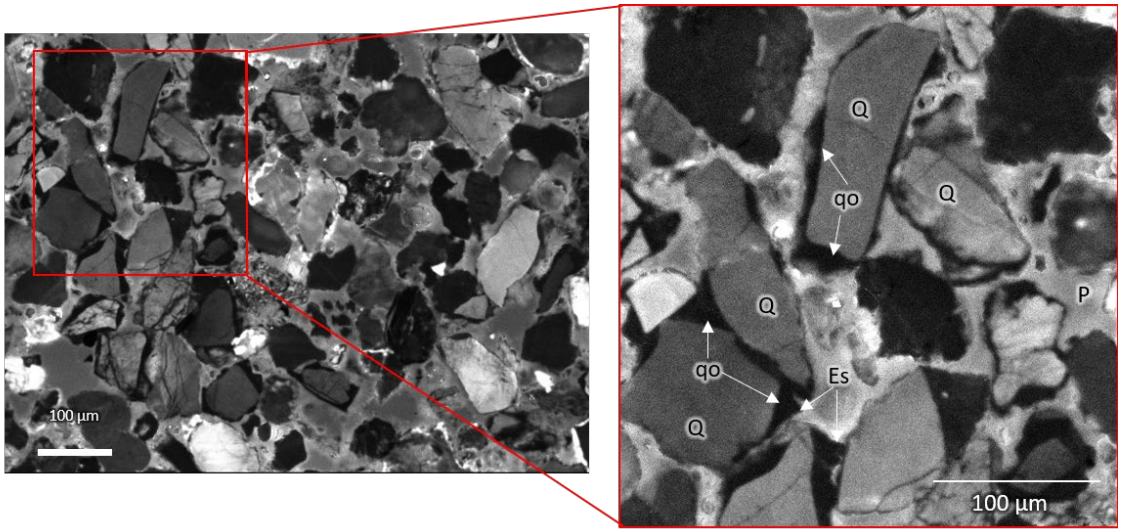


*Figure 16 Cathodoluminescence (SEM-CL). The image shows the total field view and the enlarged area. The right image shows the quartz overgrowth (qo), detrital quartz grains (Q) identification, euhedral shape produced after authigenic quartz overgrowth (Es), and the intergranular pore space (P)*

### 2.5.4 Mercury Injection Capillary pressure (MICP)

MICP is a technique first proposed and implemented by Shell in 1947. Since then, the technique has experienced several improvements (Thomeer & Murphy, 2000). During this test, mercury (non-wetting phase) is injected at increasing pressures in an evacuated sample initially filled by air (wetting phase) (Anovitz & Cole, 2015).

Mercury injection method was used to evaluate the porosity and pore size distribution in the samples at the Hibernia EOR lab at Memorial University. The measurements were carried out using AutoPore® IV 9500 equipment. At the beginning of the test, the clean and dry sample was placed into the penetrometer, the gas (air) was evacuated, and the space between the sample and the cell was filled by mercury. Increasing pressure was applied against the sample from the surrounding mercury to achieve e intrusion in smaller pores. The pore volume available to be intruded by mercury is equivalent to the connected pore volume.

The pore volume available to be intruded by mercury is equivalent to the connected pore volume. The volume of mercury forced into the pore space increases with the pressure. At the end of the test at 33,000 psi (2275 bars), even the smaller pores (~0.005μm) will be filled by mercury. The total volume of mercury intruded into the sample is measured as the reduction in the length of the mercury column in the penetrometer stem.

The volume of mercury that is intruded into the sample at a known pressure can be related to the pore throat diameter using a modification of the Young-Laplace equation for cylindrical pores (Equation 7).

$$D = \frac{\gamma\,(-4\,\cos\theta)}{P_c}$$

*Equation 7 Young-Laplace equation for cylindrical pores*

To estimate the experimental errors of these measurements, the precision in the porosity measurement was determined by running repetition samples on 10% of the sampling points.

## 2.6 Results

### 2.6.1 Petrographic description

In the Hebron Field, the facies are typically fine to very fine, moderate to well sorted sandstones with some carbonate-cemented beds. The SEM-MLA results (Figure 17) indicate that the rock is dominated by quartz (~80%), followed by feldspars, mainly the alkaline Orthoclase (~5%) and sodium plagioclase, Albite (~3%). The total clay content was found to be less than 5%. The detrital quartz grains seem clean, discarting the presence of an important amount of coating materials on the grains. Based on the Udden-Wentworth classification (Ulmer-Scholle et al., 2014), the grain size is considered fine to very fine grains. In general, the grains were observed to be moderately to well sorted, with sub-rounded and sub-angular shapes. The rock fabric has loose packing with significant intergranular pore space. The samples were found to be poorly consolidated with low matrix and cement.

The petrographic analyses suggest that the samples were mineralogically and texturally similar. An exception was the sample SP-6A which corresponds to a carbonate-cemented bed with negligible porosity and permeability. In this sample, the quartz grains are also the main framework component. However, the intergranular space is filled by carbonate

cement, giving consolidated properties to the sample. This sample was included just for the petrographic analysis and was excluded from the follow-up tests.

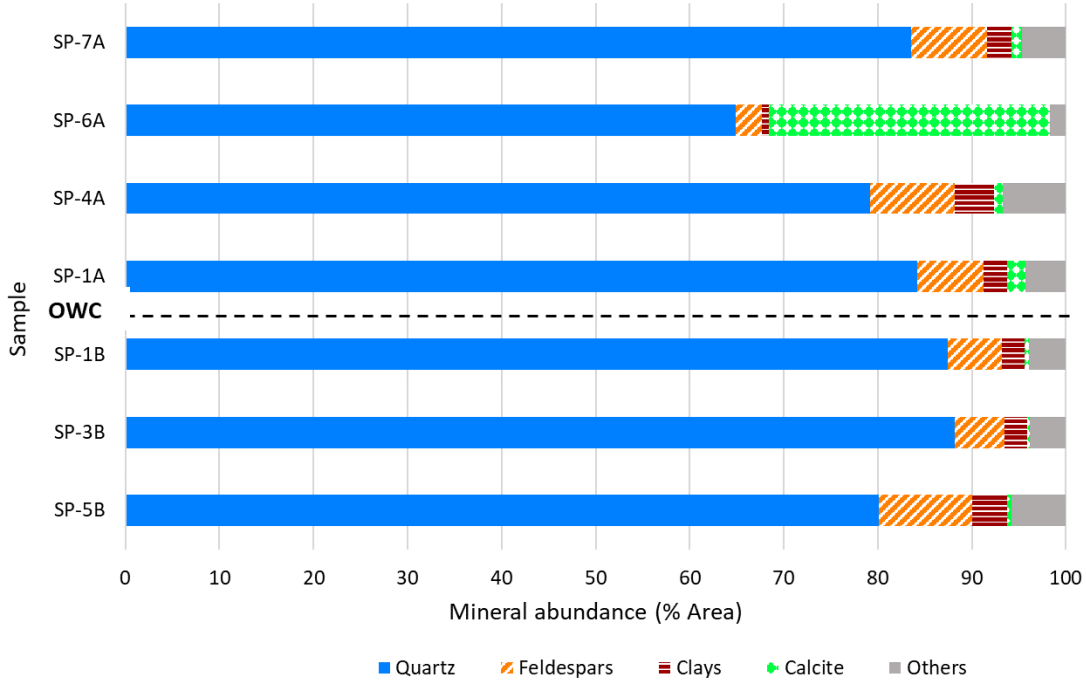


*Figure 17 SEM-MLA analysis results. See Figure 15 for location of the samples*

### 2.6.2 Quartz cementation

Analysis carried out on the SEM-CL images were used to distinguish between detrital and authigenic quartz. Quartz overgrowth was quantified, and the average is expressed as a percentage of grain area (Figure 18).

Quartz overgrowth is in general more abundant in the water-leg section of the reservoir, varying from 4 to 6 % compared to 3 to 4% in the oil-leg section suggesting a clear trend of greater abundance in the higher water-saturated rocks. The data dispersion from the average value (red line in Figure 18) varies from 0.3 to 0.7. It is possible to observe that the amount of quartz overgrowth tends to overlap in the samples located closer to the OWC,

becoming more defined in sample more distant to the OWC, even if the data dispersion is considered.

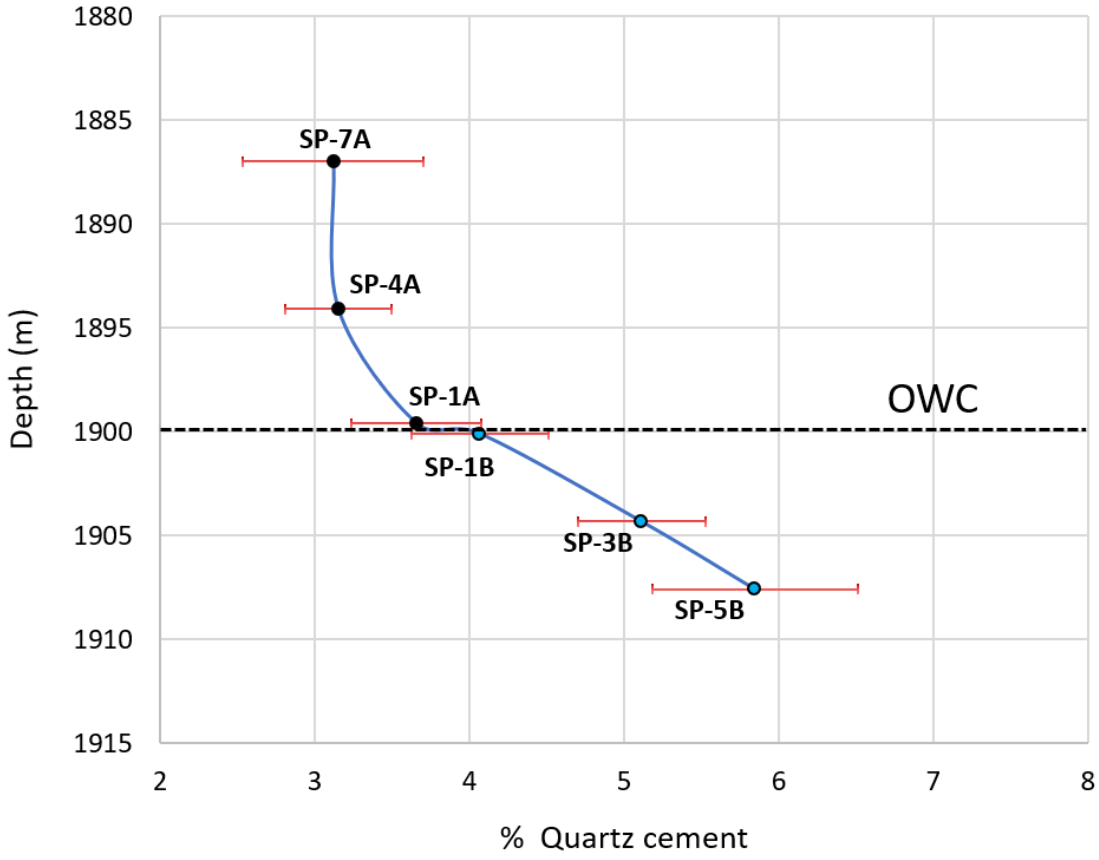


*Figure 18 Quartz overgrowth quantification. Black point indicates samples above the OWC. Blue points indicate samples below the OWC. The red line represents the dispersion from the average value*

### 2.6.3 Porosity and pore size distribution

The total porosity obtained ranges from 27 to 31% with no systematic trend (Figure 19A). The samples above and below the OWC exhibited similar average porosity regardless of the amounts of quartz overgrowth. This could mean that rock samples with very similar textural characteristics and porosities do not necessarily indicate that quartz cementation continues undisturbed after the oil emplacement since the porosity does not provide any information about the pore throat size and distribution.

The dominant pore throat size diameter of the control samples (Figure 19B) was found to be between 15 and 20 µm. showing no defined trend corresponding to the amount of quartz overgrowth. Apparently, the difference in the percentage of quartz overgrowth is not notably affecting the dominant pore throat size distribution in this system dominated by macropores. Based on porosity and most frequent pore size there is no noticeable difference in samples above and below the OWC.

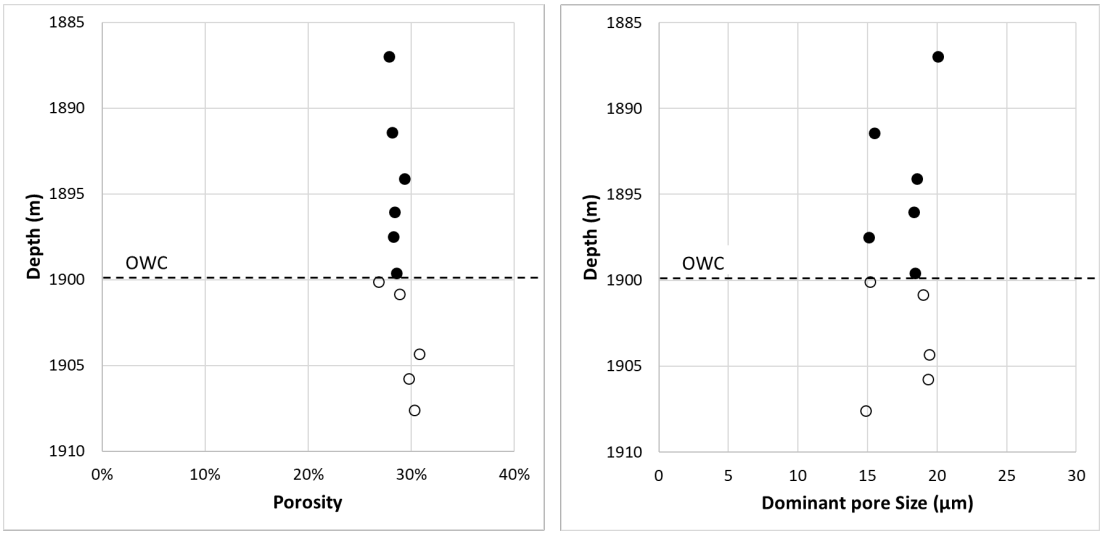


*Figure 19 (A) Porosity distribution and (B) dominant pore size for samples above and below the OWC. The solid black circles (●) indicate samples above the OWC and the clear circles (○) indicate samples below the OWC*

## 2.7 Discussion

In the Ben Nevis Formation, the percentage of quartz overgrowth was found to have a clear trend to increase towards the water leg. In contrast, the effect of the quartz overgrowth difference in the porosity and main pore size distribution is not very well defined in the interval close to the OWC indicating that the quartz overgrowth do not have a noticeable impact on the pore structure.

In samples located close to the OWC, we found that the rock samples from the water-leg have greater quartz cementation. In the Hebron Field located at less than 2 km deep and temperatures around 50- 70 °C, our results suggest that quartz cement precipitation will tend to be favored in an aqueous medium. This trend is similar to Marchand et al. (2001), Marchand, Smalley, et al. (2002), Saigal et al. (1992), and Worden et al. (2018) analyses in deeper buried and more cemented sandstone located at 3-4 km, and temperatures higher than 100 °C.

There is very little fluid inclusion data in the study area. Considering analogies with fields in the North Sea, most of the quartz cementation commonly occurs at temperatures greater than about 70 °C with important amounts found at depth between 3 to 4.5 km (Bjørlykke & Egeberg, 1993; Gluyas et al., 1993); however, temperature as low as 40 °C have been reported in the Cisco group in Texas and the Lousiana Gulf coast (McBride, 1989). The subsidence and paleotemperature 1D basin modelling (Shimeld et al., 2005) indicates that the Ben Nevis Formation was exposed at temperatures lower than 60 °C when the first pulse of oil migration occurred, and have been exposed to temperatures lower than 70 °C since then until the present (Figure 11). This could indicate that optimal burial and temperatures have not been reached to favour important amounts of quartz overgrowth to be formed, thus the quartz overgrowth is at an early stage.

The timing between the oil emplacement and quartz cement precipitation have been found to be a key factor controlling either reservoir quality preservation or deterioration (Emery et al., 1993). The paragenetic phases in the Ben Nevis Formation described by Stasiuk (2001) indicate that most of the chemical diagenetic changes in the rock took place prior to

oil migration into the system. Quartz overgrowth is interpreted to precede the oil emplacement, which supports the observed presence of quartz overgrowth in the oil zone. Another possibility is that the quartz overgrowth formed after oil emplacement (Walderhaug, 1990) but at retarded rates as have been found by Saigal et al. (1992). Either way, our observations suggest that the formation of quartz overgrowth is halted or retarded by oil intrusion and continues in the rock with higher water saturation.

## 2.8 Conclusions

We provide insight into the debate on whether pore water displacement by hydrocarbons can halt or retard the diagenetic chemical processes in reservoirs shallower than 2 km and temperature around 50 to 70 °C.

Based on the petrographic analysis, we observed that quartz overgrowth tends to be more abundant when the pore medium is occupied by water, indicating differences in the diagenetic process. However, it does not have a significant impact on the pore structure.

Quartz cementation does not appear to be the main porosity control in the Ben Nevis Formation, Hebron Field. Quartz overgrowths are not very well developed, indicating that the rock has not reached or remained at optimal conditions long enough where most of the quartz tends to precipitate in a percentage that causes a substantial impact in the general pore structure.

Similar porosity in samples above and below the OWC does not necessarily indicate that chemical diagenetic processes in quartz overgrowth are not affected by the pore water replacement by oil.

## 2.9 Acknowledgements

We thank the Natural Sciences and Engineering Research Council of Canada (NSERC), Research and Development Corporation of Newfoundland and Labrador (RDC) (now TCII), Hibernia Management and Development Company (HMDC), Chevron Canada Limited, and the Hibernia EOR Research Group for technical and financial support. The Canada-Newfoundland and Labrador Offshore Petroleum Board (C-NLOPB) provided the rock samples and Hebron field information. TechCore provided the service of cutting the core plugs with their equipment and facilities. The CREAIT network at MUN is thanked for support during the SEM-MLA-CL analyses. IHS Markit provided the well-logs.The third author was supported by the Research Council of Norway through its Centres of Excellence funding scheme, project number 262644.

## 2.10 References

Anovitz, L. M., & Cole, D. R. (2015). Characterization and Analysis of Porosity and Pore Structures. *Reviews in Mineralogy and Geochemistry*, *80*(1), 61–164. https://doi.org/10.2138/rmg.2015.80.04

Barclay, S. A., & Worden, R. H. (2000). Petrophysical and petrographical analysis of quartz cement volumes across oil–water contacts in the Magnus Field, northern North Sea. *Quartz Cementation in Sandstones*, *29*, 147–161.

Bjørlykke, K., & Egeberg, P. K. (1993). Quartz cementation in sedimentary basins. *The American Association of Petroleum Geologist*, *77*(9), 1538–1548. https://doi.org/10.1306/BDFF8EE8-1718-11D7-8645000102C1865D

C-NLOPB. (2019). Resource Information. Retrieved from https://www.cnlopb.ca/wp-content/uploads/estrr_heb.pdf

Choquette, P. W., & Pray, L. C. (1970). Geologic Nomenclature and Classification of Porosity in Sedimentary Carbonates. *The American Association of Petroleum Geologist*, *54*(2), 207–250.

Cornaglia, V. (2018). Geoscience Overview of the Hebron Field. In *Offshore Technology Conference*. Houston, Texas: Society of Petroleum Engineers.

Darrell, H. (2016). Scanning Electron Microscopy - Cathodoluminescence (SEM-CL). Retrieved from https://serc.carleton.edu/research_education/geochemsheets/semcl.html

DeSilva, N. R. (1999). Sedimentary basins and petroleum systems offshore Newfoundland and Labrador. *Geological Society, London, Petroleum Geology Conference Series*, *5*(1), 501–515. https://doi.org/10.1144/0050501

Dixon, S. A., Summers, D. M., & Surdam, R. C. (1989). Diagenesis and preservation of porosity in Norphlet Formation (Upper Jurassic), southern Alabama. *American Association of Petroleum Geologists Bulletin*, *73*(6), 707–728.

Driscoll, N. W., & Hogg, J. R. (1995). Stratigraphic response to basin formation: Jeanne d'Arc Basin, offshore Newfoundland. In J. . J. Lambiase (Ed.), *Hydrocarbon Habitat in Rift Basins* (Vol. 80, pp. 145–163). London, United Kingdom: Geological Society. https://doi.org/10.1144/GSL.SP.1995.080.01.07

Emery, D., Smalley, P. C., & Oxtoby, N. H. (1993). Synchronous oil migration and cementation in sandstone reservoirs demonstrated by quantitative description of diagenesis. *Philosophical Transactions of the Royal Society of London. Series A: Physical and Engineering Sciences*, *344*, 115–125. https://doi.org/10.1098/rsta.1993.0080

Enachescu, M. E. (1987). Tectonic and structural framework of the northeast Newfoundland continental margin. In C. Beaumont & A. J. Tankard (Eds.), *Sedimentary Basins and Basin-Forming Mechanisms* (Vol. 12, pp. 117–146). Canadian Society of Petroleum Geologists.

Evans, J., Hogg, A. J. C., Hopkins, M. S., & Howarth, R. J. (1994). Quantification of quartz cements using combined SEM, CL, and image analysis. *Journal of Sedimentary Research Section A*, *64*(2), 334–338. https://doi.org/10.1306/D4267D93-2B26-11D7-8648000102C1865D

ExxonMobil Canada. (2011). *Hebron project Development plan*. St John's. Retrieved from https://www.cnlopb.ca/information/development/

Folk, R. L. (1980). Petrology of sedimentary rocks. *Hemphll Publishing Company, Austin*, 170. https://doi.org/10.1017/CBO9781107415324.004

Gluyas, J. G., Robinson, A. G., Emery, D., Grant, S. M., & Oxtoby, N. H. (1993). The link between petroleum emplacement and sandstone cementation. *Geological Society, London, Petroleum Geology Conference Series*, *4*(1), 1395–1402. https://doi.org/10.1144/0041395

Gu, Y. (2003). Automated scanning electron microscope based mineral liberation analysis. *Journal of Minerals and Materials Characterization and Engineering*, *2*(1), 33–41. Retrieved from http://www.scirp.org/journal/PaperDownload.aspx?FileName=JMMCE20030100003_64231986.pdf&paperID=20244

Magoon, L. B., Hudson, T. L., & Peters, K. E. (2005). Egret-Hibernia(!), a significant petroleum system, northern Grand Banks area, offshore eastern Canada. *AAPG Bulletin*, *89*(9), 1203–1237. https://doi.org/10.1306/05040504115

Marchand, A. M. E., Haszeldine, R. S., Macaulay, C. I., Swennen, R., & Fallick, A. E. (2002). Quartz cementation inhibited by crestal oil charge: Miller deep water sandstone, UK North Sea. *Clay Minerals*, *35*(01), 201–210. https://doi.org/10.1180/000985500546585

Marchand, A. M. E., Haszeldine, R. S., Smalley, P. C., Macaulay, C. I., & Fallick, A. E. (2001). Evidence for reduced quartz-cementation rates in oil-filled sandstones. *Geology*, *29*(10), 915–918. https://doi.org/10.1130/0091-7613(2001)029<0915:EFRQCR>2.0.CO;2

Marchand, A. M. E., Smalley, P. C., Haszeldine, R. S., & Fallick, A. E. (2002). Note on the importance of hydrocarbon fill for reservoir quality prediction in sandstones. *AAPG Bulletin*, *86*(9), 1561–1571.

McAlpine, K. D. (1990). Mesozoic stratigraphy, sedimentary evolution, and petroleum potential of the Jeanne d'Arc Basin, Grand Banks of Newfoundland. *Geological Survey of Canada*, *89–17*, 50. https://doi.org/-

Mcbride, E. F. (1963). A Classification of Common Sandstones. *SEPM Journal of Sedimentary Research*, *33*(3), 664–669. https://doi.org/10.1306/74d70ee8-2b21-11d7-8648000102c1865d

Mcbride, E. F. (1989). Quartz Cement in Sandstones : A Review. *Earth-Science Reviews*, *26*, 69–112.

Midtbø, R. E. A., Rykkje, J. M., & Ramm, M. (2000). Deep burial diagenesis and reservoir quality along the eastern flank of the Viking Graben. Evidence for illitization and quartz cementation after hydrocarbon emplacement. *Clay Minerals*, *35*(01), 227–237. https://doi.org/10.1180/000985500546602

Molenaar, N., Cyziene, J., Sliaupa, S., & Craven, J. (2008). Lack of inhibiting effect of oil emplacement on quartz cementation: Evidence from Cambrian reservoir sandstones, Paleozoic Baltic Basin. *Bulletin of the Geological Society of America*, *120*(9–10), 1280–1295. https://doi.org/10.1130/B25979.1

MUN CREAIT. (2012). SEM - MLA. Retrieved December 1, 2017, from https://www.mun.ca/research/resources/creait/physical-sci/maf/sem

Nanakoudis, A. (2018). What is SEM? Scanning electron microscope technology explained. Retrieved from https://blog.phenom-world.com/what-is-sem

Nicoud, B. D. (2000). *Hebron D-94 Special Core Analysis - Internal Report*. (R. ExxonMobil Upstream, Ed.). Houston, Texas.

Pagel, M., Barbin, V., Blanc, P., & Ohnenstetter, D. (2000). *Cathodoluminescence in geosciences*. Springer Berlin Heidelberg.

Petro-Canada, Chevron-Canada, resources L., Mobil Oil, C., & Hydro, N. (1999). *Hebron D-94 Well history Report*. Newfoundland, Canada.

Pettijohn, F. J., Potter, P. E., & Siever, R. (1987). *Sand and Sandstone* (2nd ed.). New York: Springer-Verlag.

Saigal, G. C., Bjørlykke, K., & Larter, S. (1992). The effects of oil emplacement on diagenetic processes - examples from the Fulmar Reservoir sandstones, central North Sea. *American Association of Petroleum Geologists Bulletin*, *76*(7), 1024–1033.

Schindelin, J., Arganda-Carreras, I., Frise, E., Kaynig, V., Longair, M., Pietzsch, T., … Cardona, A. (2012). Fiji: an open-source platform for biological-image analysis. *Nature Methods*, *9*, 676–682. Retrieved from https://doi.org/10.1038/nmeth.2019

Shimeld, J. W., Altheim, B. K., MacRae, R. A., Grist, A. M., & Moir, P. N. (2001). Paleotemperature estimates. In J. W. Shimeld & P. . Moir (Eds.), *Heavy Oil Accumulations in the Jeanne d'Arc Basin: A Case Study in the Hebron, Ben Nevis, and West Ben Nevis Oil Fields* (OPen file, pp. 44–50). Geological Survey of Canada.

Shimeld, J. W., MacRae, R. A., Moir, P. N., Fowler, M. G., & Stasiuk, L. D. (2005). Heavy oil in the central Jeanne d'Arc Basin and implications for exploration risk. In R. N. Hiscott & A. Pulham (Eds.), *Petroleum Resources and reservoirs of the grand banks, Eastern Canadian Margin* (43rd ed., pp. 95–109). Geological association of Canada.

Sinclair, I. K., McAlpine, K. D., Sherwin, D. ., McMillan, N. J., Taylor, G. C., Best, M. E., … Procter, R. M. (1992). *Petroleum resources of the Jeanne d'Arc basin and environs, Grand Banks, Newfoundland* (92nd–8th ed.). Geological Survey of Canada.

Stasiuk, L. D. (2001). Organic Petrology and Fluid Inclusions. In J. W. Shimeld & P. . Moir (Eds.), *Heavy Oil Accumulations in the Jeanne d'Arc Basin: A Case Study in the Hebron, Ben Nevis, and West Ben Nevis Oil Fields* (Open File, pp. 24–26). Geological Survey of Canada.

Sylvester, P. J. (2012). Use of the Mineral Liberation Analyzer (MLA) for Mineralogical Studies of Sediments and Sedimentary Rocks. *Mineralogical Association of Canada*, (42), 1–16.

Thomeer, J. H. M., & Murphy, D. P. (2000). Capillarity in rocks. Shell/OGCI PetroSkills.

Ulmer-Scholle, D., Scholle, P., Schieber, J., & Raine, R. J. (2014). *A Color Guide to the Petrography of Sandstones, Siltstones, Shales and Associated Rocks*. *Memoir 109*. The American Association of Petroleum Geologists. https://doi.org/10.1306/13521909m1093637

Walderhaug, O. (1990). A fluid inclusion study of Quartz-cemented sandstones from offshore Mid-Norway - Possible evidence for continued quartz cementation during oil emplacement. *Journal of Sedimentary Petrology*, *60*(2), 203–210.

Walderhaug, O. (1996). Kinetic Modeling of Quartz Cementation and Porosity Loss in Deeply Buried Sandstone Reservoirs. *AAPG Bulletin*, *80*(5), 731–745. Retrieved from

https://www.academia.edu/19220564/Kinetic_modelling_of_quartz_cementation_and_porosity_loss_in_deeplyburied_sandstone_reservoirs

Worden, R. H., Bukar, M., & Shell, P. (2018). The effect of oil emplacement on quartz cementation in a deeply buried sandstone reservoir. *AAPG Bulletin*, *102*(1), 49–75. https://doi.org/10.1306/02071716001

Worden, R. H., & Burley, S. D. (2003). *Sandstone Diagenesis : The Evolution of Sand to Sandstone*. (S. D. Burley & R. H. Worden, Eds.). International Association of Sedimentologists. https://doi.org/10.1002/9781444304459.ch

Worden, R. H., Oxtoby, N. H., & Smalley, P. C. (1998). Can oil emplacement prevent quartz cementation in sandstones? *Petroleum Geoscience*, *4*(2), 129–137. https://doi.org/10.1144/petgeo.4.2.129

Zhou, W., Apkarian, R., Wang, Z. L., & Joy, D. (2007). Fundamentals of Scanning Electron Microscopy (SEM). In W. Zhou & Z. L. Wang (Eds.), *Scanning Microscopy for Nanotechnology: Techniques and Applications* (pp. 1–40). New York, NY: Springer New York. https://doi.org/10.1007/978-0-387-39620-0_1

# CHAPTER 3. AN EXPERIMENTAL AND DIGITAL INVESTIGATION INTO THE IMPACT OF DIAGENESIS ABOVE AND BELOW THE OIL-WATER CONTACT

Francis Mujica[1], Lesley A. James[1], Carl F. Berg[2], Derek Wilton[1], and Salem Akarri[2]

[1] Memorial University of Newfoundland, St John's. NL, Canada.
[2] Norwegian University of Science and Technology, Trondheim, Norway.

## 3.1 Abstract

We have investigated core samples from the Ben Nevis Formation in the Hebron Field, offshore Newfoundland, Canada. This field has a short transition zone, and a clearly identified oil-water contact (OWC). Through the analysis of Scanning Electron Microscope (SEM) and Cathodoluminescence (CL) images of thin sections from samples close to the OWC, differences in diagenesis were identified above and below the OWC. In particular, more quartz cementation was observed in the water zone. This observation is in agreement with the "oil retard diagenesis" theory widely discussed in the literature. The purpose of this project was to investigate how the observed differences in diagenesis affect the pore structure through experimental and digital investigation of transport properties that are dependent on the pure structure. We have evaluated the core samples' pore throat distribution through mercury injection capillary pressure (MICP) experiments. Further, we have conducted μ-CT imaging of the core samples. On the segmented μ-CT images, we have simulated mercury injection by a quasi-static morphological method, electrical conductivity by solving the Laplace equation, and single-phase flow by solving the Stokes equation. Both, experimental and digital rock analyses (DRA) were performed on core

samples distributed across the oil and water zones. Our results suggest that despite the differences in quartz overgrowth above (<3 %) and below ( <6%) the OWC the pore structure has not been significantly changed. This indicates that the diagenetic differences observed in the rocks do not substantially affect the pore structure and flow properties. We will discuss the experimental and digital methods and why the diagenetic differences apparently have only a small influence on pore structure and transport.

## 3.2 Introduction

The Hebron Field offshore Newfoundland Canada started production in November 2017 and is Canada's newest offshore field. A very distinctive oil-water contact (OWC) was cored in the D-94 delineation well. Similar lithology and textural characteristics on both sides of this abrupt contact provide an excellent opportunity to evaluate possible differences caused by the oil emplacement, and how such differences affect the pore structure and transport properties.

We have previously conducted scanning electron microscopy (SEM) and cathodoluminescence (CL) analyses on thin sections of rock samples, revealing that quartz overgrowth is more abundant in rock samples located below the oil-water contact (Mujica, James, Berg, & Wilton, n.d.). Results indicated that the diagenetic processes are retarded by the substitution of water for oil in the porous medium.

The cementation process has been found to play an essential role in preserving or reducing porosity and permeability (Pettijohn et al., 1987). Several efforts have been made to examine the relationship between porosity and quartz cementation in the presence of oil

and water. Studies have mostly been carried out using laboratory experiments and well log data (Barclay & Worden, 2000; Dixon et al., 1989; Emery et al., 1993; Walderhaug et al., 2000) comparing water-bearing and oil-bearing rocks.

In this work, we combined laboratory experiments and digital rock analysis (DRA) to investigate the impact of differences in quartz cementation on the pore structure. We calculated permeability, electrical conductance, and quasi-static displacement (mercury intrusion). All of these rock properties are assumed to be dependent on pore structure only, hence differences in the calculated rock properties would imply differences in the pore structure.

The effect of cementation on transport properties has previously been investigated using digital models of sandstone. Berg (2014) used models of Fontainebleau sandstone, with the exact grain packing and different degrees of quartz cementation to achieve intergranular porosity variation between 8 and 26% to evaluate the effect of cementation on the electrical conductance based on pore structure descriptors such as characteristic length, tortuosity, and constriction factor. Whereas Berg (2014) digitally varied the quartz overgrowth to determine the corresponding changes, we investigated the pore structure by comparing actual core samples from above and below the OWC.

The electrical conductance is the capacity of the rock to transmit electrical current. The relation between the conductance of the electrolyte filling the rock and the conductance of the rock is giving the formation factor. Assuming that the electrical current is conducted by the pore fluids while the rock is considered a highly insulating material, then the formation factor is directly related to the porosity, and pore structure (C. F. Berg, 2012). Permeability

indicates the ability of the media to allow fluid flow. It is a material property directly affected by pore structure and pore size (C. F. Berg, 2014). The results of mercury injection are related to the pore throat size distribution. It is a standard method used to determine up to five orders of magnitude in pore throat sizes, ranging from the nano-scale to the micro-scale (0.003 μm to 360μm) (Webb, 2001). In the digital rock analysis, the minimum pore size that can be reached is controlled by the image resolution acquired by the μ-CT scanner. In our work the image resolution was 1.9 μm. Since digital and experimental methods offer advantages but also limitations, the combination of both helps to improve the confidence of the investigated properties.

In this work, the comparison of the pore throat size distribution from MICP experiments and DRA was used as a quality control of the digital pore structure before numerical simulations. Sengupta, Kittridge, & Blangy (2017) combined traditional laboratory measurements with DRA to analyse the pore system, elastic and transport properties (permeability and electrical conductivity) in sandstones of different grain size and sorting. Similarly, Kalam (2012) compared DRA and laboratory measurements of electrical and elastic properties, absolute permeability, and saturation dependant properties in carbonate reservoir rocks. Digital rock physics was applied on Fontainebleau sandstone, Berea sandstone, carbonate rocks and packed bead models to compute electrical resistivity, elastic moduli and absolute permeability. All the properties calculated were reported to be within the ranges obtained from the laboratory measurements (Andra et al., 2013). Unlike the previous studies mentioned, we combine experimental measurements and DRA to investigate the effect of diagenetic differences of quartz overgrowth on the flow properties

above and below the OWC on the imaged and segmented 3D representation of the pore morphology.

Understanding the diagenetic impact of the oil presence on the flow properties in the water and oil-bearing zones can help to optimise the design of secondary and enhanced oil recovery (EOR) methods. Additionally, to the best knowledge of the authors, there is no record of DRA publications for the Ben Nevis Formation, Hebron Field, which provides potential industrial importance to this research.

## 3.3 Study Area

The Hebron Field is located 340 km southeast of St John's, offshore Newfoundland and Labrador in eastern Canada. Hebron is surrounded by the prolific Hibernia, Terra Nova and White Rose fields (Figure 20).

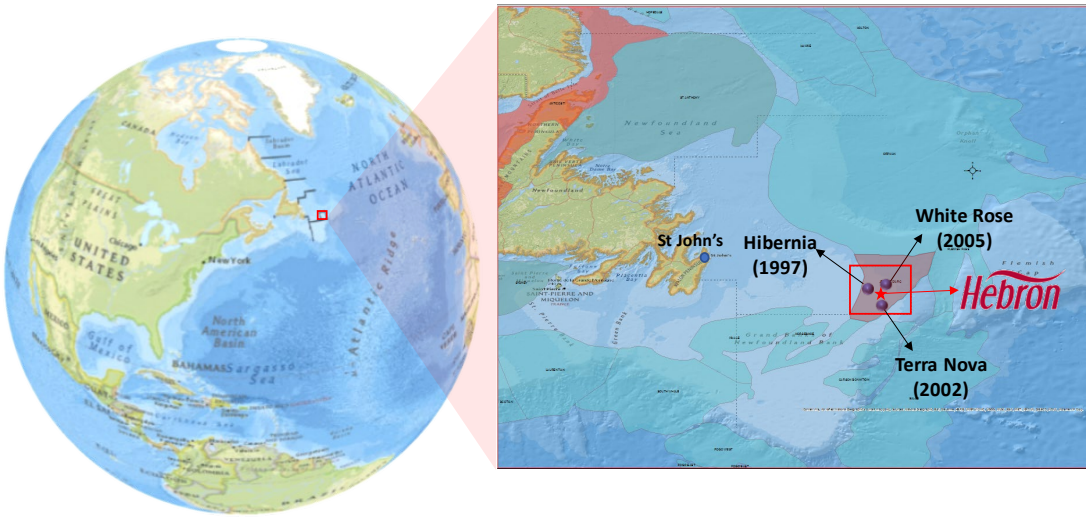


*Figure 20 Hebron Field location map, an offshore area in eastern Canada. Image to the left represents the relative location on the earth globe. The right provides a zoomed-in image of the specific Hebron Field location*

Geologically, the Hebron Field is located in the Jeanne d'Arc Basin. The Hebron-Ben Nevis complex comprises five different pools divided into three formations, i.e. Ben Nevis, Hibernia, and Jeanne d'Arc formations (Figure 21). Pool 1 is considered the main reservoir, containing around 80% of the total recoverable oil of the Hebron project (ExxonMobil Canada, 2011). Our research is focused on the Ben Nevis Formation of the Hebron Field located at 1.8 km (True Vertical Depth sub-sea - TVDSS) with temperature ranging between 50 and 70 °C, and pressures from 2600 to 2750 psi (180 to 190 bars).

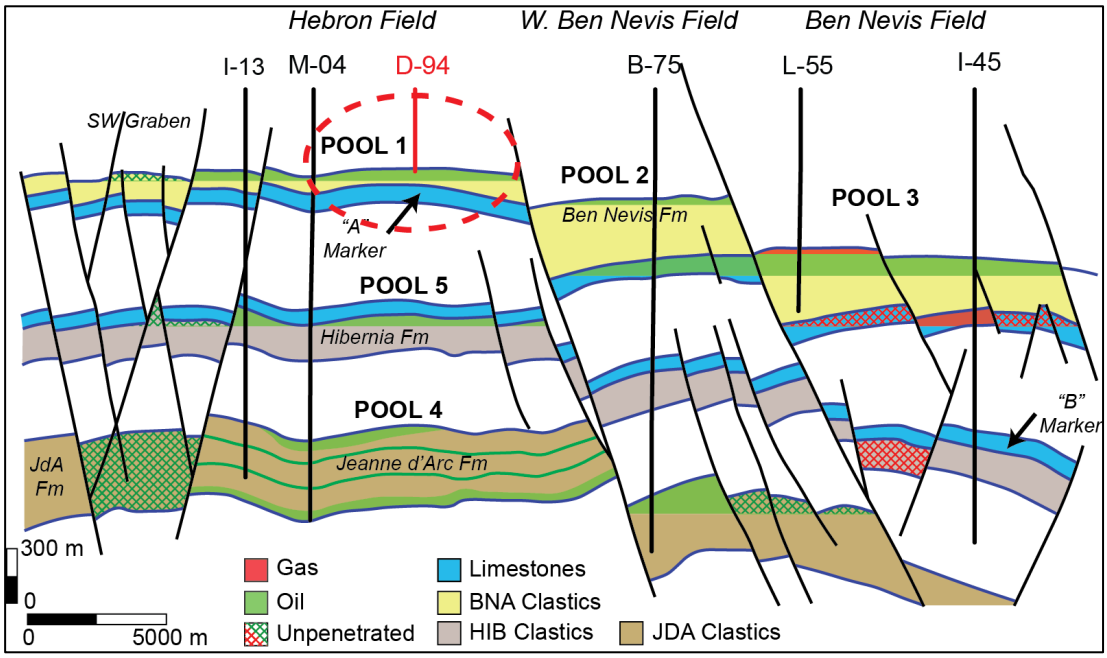


*Figure 21 Hebron Field schematic section. The red dotted ellipse shows the studied reservoir. Adapted from Cornaglia (2018)*

## 3.4 Methodology

The samples used in this work were selected from above and below the OWC in the Ben Nevis Formation. We experimentally evaluated the pore structure of core samples (SP-7A, SP-4A, SP-1A, SP-1B, SP-3B, SP-5B) from which four were also investigated digitally (SP-7A, SP-4A, SP-3B, SP-5B) (Figure 22). All the samples examined correspond to clean,

poorly cemented, and loosely consolidated sandstone. Sorting can be described from moderate to well sorted of fine to very fine grains. The rock framework is by far dominated by 80-90% quartz grains (Mujica et al., n.d.). During the sampling points definition, we integrated macroscopic characteristics from direct core observation, well log response, and core lithological description. Sample SP-6A was not included in this work since the sample corresponds to different facies of very tight calcite-cemented sections with strong HCl reaction and notable increase in the resistivity and density logs.

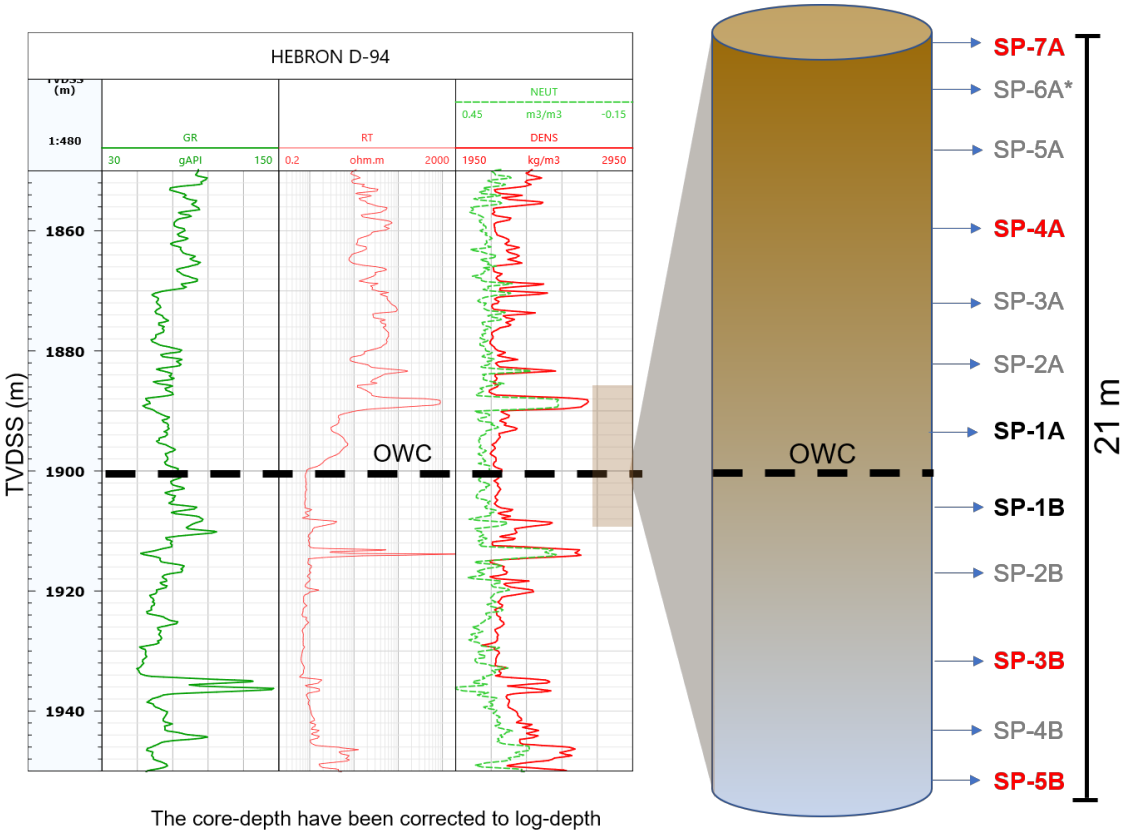


*Figure 22 Sampling points schematic location. Samples highlighted in red were used for both, the experimental and digital investigation. The * represents the carbonate cemented sample*

We physically carried out mercury injection capillary pressure (MICP) experiments and compared it to a simulated MICP virtual test virtually from high-resolution µ-CT images used to construct a digital rock. Having compared the physical and digital MICP

measurements, the "virtual laboratory" was used to simulate the electrical conductivity and absolute permeability (Figure 23).

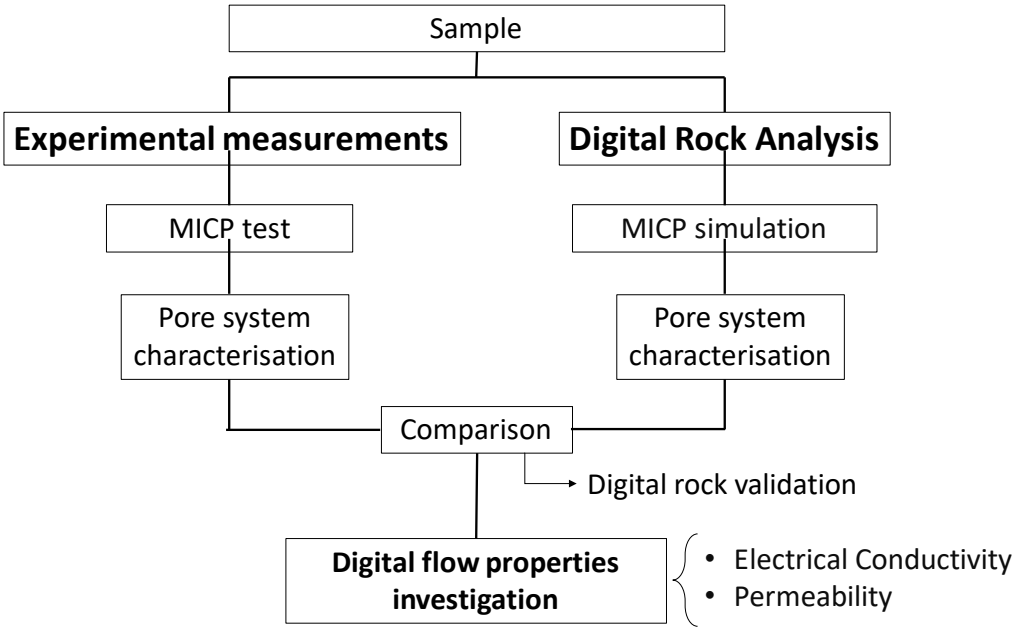


*Figure 23 General workflow diagram*

## 3.4.1 Physical rock measurements

Mercury is known to be a strong non-wetting to most solid materials and will not enter the pores by just capillary forces (Webb, 2001). The method is based on the principles governing non-wetting liquid penetrating small cylindrical pores. The Young-Laplace equation (Equation 8) for cylindrical pores is solved to estimate the pore throat diameter. The pressure-volume measurements provide excellent information to characterise the pore system (Thomeer, 1960; Washburn, 1921).

$$Pc = \frac{2\gamma \cos\theta}{r}$$

*Equation 8 Young-Laplace equation to link capillary pressure and pore size.*

The physical experiments were carried out using an AutoPore® IV 9500 (Figure 24A) in the Hibernia EOR Lab at Memorial University. The samples were first cleaned and prepared for the measurements. The first phase of the analysis was the low-pressure test (Figure 24B). During this test, the gases were evacuated (Figure 24C), and the mercury injected in the penetrometer, filling the space between the sample and the cell wall (Figure 24D) (Micromeritics Instrument, 2011).

When the low-pressure test was completed, the same penetrometer and the sample were then placed in the high-pressure chamber (Figure 24E) to measure the volume intruded at a maximum pressure of 2275 bars (33,000 psi). The mercury intrudes into the biggest pores first, and as the pressure increases, it will intrude subsequently smaller pores. The volume of mercury intruded in the sample's pores at different pressure is the same volume of mercury that decreases in the penetrometer stem (Micromeritics Instrument, 2011). Recognising that experimental errors come associated with experimental measurements, we ran a repetition sample in order to quantify the precision in the experimental results.

### 3.4.2 Digital Rock creation

Computed tomography (CT) is a useful non-destructive technique that has been successfully applied to investigate the internal structure of reservoir rocks from micro plugs of conventional core plugs. The images can then be used to produce 2D or 3D models of the pore system. The digital rock technology offers a link between geology, petrophysics, and reservoir simulations (C. F. Berg et al., 2017), whereas experimental measurements provide tools for calibration of the digital models.

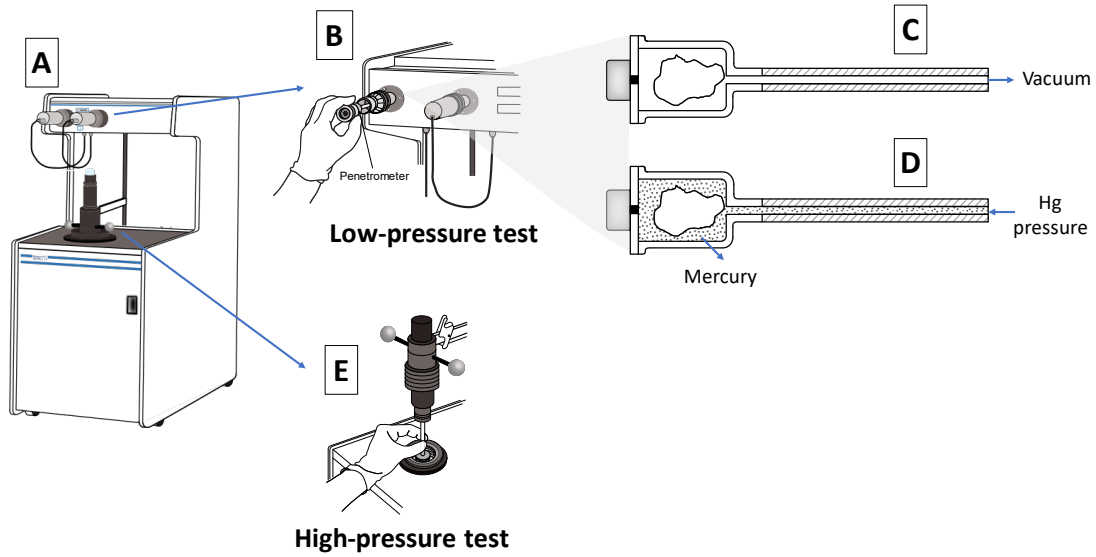


*Figure 24 MICP physical measurements. (A) AutoPore® IV 9500 equipment. (B) Low-pressure test. (C) gases evacuation and the mercury injection in the penetrometer during the low-pressure test. (d) High-pressure test. Adapted from Micromeritics Instrument (2011)*

In this work, 3D numerical simulations were performed on sub-volumes acquired from high-resolution microtomography data. There were three steps applied in this process, namely image acquisition, reconstruction, and processing.

The images were obtained using the HeliScan FEI µ-CT under dry conditions. In the µ-CT, the images are acquired by measuring the attenuation of the X-ray between the source and receptor to obtain a projection image. In our scanner, the object rotates around its axis, while both the source and receptor are static (Sasov, 1986). 1800 projected images are acquired at the same depth level at angles between 0° and 360° and then reconstructed to 2D slides. The resolution defines the minimum pore size that can be resolved, it was decided based on the MICP test, and further refined according to the validation process. Following the scanning processes, the images were reconstructed, segmented, and the pore structure was extracted (Figure 25).

Image processing was performed using Fiji - ImageJ (Rueden et al., 2017; Schindelin et al., 2012). The original image was cropped into a rectangle at the centre of the samples, avoiding the edges and discontinuities. The final cropped volume was filtered to remove noise from the original image using a non-local means denoising filter (Buades, Bartomeu, & Morel, 2011; Darbon, Cunha, Chan, Osher, & Jensen, 2008), and then segmented. For the segmentation, we used a grayscale thresholding method. We also tested the Trainable Weka Segmentation (TWS) (Arganda-Carreras et al., 2017), training an algorithm to classify grains and pores. Employing TWS yielded good results; however, the improvements were not considered sufficient to justify the significantly longer processing time. The uncertainty in the segmentation was mainly associated with the grain-pore interfaces due to the intensity-transition between the two phases (Sengupta et al., 2017).

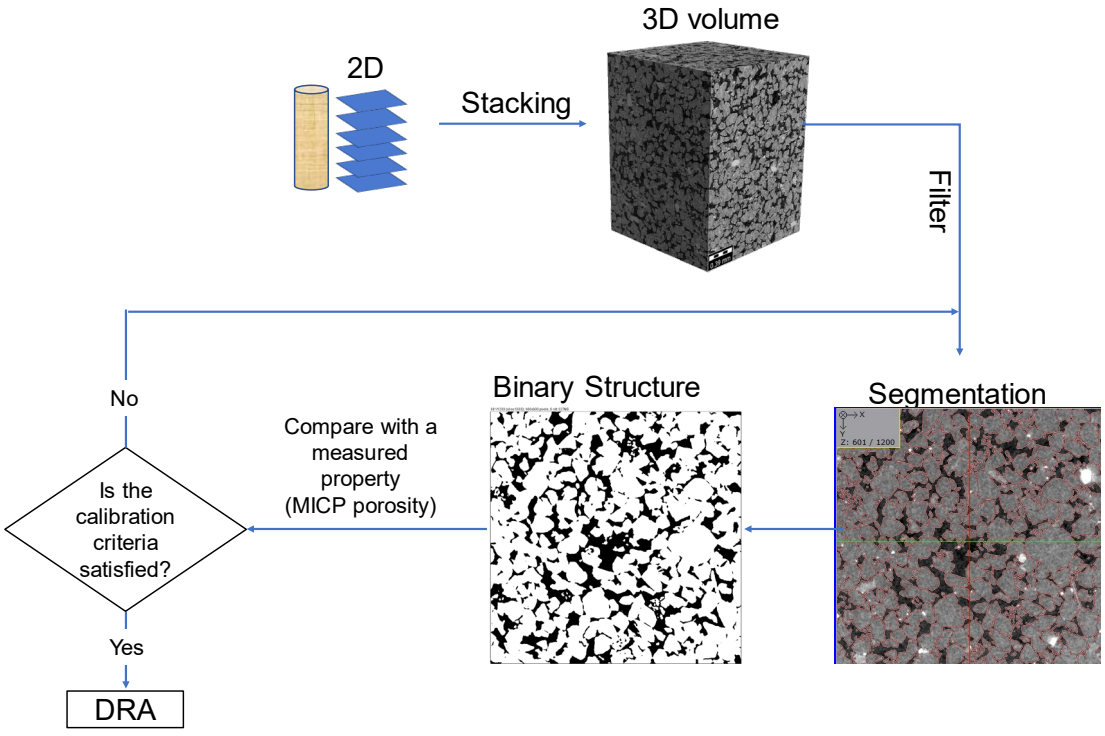


*Figure 25 Digital rock creation process*

## 3.4.3 Digital Rock simulations

### *3.4.3.1 Mercury Injection*

During drainage displacement, the invading phase, in our case mercury, displaces the defending phase (e.g. air). Like the MICP principle, the Young- Laplace equation (Equation 8) is solved to characterise the pore system and obtained the pore size distribution.

The quasi-static morphological approach has successfully simulated drainage processes (S. Berg et al., 2016a; Hilpert & Miller, 2001; Hussain et al., 2014). The imbibition process is not well described using the same approach (S. Berg et al., 2016b; Mason & Morrow, 2013). This is typically attributed to local pore-scale fluid disconnection caused by snap-off processes (Schluter et al., 2016). For the digital investigation of the pore structure, we performed numerical computations directly on the extracted 3D volume instead of idealised pore network models. The primary drainage mercury injection simulation was performed using GeoDict® from Math2Market[1]. For a given pressure, the method calculates the distribution of both, the wetting and the non-wetting phase. It assumes that gravity is negligible, the material is homogeneous, and there are only two phases considered in the system (Hilpert & Miller, 2001; Jurgen, Wiegmann, Westerteiger, Planas, & Linden, 2017). The simulated mercury injection curve was then compared to the experimental measurements to make sure that we captured the main features of the 3D pore structure to describe the transport properties. The error in the simulated pore size distribution is directly related to the size of a single pixel.

[1] Math2Market web site: https://www.math2market.com/

*3.4.3.2 Electrical conductivity*

The effective conductivity is obtained from the ratio of the electrical current to the potential drop in one-unit length, and it is used to calculate the formation factor. It is assumed that the electrical current is conducted by the pore fluids, while the rock is considered a highly insulating material. We estimated the electrical conductivity by solving the Laplace equation in the pore space using a finite difference method for steady-state conduction. The rock volume used for the numerical computation was reduced to reduce our simulations times. The formation factor can be then related to porosity through the Archie law (Equation 9). As the only input for our formation factor calculation is the pore structure, the calculated formation factor is a property of the pore structure only.

To verify the values estimated during the digital rock computations, we plotted our results against the values resulting from different empirical equations: Equation 9 from Archie (1942), and Equation 10 from Perez-Rosales (1982). We varied the cementation (m) and tortuosity (a) factors in (Equation 9). The values used were *m*=1.73 and *a*= 1.13 (Timur, Hemkins, & Worthington, 1972); and *m*=2.15 and *a*= 0.62 (Winsauer, Shearin, Masson, & Williams, 1952).

$$\frac{R_o}{R_w} = F = a\,\frac{1}{\varphi^m}$$

*Equation 9 General form of Archie's equation*

$$F = 1 + 1.03\,(\varphi^{-1.73} - 1)$$

*Equation 10 Porosity and formation factor relationship (Perez-Rosales, 1982)*

*3.4.3.3 Single Phase flow*

For slow flow the inertial forces are negligible compared with the viscous forces, giving a Reynold number close to zero. Slow flow is described by the Stokes' equation (Equation 11). Single-phase flow simulations were performed to estimate the rock permeability by solving the Stokes equation. We imposed Dirchlet boundary conditions by specifying pressures at the inlet and outlet. Relating the pressure drop to the throughput through, the Darcy equation (Equation 12) yields the permeability. The (absolute) permeability obtained is then a property of the pore structure only.

Both the flow velocity and absolute permeability numerical computations were performed using GeoDict® from Math2Market.

$$\nabla p - \mu \nabla^2 v = 0\,, \qquad \nabla . v = 0$$

*Equation 11 Stokes flow equation*

$$k = \frac{q\ \mu\ L}{\mathrm{A}\ \nabla p}$$

*Equation 12 Darcy's equation for laminar fluid flow*

Finally, we compared the results obtained from the samples above and below the OWC to evaluate the effect of the diagenetic differences on the pore structure, electrical conductivity, and absolute permeability.

## 3.5 Results and Discussion

During the scanning process, the image resolution has a significant impact on the quality and details obtained from the pore-scale and thus in the numerical computations (Sengupta et al., 2017). The images were acquired under dry conditions first at 5.2 μm per voxel of resolution, this resolution was decided based on the MICP results. However, when we tried

to reproduce the MICP measured in the lab, no satisfactory results were obtained. We then proceeded to scan the four control samples again, now using a resolution of 1,9 μm per voxel of resolution, which was good enough to reproduce the physical experiments and validate our pore morphology.

### 3.5.1 Porosity and pore structure

The porosity results are summarised in Table 1. The first column represents the name of the sample. The second column (resolved porosity) corresponds to the porosity of the sample which pore size is higher than 1.9μm (image resolution) obtained from the physical experiments; this porosity does not include the pore space of the pore size smaller than 1.9 μm. The third column represents the porosity obtained on the digital rock.

*Table 1 Experimental and digital porosity from the samples investigated*

| | **MICP** | | **DRA** |
|---|---|---|---|
| **Sample** | **Porosity** | **Resolved Porosity** | **Resolved Porosity** |
| SP-7A | 0.28 | 0.24 | 0.25 |
| SP-4A | 0.29 | 0.25 | 0.25 |
| SP-3B | 0.31 | 0.27 | 0.27 |
| SP-5B | 0.30 | 0.26 | 0.27 |

The pore throat size distribution was found to be similar on samples above and below OWC under the mercury injection test. Figure 26 represents the pore size distribution obtained from the MICP of the control samples. The majority of the pore size falls in the macropore class with pore throat diameter between 14 and 21 μm for the samples above and below.

There is not a notable trend in the pore throat size distribution responding to the quartz overgrowth. The pore throat size from the two samples above the OWC (SP-7A and SP-

4A) has the same main pore throat diameter observed in the sample SP-3B; however, the main pore throat diameter in the lowest sample (SP-5B) shows a slightly smaller size in the distribution curve even though the porosity is higher than the two samples above the OWC.

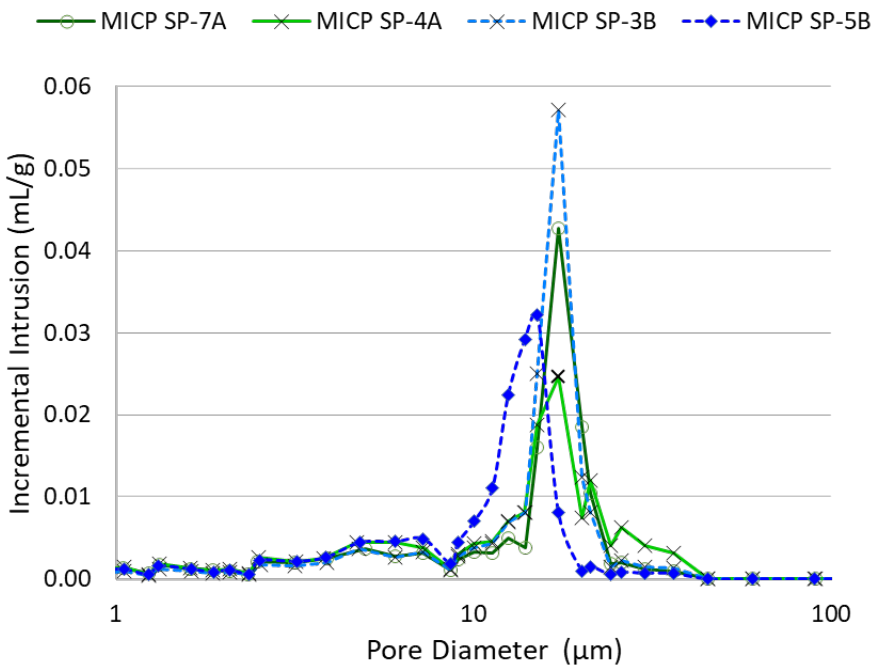


*Figure 26 Pore throat size distribution obtained from the MICP test in control samples above and below OWC*

Apparently, the quartz overgrowth does not have a notable impact on the pore throat size distribution when it is present in a small percentage in a system dominated by macropore throats. The general trend is to decrease in pore throat size when comparing the uppermost and the lowest samples; however, the variation is still not enough to observe a significant effect.

The pore system investigated by experimental MICP measurements was also examined using DRA by simulating the mercury injection. The resulting curves from both methods

were used to calibrate the digital rock. We used the log differential specific intrusion and the capillary pressure plots as a reference in the validation process (Figure 27).

The standard deviation of the pore volume from the MICP was estimated to be less than 0.003. The error associated with the computed porosity of consecutive values in the greyscale is around 0.005. The pore throat size distribution used for the calibration has an estimated error of 1.9 μm. The RSQ (Square of the Pearson correlation coefficient) between the MICP curve from physical measurements and the digital rock simulation was estimated to be 0.9 for all the samples. The good match obtained between both datasets, experimental and simulated, indicates that the main features of the pore structure were captured. Therefore, the segmented pore structure was considered representative for the core samples, and thus suitable for predictive numerical simulations.

### 3.5.2 Electrical conductivity

The results obtained from the numerical simulations are shown in Table 2. The formation factor values for the four control samples range from 10.8 to 13.3. The results obtained from our digital rock are in good agreement with the expected values (Figure 28). The tortuosity extracted from the formation factor simulations showed no significant variations above and below the OWC. The constriction factors, on the other hand, showed a trend to increase in the samples below the OWC, changing from 1.54 in the uppermost sample to 1.75 in the lowest one; however, the samples SP-4A and SP-3B showed the same constriction factor (1.55).

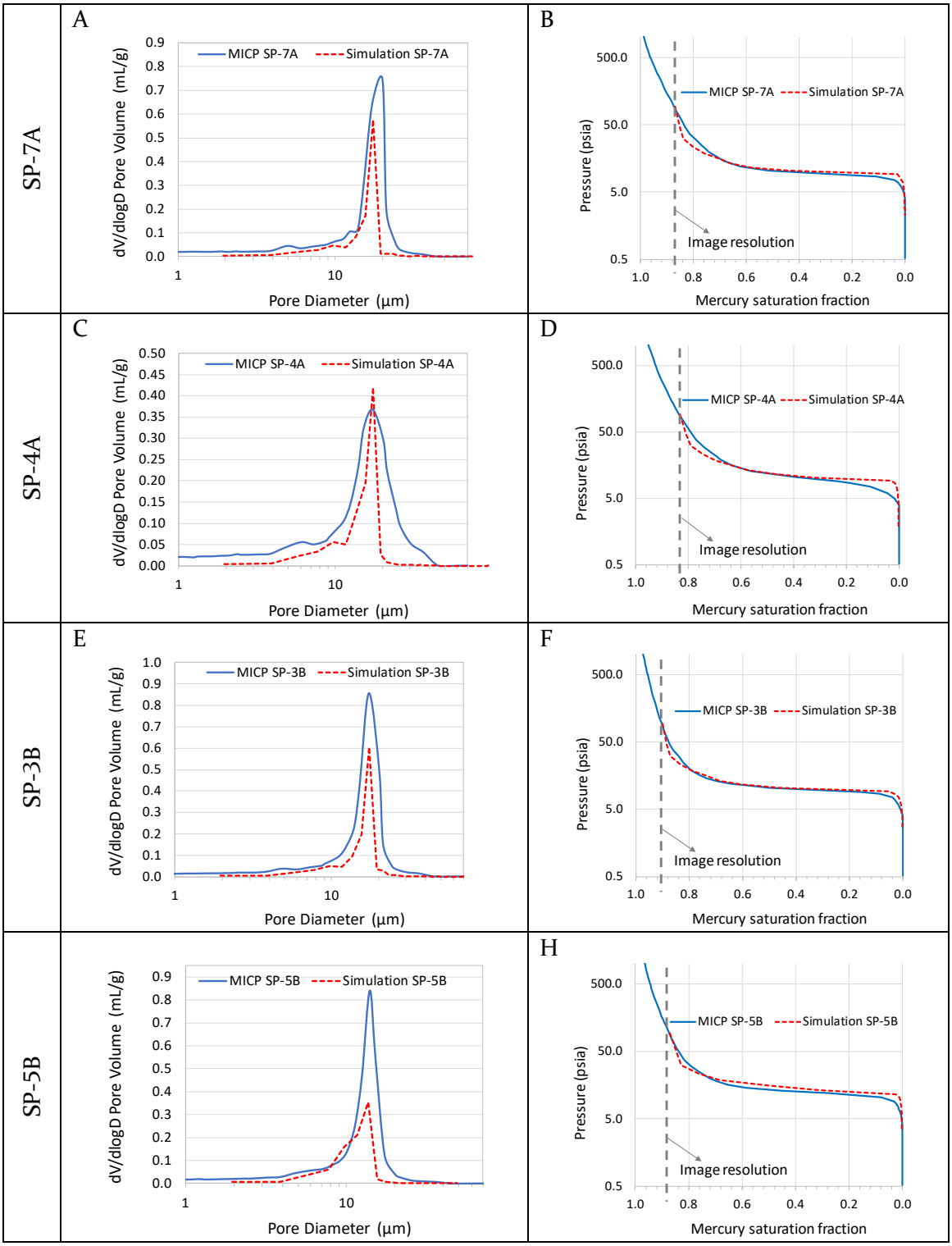


*Figure 27 Plots of MICP experimental (blue line) and simulated data (red dotted line). A, C, E and G show the log differential specific intrusion vs pore size plot. B, D, F and H show the capillary pressure vs mercury saturation fraction*

The quartz overgrowth differences do not appear to have a notable impact on the electrical conductivity, tortuosity and constriction factor; nevertheless, the variations observed are in harmony with the expected trend. If we compare the two endpoints, the formation factor tends to increase; even though the variation is considered not conclusive enough. The constriction factor is a pure pore structure measure. More quartz overgrowth should imply a higher constriction factor (C. F. Berg & Held, 2016). While the change in constriction factor is small, it is consistent with the presumed trend. Also, the slight change in tortuosity is also in accordance with the expected trend.

*Table 2 Formation factor results obtained from numerical simulations in the digital rock*

| Sample | Formation Factor | Tortuosity | Constriction factor |
|---|---|---|---|
| SP-7A | 10.9 | 0.76 | 1.54 |
| SP-4A | 11.5 | 0.76 | 1.55 |
| SP-3B | 10.8 | 0.76 | 1.55 |
| SP-5B | 13.3 | 0.75 | 1.75 |

### 3.5.3 Absolute permeability

For digital estimations of absolute permeability, it is necessary to compute the velocities and further calculate the permeability using Darcy's equation. The flow velocity in X, Y and Z direction estimated by numerically solving the Stokes equation within the digital pore space are in order of magnitude of $10^{-9}$ m/s. Figure 29 shows the flow velocities in the Z direction. The warmest colours represent the fastest flows with velocities around $300x10^{-9}$ (m/s), and the coldest colours represent the slowest fluid velocities in the digital rock.

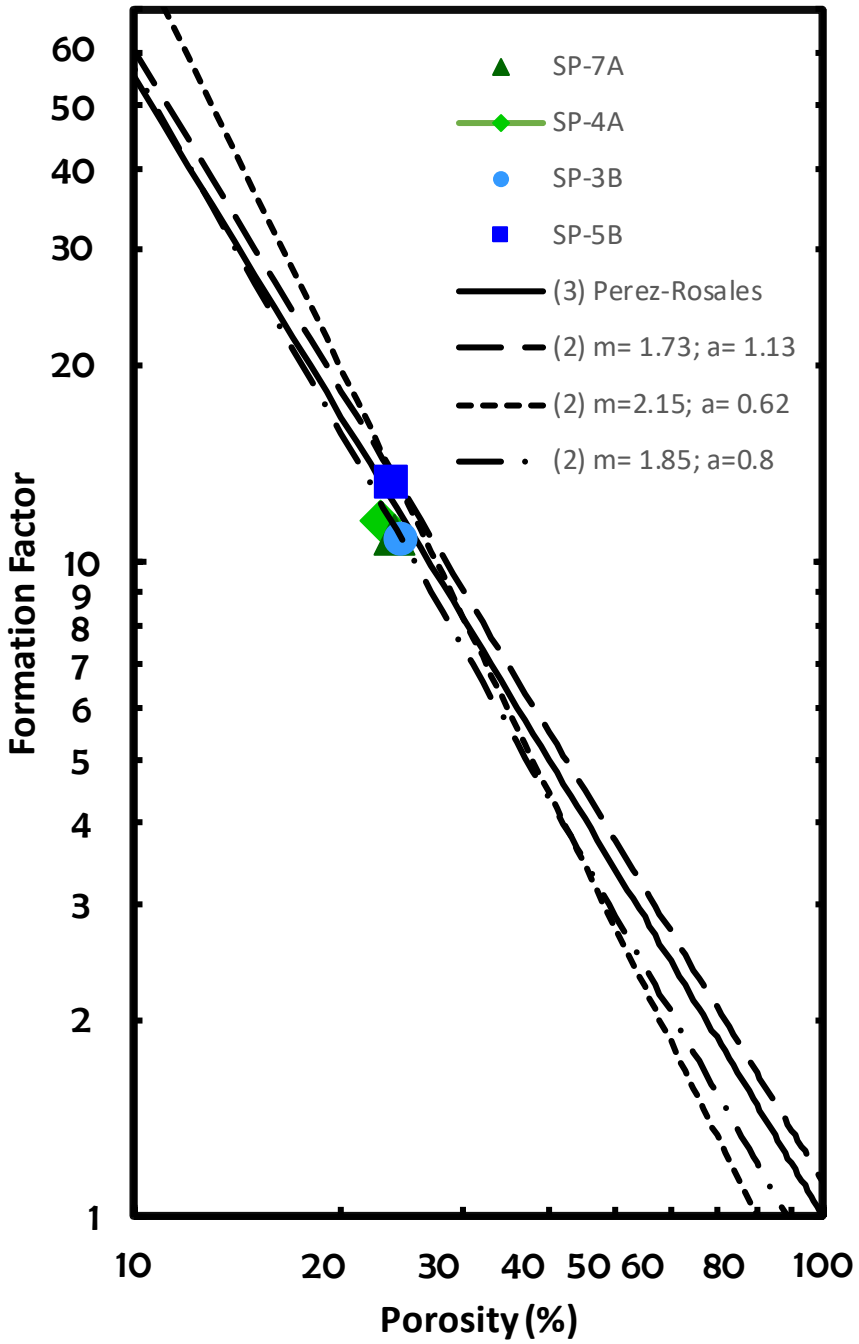


*Figure 28 Formation factor results compared with the relationship from different empirical equations*

The permeabilities obtained from the calculations are shown in Table 3. These permeability values were compared with previous core analysis carried out in four different wells where the Ben Nevis Formation was penetrated in the Hebron Asset (Figure 30). Three of these

wells are located in the Hebron Field, and one is located in the West Ben Nevis block. In the core porosity – air permeability general relationship (Figure 30), the blue squares correspond to the core analysis from Hebron D-94 well, and the grey areas represent the expected permeability for the porosity range of the samples used in this work. The absolute brine permeability from the USBM wettability test was reported as 1427 mD (Nicoud, 2000) showing good agreement to the simulated values.

The digital rock simulation does not show notable changes in permeability between the samples above and below the OWC. Even when a slight trend is observed to decrease the permeability in the water zone, the trend is not well defined, and no certain conclusions can be made.

### 3.5.4 Digital and experimental methods

There are several advantages and disadvantages related to each of these methods. Two main disadvantages are presented by the mercury injection method: 1- the method destroys the sample, and 2- the conversion necessary to correlate the results to a different fluids system. In the DRA, the main uncertainty is related to the image resolution and the segmentation process.

Since MICP requires little time during the experimental measurements and provides excellent information of the pore system, it presents an excellent opportunity for the digital rock calibration and further flow properties simulations. It seems that combining both methods, we can increase our confidence in the results and compensate for the main disadvantages presented from both techniques.

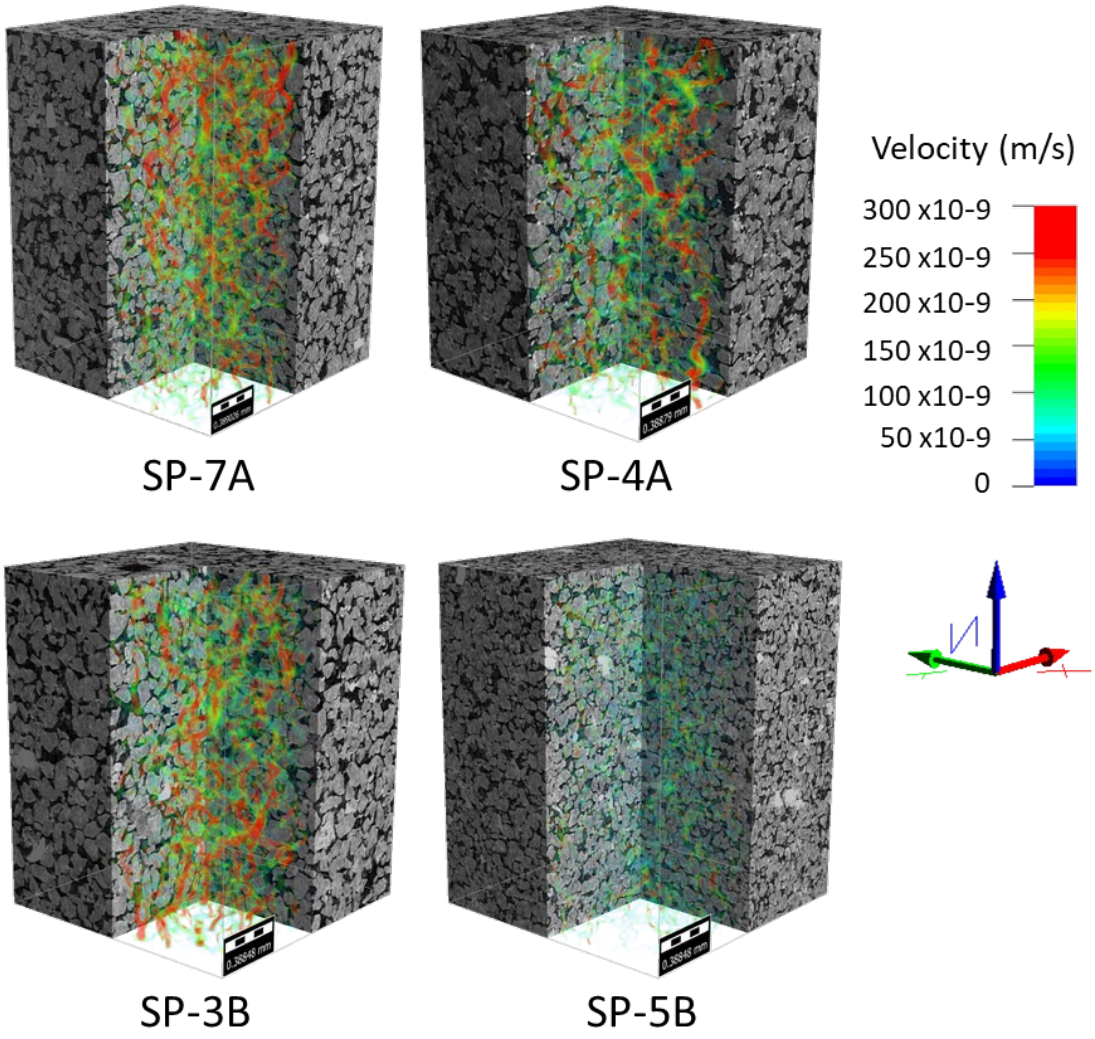


*Figure 29 Digital rock analysis. Average flow velocity in the Z direction*

*Table 3 Computed permeability in X, Y and Z directions*

| | **X-Permeability (mD)** | **Y-Permeability (mD)** | **Z-Permeability (mD)** |
|---|---|---|---|
| SP-7A | 1526 | 1515 | 1091 |
| SP-4A | 1415 | 1256 | 760 |
| SP-3B | 1734 | 1790 | 1114 |
| SP-5B | 941 | 925 | 514 |

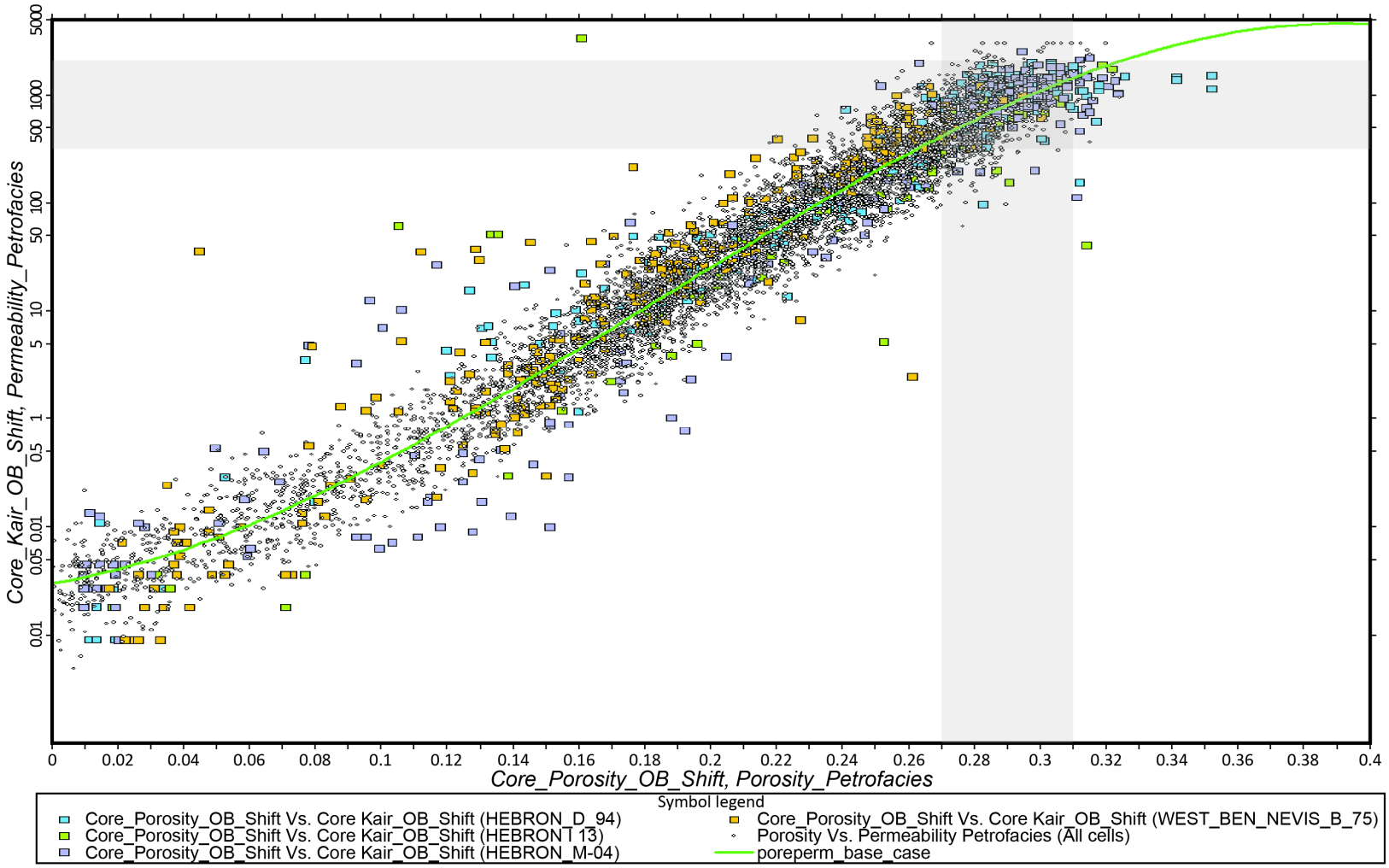


*Figure 30 Porosity and permeability relationship from core analysis in different wells, Ben Nevis Formation, Hebron Field from ExxonMobil Canada (2011)*

## 3.6 Conclusions

We have conducted experiments and simulated transport properties that depends solely on the pore structure. Based on our experimental and digital rock investigations, the diagenetic differences observed in quartz overgrowth for the samples above and below the OWC do not have a significant impact on the pore structure. However, the observed changes in pore structure descriptors such as constriction factor are in accordance with expected trends. This could indicate that the quartz overgrowth has not been developed enough to cause a significant reduction of the pores and/or pore throats to impact the flow properties.

The morphological quasi-static method was successfully used to validate our pore structure by simulating the mercury injection during primary drainage processes.

We successfully reproduced the main features of the physical rock in our digital representation. The computed properties fall within expected theoretical and experimental ranges.

The Ben Nevis reservoir at the Hebron Field has similar transport properties above and below the OWC which is translated in an excellent chance that the underlying aquifer could help with the reservoir pressure support. Furthermore, the water injection could be successfully performed from the water zone based on the similar flow properties on both sides.

Neither physical experiments nor DRA will provide an exact answer about the transport properties; however, by combining both techniques, it is possible to increase our confidence in the results. Once the digital rock model has been validated, it is possible to provide more

comprehensive combinations of properties to investigate in a reduced time. We strongly support the combination of both physical and digital techniques to optimise the reservoir characterisation process instead of replacing one for another.

## 3.7 Acknowledgements

We thank the Natural Sciences and Engineering Research Council of Canada (NSERC), Research and Development Corporation of Newfoundland and Labrador (RDC) (now TCII), Hibernia Management and development Company (HMDC), Chevron Canada Limited, and the Hibernia EOR Research group for technical and financial support. The Canada-Newfoundland and Labrador Offshore Petroleum Board (C-NLOPB) for providing the rock samples and Hebron Field information. PetriCore for providing the opportunity to use their equipment and facilities to carry out the μ-CT scans. PoreLab at NTNU for the technical support. Mitacs for providing funding to support the international research exchange. IHS Markit for providing the well-logs. The third author was supported by the Research Council of Norway through its Centres of Excellence funding scheme, project number 262644.

## 3.8 References

Andra, H., Combaret, N., Dvorkin, J., Glatt, E., Han, J., Kabel, M., … Zhan, X. (2013). Digital rock physics benchmarks — part II : Computing effective properties. *Computers & Geosciences Journal*, *50*, 33–43. https://doi.org/10.1016/j.cageo.2012.09.008

Archie, G. E. (1942). The Electrical Resistivity Log as an Aid in Determining Some Reservoir Characteristics. *Transactions of the AIME*, *146*(01), 54–62. https://doi.org/10.2118/942054-G

Arganda-Carreras, I., Kaynig, V., Rueden, C. T., Schindelin, J., Eliceiri, K. W., Cardona, A., & Sebastian Seung, H. (2017). Trainable Weka Segmentation: a machine learning tool for microscopy pixel classification. *Bioinformatics*, *33*(15), 2424–2426.

https://doi.org/10.1093/bioinformatics/btx180

Barclay, S. A., & Worden, R. H. (2000). Petrophysical and petrographical analysis of quartz cement volumes across oil–water contacts in the Magnus Field, northern North Sea. *Quartz Cementation in Sandstones*, *29*, 147–161.

Berg, C. F. (2012). Re-examining Archie ' s law : Conductance description by tortuosity and constriction. *Physical Review*, *86*(046314), 1–9. https://doi.org/10.1103/PhysRevE.86.046314

Berg, C. F. (2014). Permeability Description by Characteristic Length , Tortuosity , Constriction and Porosity. *Transp Porous Med*, *103*, 381–400. https://doi.org/10.1007/s11242-014-0307-6

Berg, C. F., & Held, R. (2016). Fundamental Transport Property Relations in Porous Media Incorporating Detailed Pore Structure Description. *Transport in Porous Media*, *112*(2), 467–487. https://doi.org/10.1007/s11242-016-0661-7

Berg, C. F., Lopez, O., & Berland, H. (2017). Industrial applications of digital rock technology. *Petroleum Science and Engineering*, 35. https://doi.org/10.1016/j.petrol.2017.06.074

Berg, S., Rücker, M., Ott, H., Georgiadis, A., Linde, H. Van Der, Enzmann, F., … Wiegmann, A. (2016a). Connected Pathway Relative Permeability from Pore-Scale Imaging of Imbibition. *Advances in Water Resources*, (2). https://doi.org/10.1016/j.advwatres.2016.01.010

Berg, S., Rücker, M., Ott, H., Georgiadis, A., Linde, H. Van Der, Enzmann, F., … Wiegmann, A. (2016b). Modelling of imbibition relative permeability by direct quasi-static approach. In *International Symposium of the Society of Core Analysts* (Vol. 007, pp. 1–12).

Buades, A., Bartomeu, C., & Morel, J.-M. (2011). Non-Local Means Denoising. *Image Processing On Line*, *1*. https://doi.org/10.5201/ipol.2011.bcm_nlm

Cornaglia, V. (2018). Geoscience Overview of the Hebron Field. In *Offshore Technology Conference*. Houston, Texas: Society of Petroleum Engineers.

Darbon, J., Cunha, A., Chan, T. F., Osher, S., & Jensen, G. J. (2008). Fast nonlocal filtering applied to electron cryomicroscopy. *Technology*, 1331–1334.

Dixon, S. A., Summers, D. M., & Surdam, R. C. (1989). Diagenesis and preservation of porosity in Norphlet Formation (Upper Jurassic), southern Alabama. *American Association of Petroleum Geologists Bulletin*, *73*(6), 707–728.

Emery, D., Smalley, P. C., & Oxtoby, N. H. (1993). Synchronous oil migration and cementation in sandstone reservoirs demonstrated by quantitative description of diagenesis. *Philosophical Transactions of the Royal Society of London. Series A: Physical and Engineering Sciences*, *344*, 115–125. https://doi.org/10.1098/rsta.1993.0080

ExxonMobil Canada. (2011). *Hebron project Development plan*. St John's. Retrieved from https://www.cnlopb.ca/information/development/

Hilpert, M., & Miller, C. T. (2001). Pore-morphology-based simulation of drainage in totally wetting porous media. *Advances in Water Resources*, *24*, 243–255.

Hussain, F., Pinczewski, W. V, Cinar, Y., Arns, J. Y., Arns, C. H., & Turner, M. L. (2014). Computation of Relative Permeability from Imaged Fluid Distributions at the Pore Scale. *Transp Porous Med*, (104), 91–107. https://doi.org/10.1007/s11242-014-0322-7

Jurgen, B., Wiegmann, A., Westerteiger, R., Planas, B., & Linden, S. (2017). SatuDict. Kaiserslautern, Germany: MATH2MARKET GMBH. Retrieved from www.geodict.com

Kalam, M. Z. (2012). Digital Rock Physics for Fast and Accurate Special Core Analysis in Carbonates. In J. S. Gomes (Ed.), *New Technologies in the Oil and Gas Industry*. InTechOpen. https://doi.org/10.5772/3216

Mason, G., & Morrow, N. R. (2013). Developments in spontaneous imbibition and possibilities for future work. *Journal of Petroleum Science and Engineering*, *110*, 268–293. https://doi.org/10.1016/j.petrol.2013.08.018

Math2Market. (n.d.). GeoDict. *Https://Www.Math2market.Com*. Retrieved from https://www.math2market.com/

Micromeritics Instrument. (2011). Autopore IV 9500 Operator's Manual.

Mujica, F., James, L. A., Berg, C. F., & Wilton, D. H. (n.d.). Fundamental understanding of how the presence of oil impacts diagenesis by investigating rock samples close to the Oil-Water contact (OWC). Manuscript in preparation. (to be published).

Nicoud, B. D. (2000). *Hebron D-94 Special Core Analysis - Internal Report*. (R. ExxonMobil Upstream, Ed.). Houston, Texas.

Perez-Rosales, C. (1982). On the Relationship Between Formation Resistivity Factor and Porosity. *Society of Petroleum Engineers Journal*, *22*(04), 531–536. https://doi.org/10.2118/10546-pa

Pettijohn, F. J., Potter, P. E., & Siever, R. (1987). *Sand and Sandstone* (2nd ed.). New York: Springer-Verlag.

Rueden, C. T., Schindelin, J., Hiner, M. C., DeZonia, B. E., Walter, A. E., Arena, E. T., & Eliceiri, K. W. (2017). ImageJ2: ImageJ for the next generation of scientific image data. *BMC Bioinformatics*, *18*(1), 529. https://doi.org/10.1186/s12859-017-1934-z

Sasov, A. Y. (1986). Microtomography I. Methods and equipment. *Journal of Microscopy*, *147*, 169–178. https://doi.org/10.1111/j.1365-2818.1987.tb02829.x

Schindelin, J., Arganda-Carreras, I., Frise, E., Kaynig, V., Longair, M., Pietzsch, T., …

Cardona, A. (2012). Fiji: an open-source platform for biological-image analysis. *Nature Methods*, *9*, 676–682. Retrieved from https://doi.org/10.1038/nmeth.2019

Schluter, S., Berg, S., Rucker, M., Armstrong, R. T., Vogel, H. ., Hilfer, R., & Wildenschild, D. (2016). Pore-scale displacement mechanisms as a source of hysteresis for two-phase flow in porous media. *Water Resources Research*, *52*, 2194–2205. https://doi.org/10.1002/2015WR018254

Sengupta, M., Kittridge, M. G., & Blangy, J.-P. (2017). Using digital rocks and simulations of pore-scale multiphysics to characterize a sandstone reservoir. *Interpretation of Lab Rock-Physics Data by Numerical Simulations*, *5*(1), 33–43. https://doi.org/10.1190/INT-2016-0068.1

Thomeer, J. H. M. (1960). Introduction of a Pore Geometrical Factor Defined by the Capillary Pressure Curve. *Journal of Petroleum Engineers*, *12*(03), 73–77. https://doi.org/https://doi.org/10.2118/1324-G

Timur, A., Hemkins, W. ., & Worthington, A. . (1972). Porosity and Pressure Dependence of Formation Resistivity Factor for Sandstones. In *Trans CWLS Fourth Formation Evaluation Symposium* (p. 30). Calgary: Society of Well Logging.

Walderhaug, O., Lander, R. ., Bjørkum, P. A., Oelkers, E. H., Bjørlykke, K., & Nadeau, P. H. (2000). Modelling quartz cementation and porosity in reservoir sandstones: examples from the Norwegian continental shelf. *Quartz Cementation in Sandstones*, *29*, 39–49.

Washburn, E. W. (1921). Note on a method of determining the distribution of pore sizes in a porous material. In *Natl. Acad. Sci.* (Vol. 7, pp. 115–116).

Webb, P. A. (2001, January). An Introduction To The Physical Characterization of Materials by Mercury Intrusion Porosimetry with Emphasis On Reduction And Presentation of Experimental Data. *Micromeritics Instrument Corp*, (01), 23. https://doi.org/10.1177/004057368303900411

Winsauer, W. ., Shearin, H. . J., Masson, P. H., & Williams, M. (1952). Resistivity of Brine-Saturated Sands in Relation to Pore Geometry. *AAPG Bulletin*, (36), 253–277.

# CHAPTER 4. SUMMARY

This research provided insight into the debate on whether pore water displacement by hydrocarbons can halt/retard or even stop the diagenetic chemical processes in reservoirs shallower than 2 km and temperature around 50 to 70 °C. The methodology applied involves the combination of SEM-MLA, SEM-CL, MICP, and DRA to compare the effect of diagenetic differences on samples located close to the OWC.

The Ben Nevis Formation in the Hebron Field exhibits a very distinctive OWC observed in core and well logs. The SEM-MLA analysis showed that samples from above and below the OWC where mineralogically and texturally very similar. These similarities were used to analyse the oil effect in the diagenetic process, particularly in quartz overgrowth. From the SEM-CL analysis, a clear trend was observed for the quartz overgrowth to be more abundant in the sample with higher water saturation, indicating differences in the diagenetic process.

Pore throat size distribution, pore structure descriptors, and electrical conductivity analysis were used to investigate the effect in transport properties caused by quartz overgrowth differences. Simulated transport properties that depend solely on the pore structure indicated that formation and constriction factors tend to increase while tortuosity tends to decrease. Even though the differences between the sample above and below the OWC are not conclusive enough, the observed changes are in harmony with the expected trend.

The reservoir rock has not reached or been long enough under conditions giving a high rate of quartz precipitation. Therefore, the amount of quartz cementation is not large enough to

cause a substantial impact on the pore structure and rock transport properties. Good reservoir quality above and below the OWC can enable the underlying aquifer to support the reservoir pressure during hydrocarbon production. It might also enable successful drainage of hydrocarbons by water injection into the water zone.

Instead of replacing one for another, the combination of both physical and digital techniques is strongly advised to optimise the reservoir characterisation process. In this research work, we successfully reproduced the main features of the physical rock in a digital representation. The results obtained from the digital rock simulations were validated against laboratory measurements and theoretical values. Having the digital rock calibrated opens the possibility to explore and compare additional reservoir properties and behaviour. We presented the first 3D rock volume from μ-CT scans and digital rock analysis (DRA) in the study area.

## 4.1 FUTURE WORK

The following ideas are recommended to better understand the oil presence impacts diagenesis and the resulting effect in the rock and transport properties

- Investigate fluid inclusion in the quartz cement to more accurately decide the time for oil migration into the Ben Nevis Formation, Hebron Field.
- Based on basin models, extend the present research to the Hibernia and Jeanne d'Arc formations in the Hebron Field. Both formations have experienced more burial, and higher temperature so one would expect the quartz cementation to have a bigger impact on the pore structure and transport properties.

- Carefully investigate and quantify the presence and type of grain coating materials for possible relationship with quartz cementation
- The calibrated digital rock model opens wide possible applications for better reservoir characterisation of the Ben Nevis Formation in the Hebron Field.

# REFERENCES


Amyx, J. W., Bass, D. M., & Whiting, R. L. (1960). *Petroleum Reservoir Engineering Physical Properties*. New York: McGraw-Hill Book Company. Retrieved from https://vdocuments.mx/amyx-petroleum-reservoir-engineering.html

Andra, H., Combaret, N., Dvorkin, J., Glatt, E., Han, J., Kabel, M., … Zhan, X. (2013). Digital rock physics benchmarks — part II : Computing effective properties. *Computers & Geosciences Journal*, *50*, 33–43. https://doi.org/10.1016/j.cageo.2012.09.008

Anovitz, L. M., & Cole, D. R. (2015). Characterization and Analysis of Porosity and Pore Structures. *Reviews in Mineralogy and Geochemistry*, *80*(1), 61–164. https://doi.org/10.2138/rmg.2015.80.04

Archie, G. E. (1942). The Electrical Resistivity Log as an Aid in Determining Some Reservoir Characteristics. *Transactions of the AIME*, *146*(01), 54–62. https://doi.org/10.2118/942054-G

Arganda-Carreras, I., Kaynig, V., Rueden, C. T., Schindelin, J., Eliceiri, K. W., Cardona, A., & Sebastian Seung, H. (2017). Trainable Weka Segmentation: a machine learning tool for microscopy pixel classification. *Bioinformatics*, *33*(15), 2424–2426. https://doi.org/10.1093/bioinformatics/btx180

Barclay, S. A., & Worden, R. H. (2000). Petrophysical and petrographical analysis of quartz cement volumes across oil–water contacts in the Magnus Field, northern North Sea. *Quartz Cementation in Sandstones*, *29*, 147–161.

Bear, J. (1988). *Dynamics of fluids in porous media*. New York: Dover.

Berg, C. F. (2012). Re-examining Archie ' s law : Conductance description by tortuosity and constriction. *Physical Review*, *86*(046314), 1–9. https://doi.org/10.1103/PhysRevE.86.046314

Berg, C. F. (2014). Permeability Description by Characteristic Length , Tortuosity , Constriction and Porosity. *Transp Porous Med*, *103*, 381–400. https://doi.org/10.1007/s11242-014-0307-6

Berg, C. F., & Held, R. (2016). Fundamental Transport Property Relations in Porous Media Incorporating Detailed Pore Structure Description. *Transport in Porous Media*, *112*(2), 467–487. https://doi.org/10.1007/s11242-016-0661-7

Berg, C. F., Lopez, O., & Berland, H. (2017). Industrial applications of digital rock technology. *Petroleum Science and Engineering*, 35. https://doi.org/10.1016/j.petrol.2017.06.074

Berg, S., Rücker, M., Ott, H., Georgiadis, A., Linde, H. Van Der, Enzmann, F., … Wiegmann, A. (2016a). Connected Pathway Relative Permeability from Pore-Scale

Imaging of Imbibition. *Advances in Water Resources*, (2). https://doi.org/10.1016/j.advwatres.2016.01.010

Berg, S., Rücker, M., Ott, H., Georgiadis, A., Linde, H. Van Der, Enzmann, F., … Wiegmann, A. (2016b). Modelling of imbibition relative permeability by direct quasi-static approach. In *International Symposium of the Society of Core Analysts* (Vol. 007, pp. 1–12).

Bjørlykke, K., & Egeberg, P. K. (1993). Quartz cementation in sedimentary basins. *The American Association of Petroleum Geologist*, *77*(9), 1538–1548. https://doi.org/10.1306/BDFF8EE8-1718-11D7-8645000102C1865D

Buades, A., Bartomeu, C., & Morel, J.-M. (2011). Non-Local Means Denoising. *Image Processing On Line*, *1*. https://doi.org/10.5201/ipol.2011.bcm_nlm

Burley, Stuart D. (1993). Models of burial diagenesis for deep exploration plays in Jurassic fault traps of the Central and Northern North Sea. In J. R. Parker (Ed.), *Petroleum Geology of Northwest Europe: Proceedings of the 4th Conference* (pp. 1353–1375). The Geological Society, London.

C-NLOPB. (2010). Lithostratigraphy of Jeanne d'Arc Basin. Retrieved October 10, 2017, from http://www.cnlopb.ca/pdfs/maps/xdb_lith.pdf

C-NLOPB. (2012). *Staff analysis Hebron Development Plan*. Retrieved from https://www.cnlopb.ca/wp-content/uploads/news/sahebdevplan.pdf

C-NLOPB. (2019a). Resource Information. Retrieved from https://www.cnlopb.ca/wp-content/uploads/estrr_heb.pdf

C-NLOPB. (2019b). Well Locations - Hebron Field, Ben Nevis Reservoir. Retrieved June 20, 2019, from https://www.cnlopb.ca/information/maps/

Carman, P. C. (1937). Fluid flow through granular beds. *Trans. Instn Chem. Engrs*, *15*, 150–166. https://doi.org/10.1016/S0263-8762(97)80003-2

Choquette, P. W., & Pray, L. C. (1970). Geologic Nomenclature and Classification of Porosity in Sedimentary Carbonates. *The American Association of Petroleum Geologist*, *54*(2), 207–250.

CoreLab. (1999). *Hebron D94 Well - Core Photos*. Canada.

Cornaglia, V. (2018). Geoscience Overview of the Hebron Field. In *Offshore Technology Conference*. Houston, Texas: Society of Petroleum Engineers.

Cossé, R. (1993). *Basics of reservoir engineering*. (Editions Technip, Ed.). Paris: Gulf Publishing company.

Dake, L. P. (1997). *Fundamentals of reservoir engineering* (16th ed.). Netherlands: Elsevier Science B.V.

Darbon, J., Cunha, A., Chan, T. F., Osher, S., & Jensen, G. J. (2008). Fast nonlocal filtering

applied to electron cryomicroscopy. *Technology*, 1331–1334.

Darcy, H. (1856). *Dètermination des lois d'ècoulement de l'eau à travers le sable*. *Les Fontaines Publiques de la Ville de Dijon*. Paris. Retrieved from https://books.google.no/books?id=DOwbgyt_MzQC&printsec=frontcover&hl=en#v=onepage&q&f=false

Darrell, H. (2016). Scanning Electron Microscopy - Cathodoluminescence (SEM-CL). Retrieved from https://serc.carleton.edu/research_education/geochemsheets/semcl.html

DeSilva, N. R. (1999). Sedimentary basins and petroleum systems offshore Newfoundland and Labrador. *Geological Society, London, Petroleum Geology Conference Series*, *5*(1), 501–515. https://doi.org/10.1144/0050501

Dixon, S. A., Summers, D. M., & Surdam, R. C. (1989). Diagenesis and preservation of porosity in Norphlet Formation (Upper Jurassic), southern Alabama. *American Association of Petroleum Geologists Bulletin*, *73*(6), 707–728.

Driscoll, N. W., & Hogg, J. R. (1995). Stratigraphic response to basin formation: Jeanne d'Arc Basin, offshore Newfoundland. In J. . J. Lambiase (Ed.), *Hydrocarbon Habitat in Rift Basins* (Vol. 80, pp. 145–163). London, United Kingdom: Geological Society. https://doi.org/10.1144/GSL.SP.1995.080.01.07

Dvorkin, J., Gutierrez, M., & Grana, D. (2014). *Seismic Reflections of Rock Properties*. New york: Cambridge University Press.

Emery, D., Smalley, P. C., & Oxtoby, N. H. (1993). Synchronous oil migration and cementation in sandstone reservoirs demonstrated by quantitative description of diagenesis. *Philosophical Transactions of the Royal Society of London. Series A: Physical and Engineering Sciences*, *344*, 115–125. https://doi.org/10.1098/rsta.1993.0080

Enachescu, M. E. (1987). Tectonic and structural framework of the northeast Newfoundland continental margin. In C. Beaumont & A. J. Tankard (Eds.), *Sedimentary Basins and Basin-Forming Mechanisms* (Vol. 12, pp. 117–146). Canadian Society of Petroleum Geologists.

Evans, J., Hogg, A. J. C., Hopkins, M. S., & Howarth, R. J. (1994). Quantification of quartz cements using combined SEM, CL, and image analysis. *Journal of Sedimentary Research Section A*, *64*(2), 334–338. https://doi.org/10.1306/D4267D93-2B26-11D7-8648000102C1865D

ExxonMobil Canada. (2011). *Hebron project Development plan*. St John's. Retrieved from https://www.cnlopb.ca/information/development/

Folk, R. L. (1980). Petrology of sedimentary rocks. *Hemphll Publishing Company, Austin*, 170. https://doi.org/10.1017/CBO9781107415324.004

Giesche, H. (2006). Mercury porosimetry: A general (practical) overview. *Particle and*

*Particle Systems Characterization*, *23*(1), 9–19. https://doi.org/10.1002/ppsc.200601009

Glover, P. (2014). *Petrophysics*. *MSc Petroleum Geology*. Aberdeen: Department of Geology and Petroleum Geology, University of Aberdeen. Retrieved from http://homepages.see.leeds.ac.uk/~earpwjg/PG_EN/CD Contents/Formation Evaluation English/

Gluyas, J. G., Robinson, A. G., Emery, D., Grant, S. M., & Oxtoby, N. H. (1993). The link between petroleum emplacement and sandstone cementation. *Geological Society, London, Petroleum Geology Conference Series*, *4*(1), 1395–1402. https://doi.org/10.1144/0041395

Gu, Y. (2003). Automated scanning electron microscope based mineral liberation analysis. *Journal of Minerals and Materials Characterization and Engineering*, *2*(1), 33–41. Retrieved from http://www.scirp.org/journal/PaperDownload.aspx?FileName=JMMCE20030100003_64231986.pdf&paperID=20244

Hilpert, M., & Miller, C. T. (2001). Pore-morphology-based simulation of drainage in totally wetting porous media. *Advances in Water Resources*, *24*, 243–255.

Hussain, F., Pinczewski, W. V, Cinar, Y., Arns, J. Y., Arns, C. H., & Turner, M. L. (2014). Computation of Relative Permeability from Imaged Fluid Distributions at the Pore Scale. *Transp Porous Med*, (104), 91–107. https://doi.org/10.1007/s11242-014-0322-7

Jorden, J. R., & Campbell, F. L. (1985). *Well logging: Rock properties, borehole environment, mud and temperature logging* (Henry L. D). New York: Society of Petroleum Engineers.

Jurgen, B., Wiegmann, A., Westerteiger, R., Planas, B., & Linden, S. (2017). SatuDict. Kaiserslautern, Germany: MATH2MARKET GMBH. Retrieved from www.geodict.com

Kalam, M. Z. (2012). Digital Rock Physics for Fast and Accurate Special Core Analysis in Carbonates. In J. S. Gomes (Ed.), *New Technologies in the Oil and Gas Industry*. InTechOpen. https://doi.org/10.5772/3216

Magoon, L. B., Hudson, T. L., & Peters, K. E. (2005). Egret-Hibernia(!), a significant petroleum system, northern Grand Banks area, offshore eastern Canada. *AAPG Bulletin*, *89*(9), 1203–1237. https://doi.org/10.1306/05040504115

Marchand, A. M. E., Haszeldine, R. S., Macaulay, C. I., Swennen, R., & Fallick, A. E. (2002). Quartz cementation inhibited by crestal oil charge: Miller deep water sandstone, UK North Sea. *Clay Minerals*, *35*(01), 201–210. https://doi.org/10.1180/000985500546585

Marchand, A. M. E., Haszeldine, R. S., Smalley, P. C., Macaulay, C. I., & Fallick, A. E.

(2001). Evidence for reduced quartz-cementation rates in oil-filled sandstones. *Geology*, *29*(10), 915–918. https://doi.org/10.1130/0091-7613(2001)029<0915:EFRQCR>2.0.CO;2

Marchand, A. M. E., Smalley, P. C., Haszeldine, R. S., & Fallick, A. E. (2002). Note on the importance of hydrocarbon fill for reservoir quality prediction in sandstones. *AAPG Bulletin*, *86*(9), 1561–1571.

Mason, G., & Morrow, N. R. (2013). Developments in spontaneous imbibition and possibilities for future work. *Journal of Petroleum Science and Engineering*, *110*, 268–293. https://doi.org/10.1016/j.petrol.2013.08.018

McAlpine, K. D. (1990). Mesozoic stratigraphy, sedimentary evolution, and petroleum potential of the Jeanne d'Arc Basin, Grand Banks of Newfoundland. *Geological Survey of Canada*, *89–17*, 50. https://doi.org/-

McBride, E. F. (1963). A Classification of Common Sandstones. *SEPM Journal of Sedimentary Research*, *33*(3), 664–669. https://doi.org/10.1306/74d70ee8-2b21-11d7-8648000102c1865d

McBride, E. F. (1989). Quartz Cement in Sandstones : A Review. *Earth-Science Reviews*, *26*, 69–112.

Micromeritics Instrument. (2011). Autopore IV 9500 Operator's Manual.

Midtbø, R. E. A., Rykkje, J. M., & Ramm, M. (2000). Deep burial diagenesis and reservoir quality along the eastern flank of the Viking Graben. Evidence for illitization and quartz cementation after hydrocarbon emplacement. *Clay Minerals*, *35*(01), 227–237. https://doi.org/10.1180/000985500546602

Molenaar, N., Cyziene, J., Sliaupa, S., & Craven, J. (2008). Lack of inhibiting effect of oil emplacement on quartz cementation: Evidence from Cambrian reservoir sandstones, Paleozoic Baltic Basin. *Bulletin of the Geological Society of America*, *120*(9–10), 1280–1295. https://doi.org/10.1130/B25979.1

Morad, S., Ketzer, J. M., & De Ros, L. F. (2000). Spatial and temporal distribution of diagenetic alterations in siliciclastic rocks : implications for mass transfer in sedimentary basins. *Sedimentology*, *47*(1), 95–120.

Mujica, F., James, L. A., Berg, C. F., & Wilton, D. H. (n.d.). Fundamental understanding of how the presence of oil impacts diagenesis by investigating rock samples close to the Oil-Water contact (OWC). Manuscript in preparation. (to be published).

MUN CREAIT. (2012). SEM - MLA. Retrieved December 1, 2017, from https://www.mun.ca/research/resources/creait/physical-sci/maf/sem

Nanakoudis, A. (2018). What is SEM? Scanning electron microscope technology explained. Retrieved from https://blog.phenom-world.com/what-is-sem

Nicoud, B. D. (2000). *Hebron D-94 Special Core Analysis - Internal Report*. (R.

ExxonMobil Upstream, Ed.). Houston, Texas.

Oldenburg, D. ., & Jones, F. H. . (2007). Inversion for Applied Geophysics; Learning resources about geophysical inversion. Retrieved from https://www.eoas.ubc.ca/ubcgif/iag/foundations/properties/resistivity.htm

Øren, P. E., Bakke, S., & Arntzen, O. J. (1998). Extending Predictive Capabilities to Network Models. *SPE Journal*, *SPE 52052*(December), 324–336. Retrieved from https://www.onepetro.org/download/journal-paper/SPE-52052-PA?id=journal-paper%2FSPE-52052-PA

Osborne, M. J., & Swarbrick, R. E. (1999). Diagenesis in North Sea HPHT clastic reservoirs-consequences for porosity and overpressure prediction. *Marine and Petroleum Geology*, *16*(4), 337–353. https://doi.org/10.1016/S0264-8172(98)00043-9

Pagel, M., Barbin, V., Blanc, P., & Ohnenstetter, D. (2000). *Cathodoluminescence in geosciences*. Springer Berlin Heidelberg.

Perez-Rosales, C. (1982). On the Relationship Between Formation Resistivity Factor and Porosity. *Society of Petroleum Engineers Journal*, *22*(04), 531–536. https://doi.org/10.2118/10546-pa

Petro-Canada, Chevron-Canada, resources L., Mobil Oil, C., & Hydro, N. (1999a). *Hebron D-94 Geological Report*. Newfoundland, Canada.

Petro-Canada, Chevron-Canada, resources L., Mobil Oil, C., & Hydro, N. (1999b). *Hebron D-94 Well history Report*. Newfoundland, Canada.

Pettijohn, F. J., Potter, P. E., & Siever, R. (1987). *Sand and Sandstone* (2nd ed.). New York: Springer-Verlag.

Rueden, C. T., Schindelin, J., Hiner, M. C., DeZonia, B. E., Walter, A. E., Arena, E. T., & Eliceiri, K. W. (2017). ImageJ2: ImageJ for the next generation of scientific image data. *BMC Bioinformatics*, *18*(1), 529. https://doi.org/10.1186/s12859-017-1934-z

Saigal, G. C., Bjørlykke, K., & Larter, S. (1992). The effects of oil emplacement on diagenetic processes - examples from the Fulmar Reservoir sandstones, central North Sea. *American Association of Petroleum Geologists Bulletin*, *76*(7), 1024–1033.

Sam Boggs, J. (2006). *Principles of Sedimentology and Stratigraphy*. *Pearson* (4th ed.). Retrieved from https://www.pearson.com/us/higher-education/product/Boggs-Principles-of-Sedimentology-and-Stratigraphy-4th-Edition/9780131547285.html?tab=contents

Sandoval, M. E. (2000). *Diagenesis de areniscas*. Caracas: Universidad Central de Venezuela. Retrieved from https://books.google.ca/books?id=6Zu9hlzp9kcC&printsec=frontcover&source=gbs_vpt_read&redir_esc=y#v=onepage&q&f=false

Sasov, A. Y. (1986). Microtomography I. Methods and equipment. *Journal of Microscopy*, *147*, 169–178. https://doi.org/10.1111/j.1365-2818.1987.tb02829.x

Schindelin, J., Arganda-Carreras, I., Frise, E., Kaynig, V., Longair, M., Pietzsch, T., … Cardona, A. (2012). Fiji: an open-source platform for biological-image analysis. *Nature Methods*, *9*, 676–682. Retrieved from https://doi.org/10.1038/nmeth.2019

Schluter, S., Berg, S., Rucker, M., Armstrong, R. T., Vogel, H. ., Hilfer, R., & Wildenschild, D. (2016). Pore-scale displacement mechanisms as a source of hysteresis for two-phase flow in porous media. *Water Resources Research*, *52*, 2194–2205. https://doi.org/10.1002/2015WR018254

Schon, J. H. (2015). *Physical Properties of Rocks— Fundamentals and Principles of Petrophysics* (2nd ed.). Elsevier B.V. https://doi.org/10.1016/B978-0-444-63533-4.09991-1

Schwartz, L. M., & Kimminau, S. (1987). Analysis of electrical conduction in the grain consolidation model. *Geophysics*, *52*(10), 1402–1411.

Sengupta, M., Kittridge, M. G., & Blangy, J.-P. (2017). Using digital rocks and simulations of pore-scale multiphysics to characterize a sandstone reservoir. *Interpretation of Lab Rock-Physics Data by Numerical Simulations*, *5*(1), 33–43. https://doi.org/10.1190/INT-2016-0068.1

Shimeld, J. W., Altheim, B. K., MacRae, R. A., Grist, A. M., & Moir, P. N. (2001). Paleotemperature estimates. In J. W. Shimeld & P. . Moir (Eds.), *Heavy Oil Accumulations in the Jeanne d'Arc Basin: A Case Study in the Hebron, Ben Nevis, and West Ben Nevis Oil Fields* (OPen file, pp. 44–50). Geological Survey of Canada.

Shimeld, J. W., MacRae, R. A., Moir, P. N., Fowler, M. G., & Stasiuk, L. D. (2005). Heavy oil in the central Jeanne d'Arc Basin and implications for exploration risk. In R. N. Hiscott & A. Pulham (Eds.), *Petroleum Resources and reservoirs of the grand banks, Eastern Canadian Margin* (43rd ed., pp. 95–109). Geological association of Canada.

Sinclair, I. K., McAlpine, K. D., Sherwin, D. ., McMillan, N. J., Taylor, G. C., Best, M. E., … Procter, R. M. (1992). *Petroleum resources of the Jeanne d'Arc basin and environs, Grand Banks, Newfoundland* (92nd–8th ed.). Geological Survey of Canada.

Southard, J. (2007). Diagenesis. In *Sedimentary Geology* (pp. 148–168). Massachusetts Institute of Technology: MIT OpenCourseWare. Retrieved from https://ocw.mit.edu/courses/earth-atmospheric-and-planetary-sciences/12-110-sedimentary-geology-spring-2007/lecture-notes/ch7.pdf

Stasiuk, L. D. (2001). Organic Petrology and Fluid Inclusions. In J. W. Shimeld & P. . Moir (Eds.), *Heavy Oil Accumulations in the Jeanne d'Arc Basin: A Case Study in the Hebron, Ben Nevis, and West Ben Nevis Oil Fields* (Open File, pp. 24–26). Geological Survey of Canada.

Sylvester, P. J. (2012). Use of the Mineral Liberation Analyzer (MLA) for Mineralogical

Studies of Sediments and Sedimentary Rocks. *Mineralogical Association of Canada*, (42), 1–16.

Tarbuck, E., & Lutgens, F. (2005). *An Introduction to physical Geology* (Canadian e). Toronto : Pearson Prentice Hall c2005.

Thomeer, J. H. M. (1960). Introduction of a Pore Geometrical Factor Defined by the Capillary Pressure Curve. *Journal of Petroleum Engineers*, *12*(03), 73–77. https://doi.org/https://doi.org/10.2118/1324-G

Thomeer, J. H. M., & Murphy, D. P. (2000). Capillarity in rocks. Shell/OGCI PetroSkills.

Tiab, D., & Donaldson, E. C. (2016). Porosity and Permeability. In *Petrophysics* (4th ed., pp. 67–186). Elsevier Inc. https://doi.org/10.1016/B978-0-12-803188-9.00003-6

Timur, A., Hemkins, W. ., & Worthington, A. . (1972). Porosity and Pressure Dependence of Formation Resistivity Factor for Sandstones. In *Trans CWLS Fourth Formation Evaluation Symposium* (p. 30). Calgary: Society of Well Logging.

Torsæter, O., & Abtahi, M. (2003). *Experimental Reservoir Engineering*. Department of petroleum Engineering and applied Geophysics.

Ulmer-Scholle, D., Scholle, P., Schieber, J., & Raine, R. J. (2014). *A Color Guide to the Petrography of Sandstones, Siltstones, Shales and Associated Rocks*. *Memoir 109*. The American Association of Petroleum Geologists. https://doi.org/10.1306/13521909m1093637

Van Brakel, J., Modrý, S., & Svatá, M. (1981). Mercury porosimetry: state of the art. *Powder Technology*, *29*(1), 1–12. https://doi.org/10.1016/0032-5910(81)85001-2

Walderhaug, O. (1990). A fluid inclusion study of Quartz-cemented sandstones from offshore Mid-Norway - Possible evidence for continued quartz cementation during oil emplacement. *Journal of Sedimentary Petrology*, *60*(2), 203–210.

Walderhaug, O. (1996). Kinetic Modeling of Quartz Cementation and Porosity Loss in Deeply Buried Sandstone Reservoirs. *AAPG Bulletin*, *80*(5), 731–745. Retrieved from https://www.academia.edu/19220564/Kinetic_modelling_of_quartz_cementation_and_porosity_loss_in_deeplyburied_sandstone_reservoirs

Walderhaug, O., Lander, R. ., Bjørkum, P. A., Oelkers, E. H., Bjørlykke, K., & Nadeau, P. H. (2000). Modelling quartz cementation and porosity in reservoir sandstones: examples from the Norwegian continental shelf. *Quartz Cementation in Sandstones*, *29*, 39–49.

Washburn, E. W. (1921). Note on a method of determining the distribution of pore sizes in a porous material. In *Natl. Acad. Sci.* (Vol. 7, pp. 115–116).

Webb, P. A. (2001, January). An Introduction To The Physical Characterization of Materials by Mercury Intrusion Porosimetry with Emphasis On Reduction And Presentation of Experimental Data. *Micromeritics Instrument Corp*, (01), 23.

https://doi.org/10.1177/004057368303900411

Winsauer, W. ., Shearin, H. . J., Masson, P. H., & Williams, M. (1952). Resistivity of Brine-Saturated Sands in Relation to Pore Geometry. *AAPG Bulletin*, (36), 253–277.

Worden, R. H., Bukar, M., & Shell, P. (2018). The effect of oil emplacement on quartz cementation in a deeply buried sandstone reservoir. *AAPG Bulletin*, *102*(1), 49–75. https://doi.org/10.1306/02071716001

Worden, R. H., & Burley, S. D. (2003). *Sandstone Diagenesis : The Evolution of Sand to Sandstone*. (S D Burley & R. H. Worden, Eds.). International Association of Sedimentologists. https://doi.org/10.1002/9781444304459.ch

Worden, R. H., & Morad, S. (2000). Quartz cementation in oil field sandstones : a review of the key controversies, (2000), 20.

Worden, R. H., Oxtoby, N. H., & Smalley, P. C. (1998). Can oil emplacement prevent quartz cementation in sandstones? *Petroleum Geoscience*, *4*(2), 129–137. https://doi.org/10.1144/petgeo.4.2.129

Zhou, W., Apkarian, R., Wang, Z. L., & Joy, D. (2007). Fundamentals of Scanning Electron Microscopy (SEM). In W. Zhou & Z. L. Wang (Eds.), *Scanning Microscopy for Nanotechnology: Techniques and Applications* (pp. 1–40). New York, NY: Springer New York. https://doi.org/10.1007/978-0-387-39620-0_1

# APPENDICES

**Appendix A** Hebron D-94 Well, Core 6 original ("Fresh") core photos (CoreLab, 1999). Sample location in the core. Boxes 1-34/34


7/34
1909.0 m
8/34
SP-5A
9/34
1910.0 m
10/34
11/34
1911.0 m
12/34

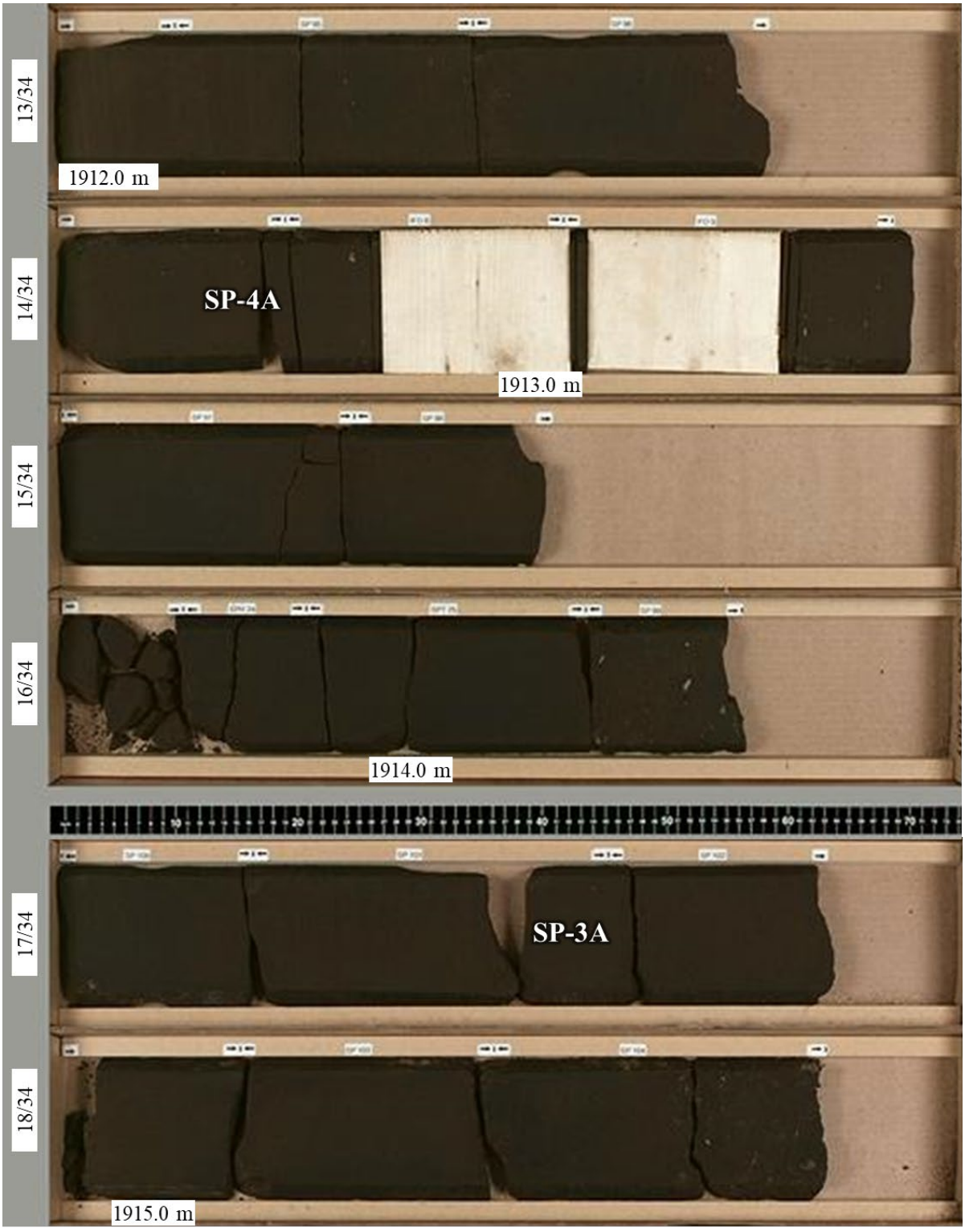
13/34
1912.0 m
14/34
SP-4A
1913.0 m
15/34
16/34
1914.0 m
17/34
SP-3A
18/34
1915.0 m

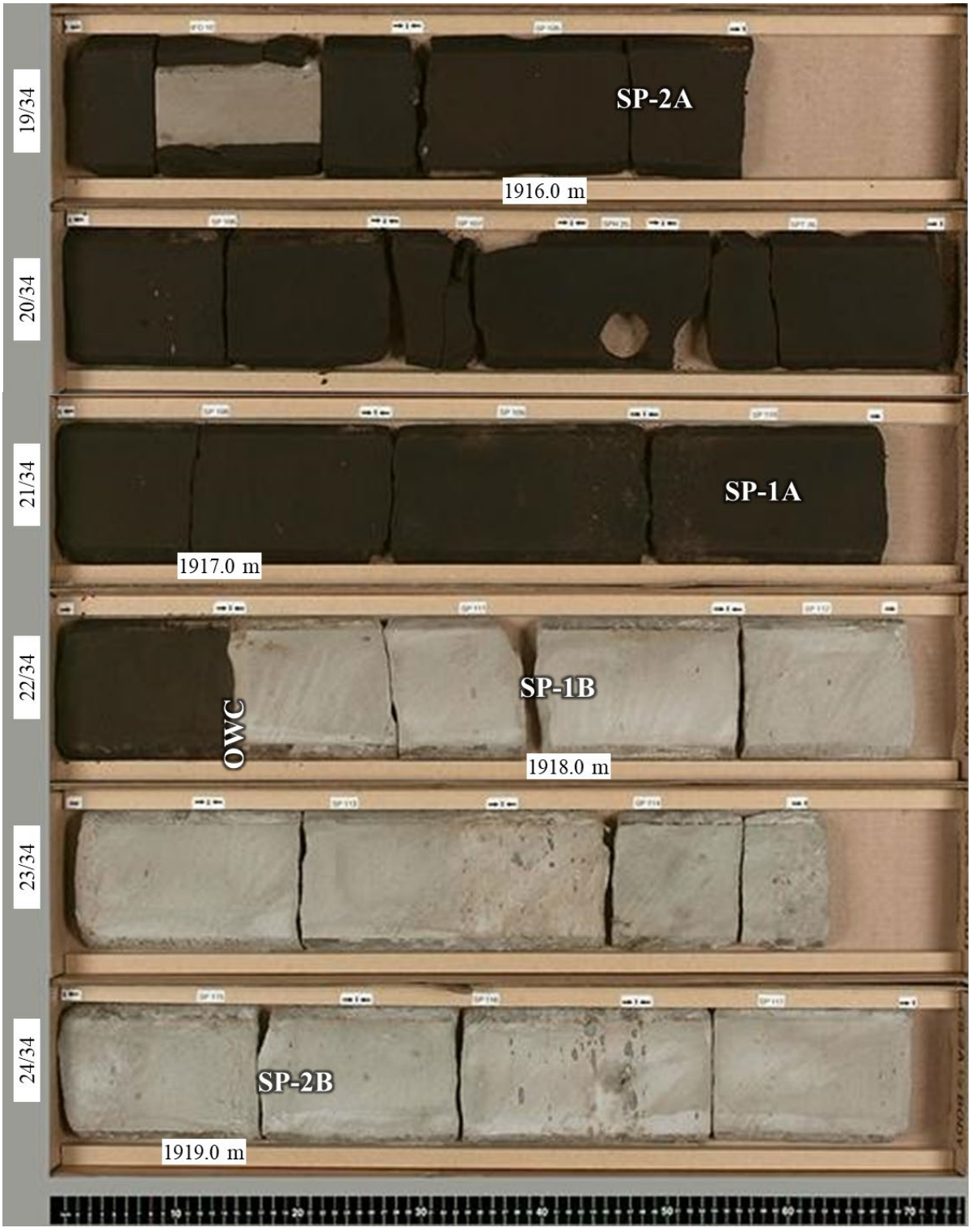
19/34
SP-2A
1916.0 m
20/34
21/34
SP-1A
1917.0 m
22/34
SP-1B
OWC
1918.0 m
23/34
24/34
SP-2B
1919.0 m

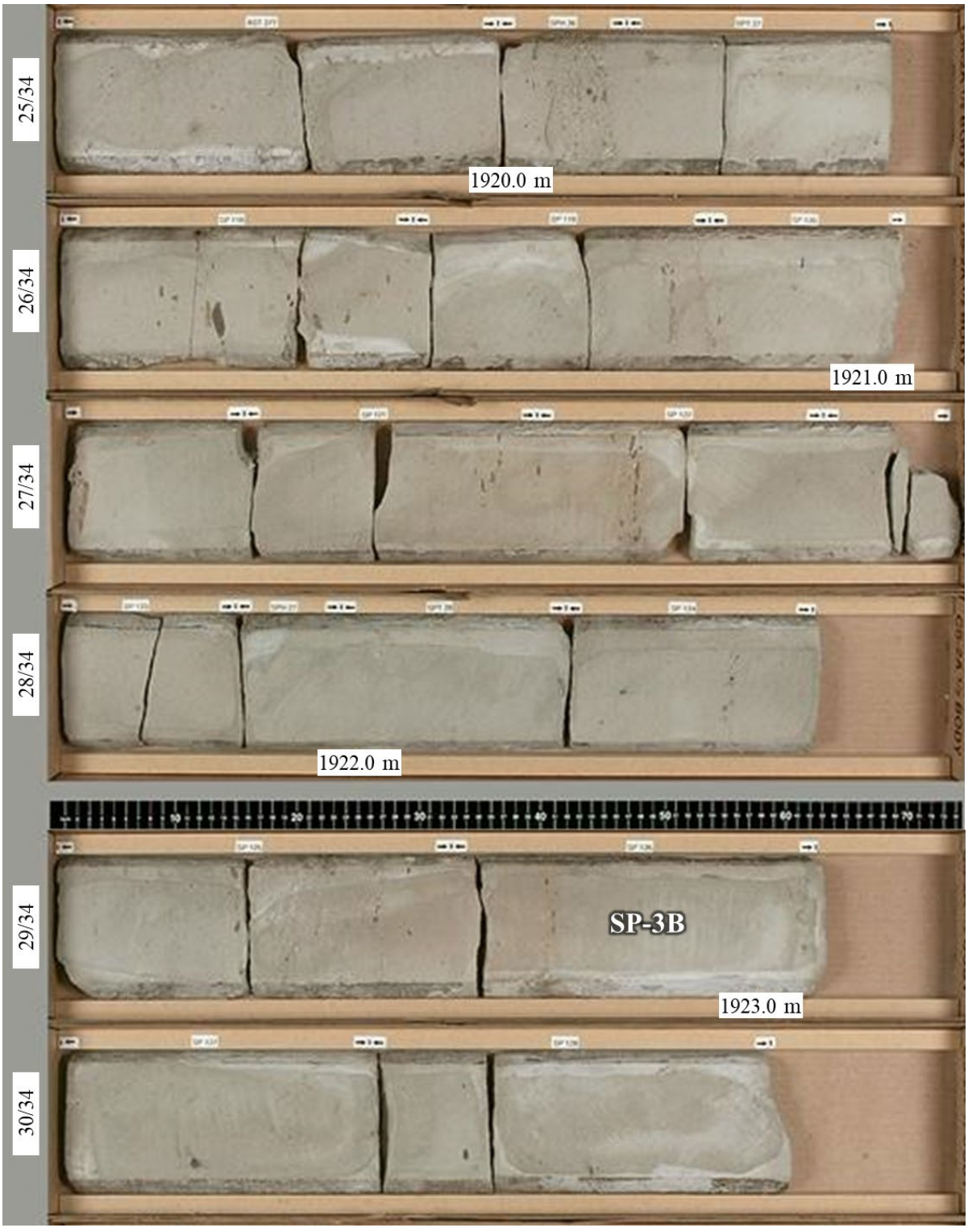
25/34
1920.0 m
26/34
1921.0 m
27/34
28/34
1922.0 m
SP-3B
29/34
1923.0 m
30/34

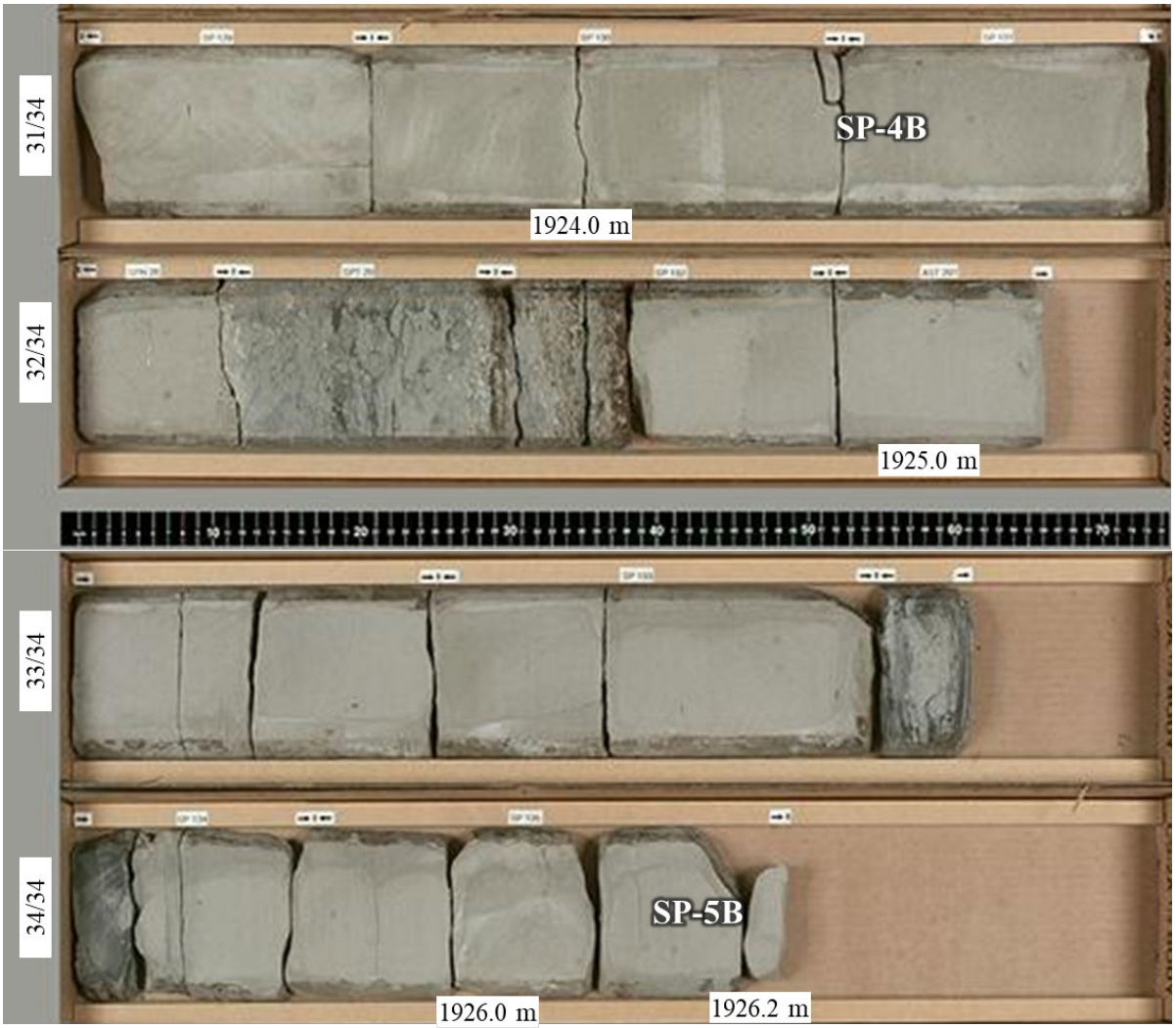
31/34
SP-4B
1924.0 m
32/34
1925.0 m
33/34
34/34
SP-5B
1926.0 m
1926.2 m

**Appendix B** Mercury injection capillary pressure (MICP) test summary for all the samples.

| | Sample weight | Pore Volume | Bulk Volume | Porosity | Apparent (skeletal) Density | Threshold Pressure |
|---|---|---|---|---|---|---|
| | g | mL | mL | Fraction | g/mL | Psi |
| **SP-7A** | 0.98 | 0.15 | 0.53 | 0.28 | 2.57 | 9.0 |
| **SP-5A** | 1.39 | 0.21 | 0.74 | 0.28 | 2.61 | 11.7 |
| **SP-4A** | 0.72 | 0.11 | 0.38 | 0.29 | 2.64 | 9.7 |
| **SP-3A** | 1.13 | 0.17 | 0.61 | 0.28 | 2.60 | 9.9 |
| **SP-2A** | 1.01 | 0.15 | 0.54 | 0.28 | 2.61 | 12.0 |
| **SP-1A** | 1.34 | 0.21 | 0.72 | 0.29 | 2.61 | 9.8 |
| **SP-1B** | 0.78 | 0.11 | 0.41 | 0.27 | 2.59 | 11.9 |
| **SP-1B*** | 1.80 | 0.27 | 0.95 | 0.27 | 2.62 | 11.6 |
| **SP-2B** | 0.92 | 0.14 | 0.50 | 0.29 | 2.58 | 9.5 |
| **SP-2B*** | 1.24 | 0.19 | 0.66 | 0.29 | 2.62 | 10.2 |
| **SP-3B** | 1.27 | 0.22 | 0.70 | 0.31 | 2.62 | 9.3 |
| **SP-4B** | 1.06 | 0.17 | 0.58 | 0.30 | 2.61 | 9.3 |
| **SP-5B** | 1.41 | 0.23 | 0.77 | 0.30 | 2.62 | 12.2 |

* Repetition samples

**Appendix C** Quartz overgrowth quantification details.

| | | 1 | 2 | 3 | 4 | 5 | 6 | 7 | 8 | 9 | 10 | Mean | SD |
|---|---|---|---|---|---|---|---|---|---|---|---|---|---|
| **SP-7A** | Qo | 2.2 | 3.6 | 2.6 | 3.3 | 3.4 | 3.0 | 3.2 | 4.1 | 3.6 | 2.3 | **3.1** | **0.6** |
| | Qo area | 7205 | 11510 | 8383 | 10320 | 11171 | 9898 | 10155 | 12617 | 11843 | 7687 | | |
| | Grains area | 331602 | 318708 | 320272 | 316053 | 332076 | 330038 | 315769 | 309132 | 327810 | 341178 | | |
| **SP-4A** | Qo | 3.8 | 3.0 | 3.4 | 3.0 | 2.7 | 3.2 | 2.6 | 3.4 | 3.3 | 3.1 | **3.1** | **0.3** |
| | Qo area | 11847 | 10098 | 11745 | 10427 | 9053 | 11274 | 8422 | 11657 | 11282 | 10744 | | |
| | Grains area | 314868 | 337196 | 343927 | 350327 | 331270 | 348668 | 328378 | 346677 | 337243 | 344022 | | |
| **SP-1A** | Qo | 4.0 | 3.6 | 3.2 | 3.9 | 3.6 | 3.7 | 3.8 | 4.3 | 3.8 | 2.7 | **3.6** | **0.4** |
| | Qo area | 13369 | 12764 | 10425 | 13290 | 12398 | 11928 | 12531 | 13060 | 12859 | 8128 | | |
| | Grains area | 337812 | 353598 | 329327 | 344544 | 342173 | 318565 | 332692 | 301073 | 338808 | 299319 | | |
| **SP-1B** | Qo | 3.9 | 3.5 | 3.6 | 3.9 | 4.8 | 4.2 | 3.9 | 4.0 | 4.0 | 4.9 | **4.0** | **0.4** |
| | Qo area | 13413 | 12747 | 12396 | 13087 | 16911 | 14605 | 13107 | 13980 | 14846 | 17162 | | |
| | Grains area | 339756 | 367820 | 340941 | 339424 | 352318 | 348004 | 338855 | 350090 | 373793 | 347341 | | |
| **SP-3B** | Qo | 5.2 | 5.4 | 4.7 | 4.6 | 5.1 | 5.3 | 5.4 | 5.6 | 5.5 | 4.3 | **5.1** | **0.4** |
| | Qo area | 17623 | 17180 | 14563 | 14759 | 17600 | 17791 | 17054 | 19105 | 17790 | 14616 | | |
| | Grains area | 340704 | 318803 | 307093 | 320035 | 343264 | 337765 | 317143 | 338334 | 322927 | 341178 | | |
| **SP-5B** | Qo | 6.7 | 5.4 | 5.3 | 6.6 | 6.3 | 5.5 | 5.4 | 6.8 | 5.7 | 4.8 | **5.8** | **0.7** |
| | Qo area | 22739 | 17468 | 17134 | 21546 | 21790 | 18639 | 18028 | 22599 | 18926 | 14114 | | |
| | Grains area | 340277 | 323543 | 324065 | 326056 | 347673 | 336106 | 336058 | 330180 | 334067 | 294389 | | |

**Appendix D** Examples of Quartz overgrwoths (Qo) in SEM-CL images.

SP-7A

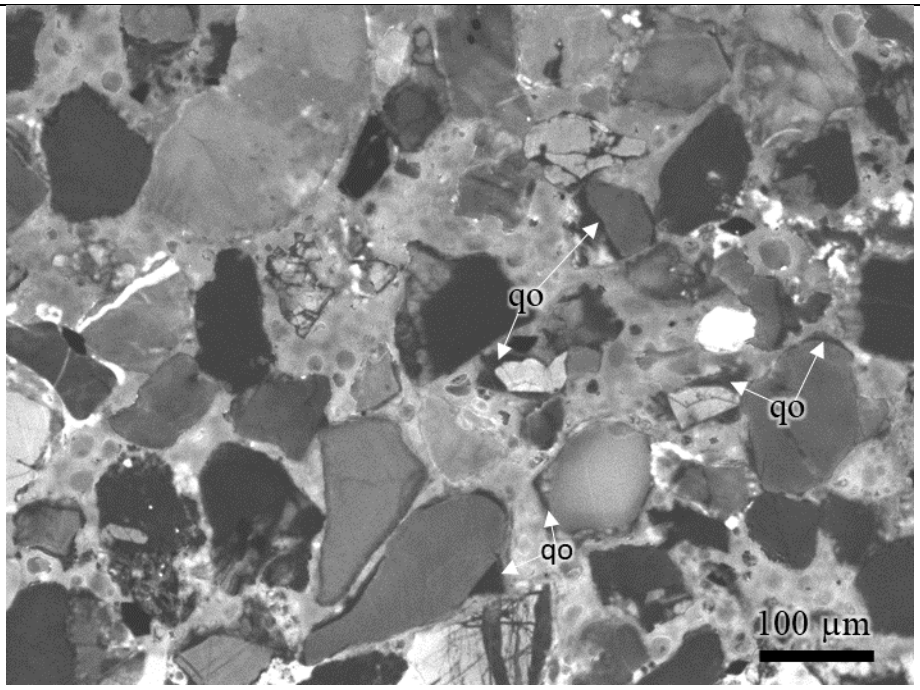


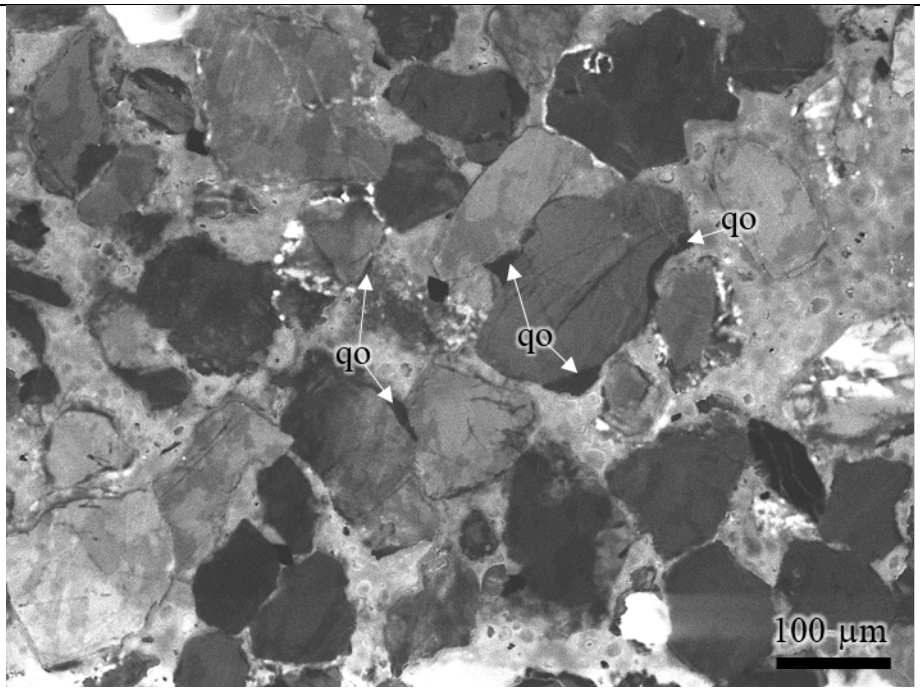

SP-4A

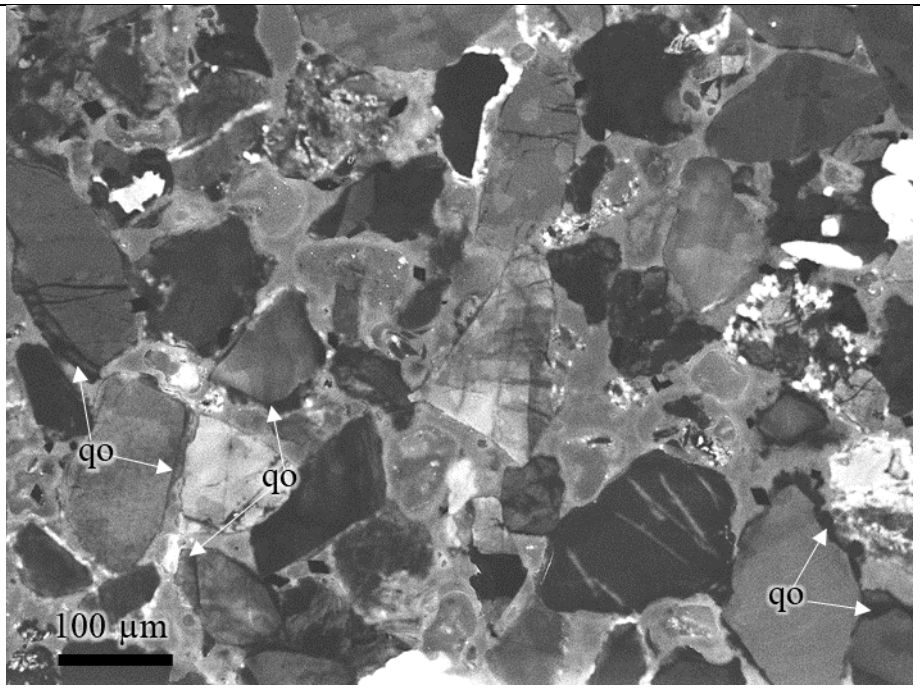


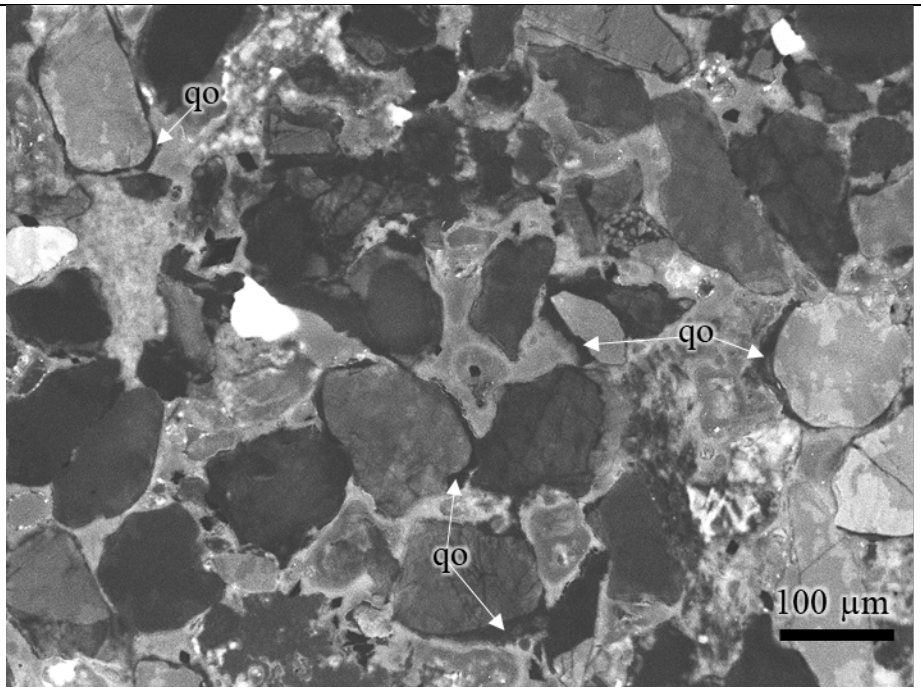

SP-1A

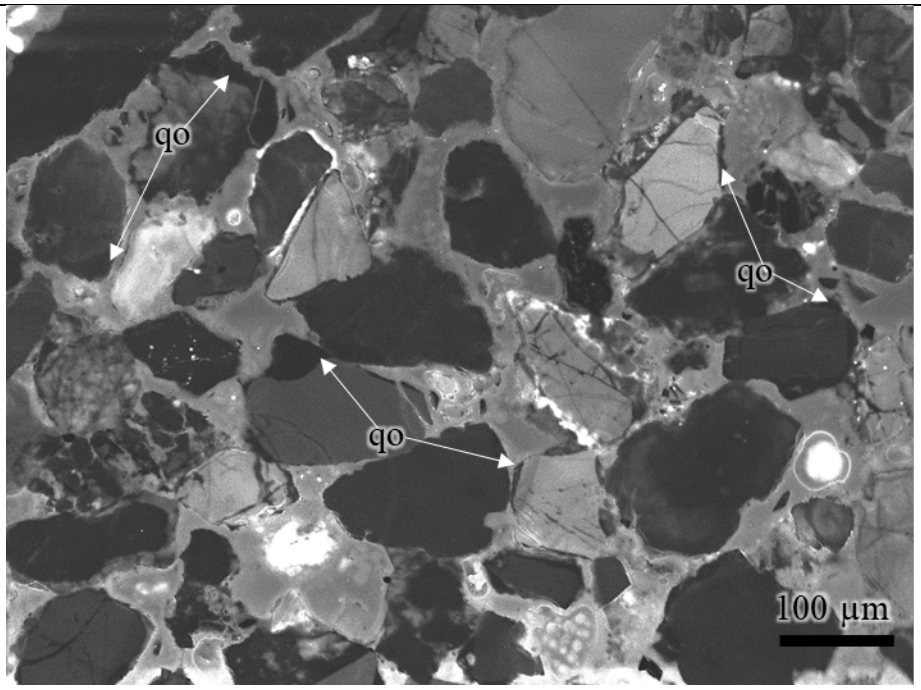


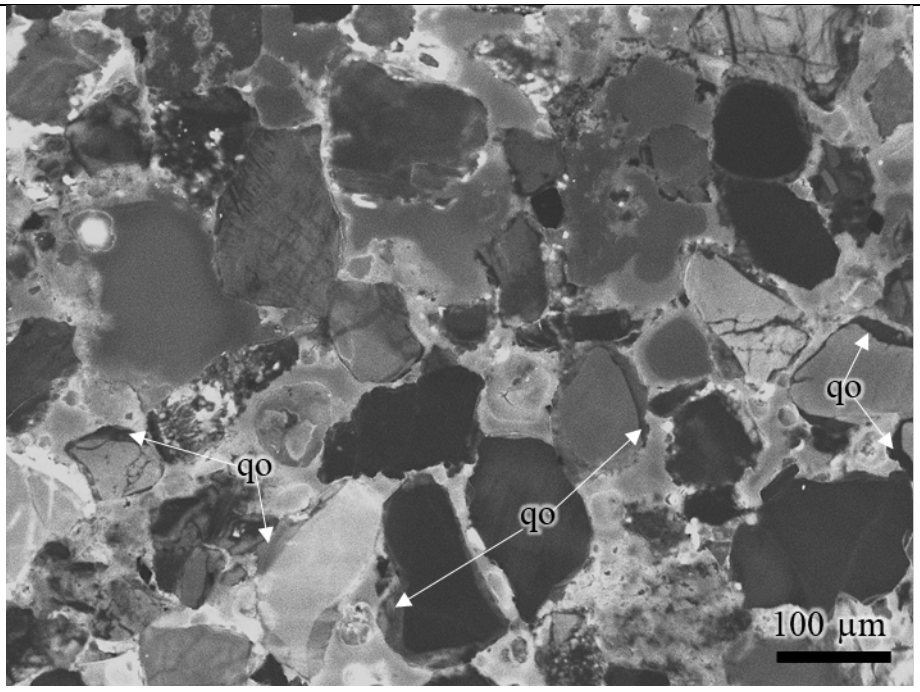

SP-1B

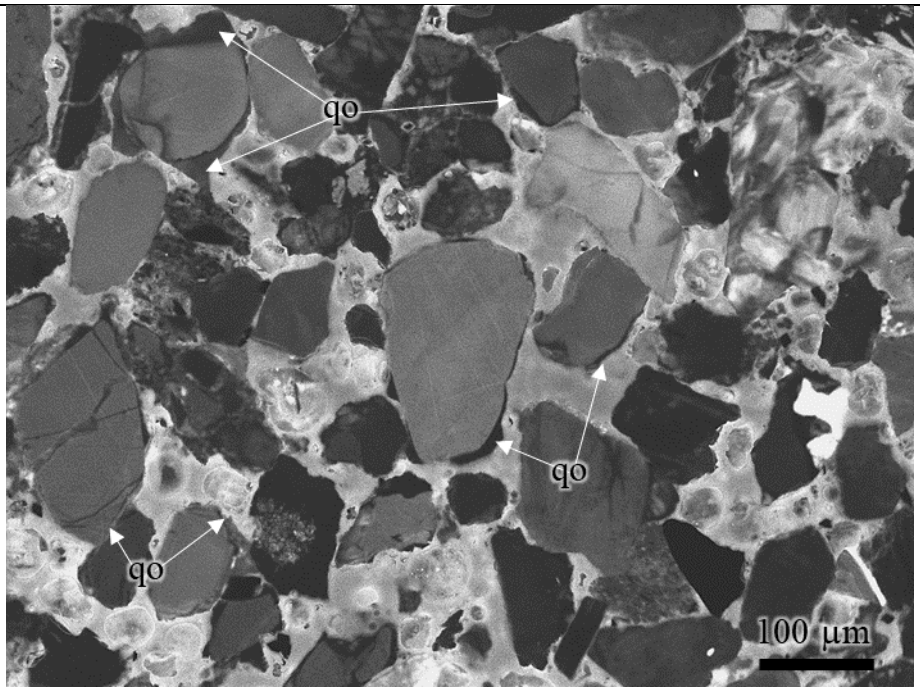


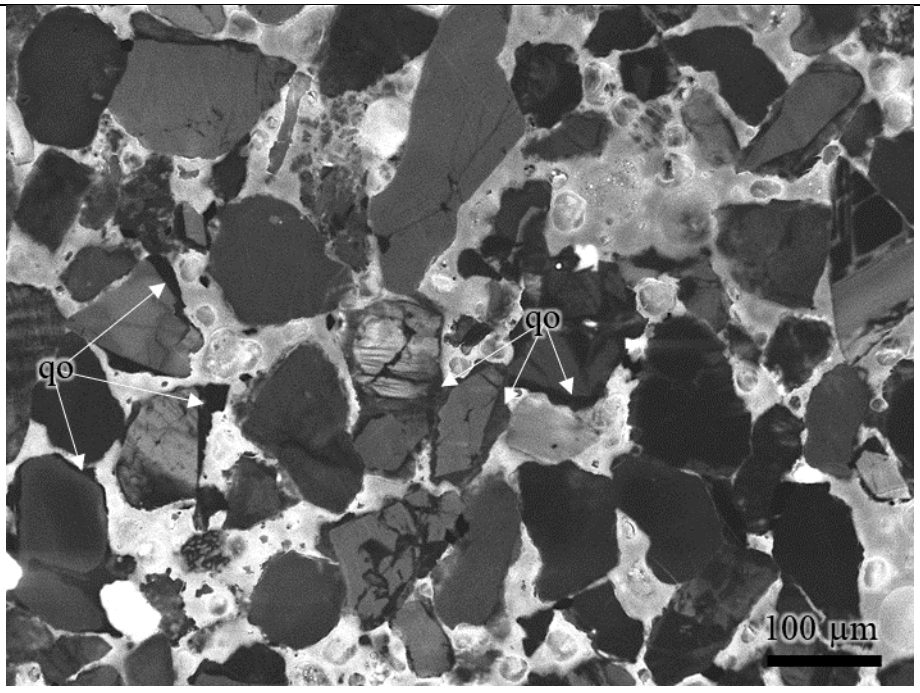

SP-3B

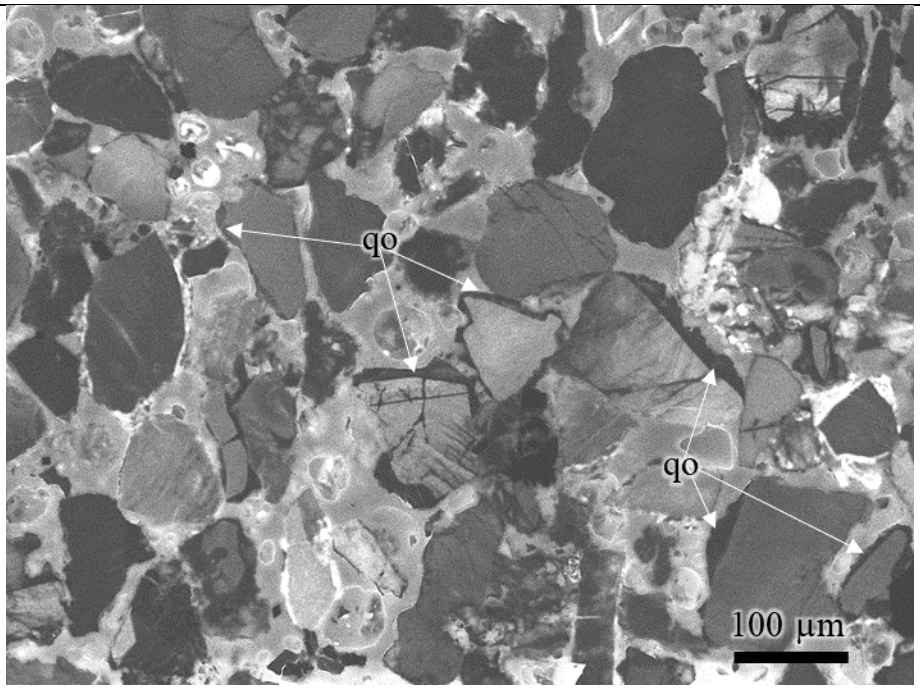


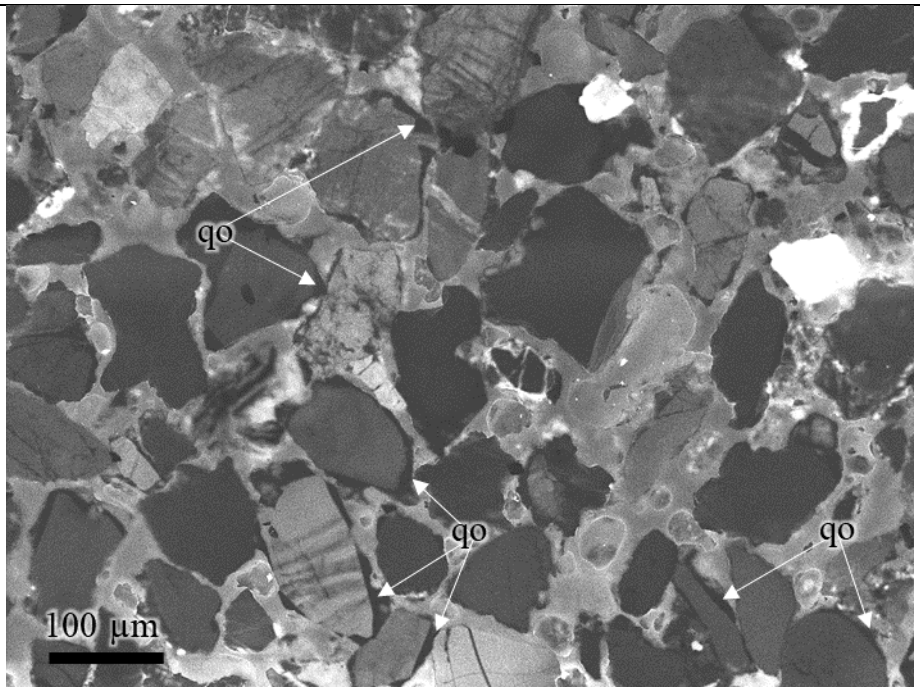

SP-5B

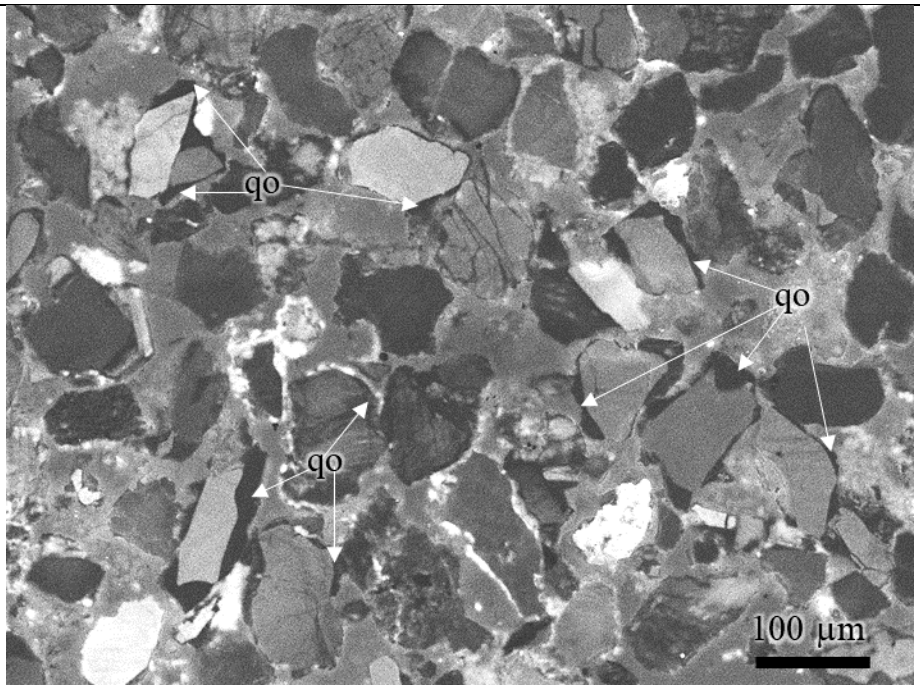


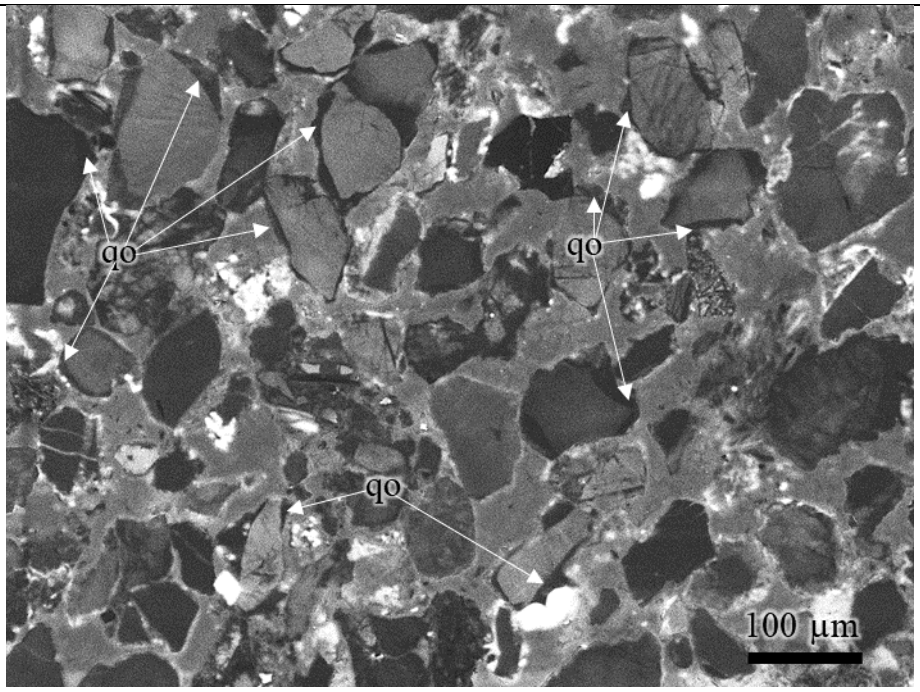

**Appendix E** Micro-computed tomography (µ-CT) images. Examples at 5.2 µm and 1.9 of resolution.

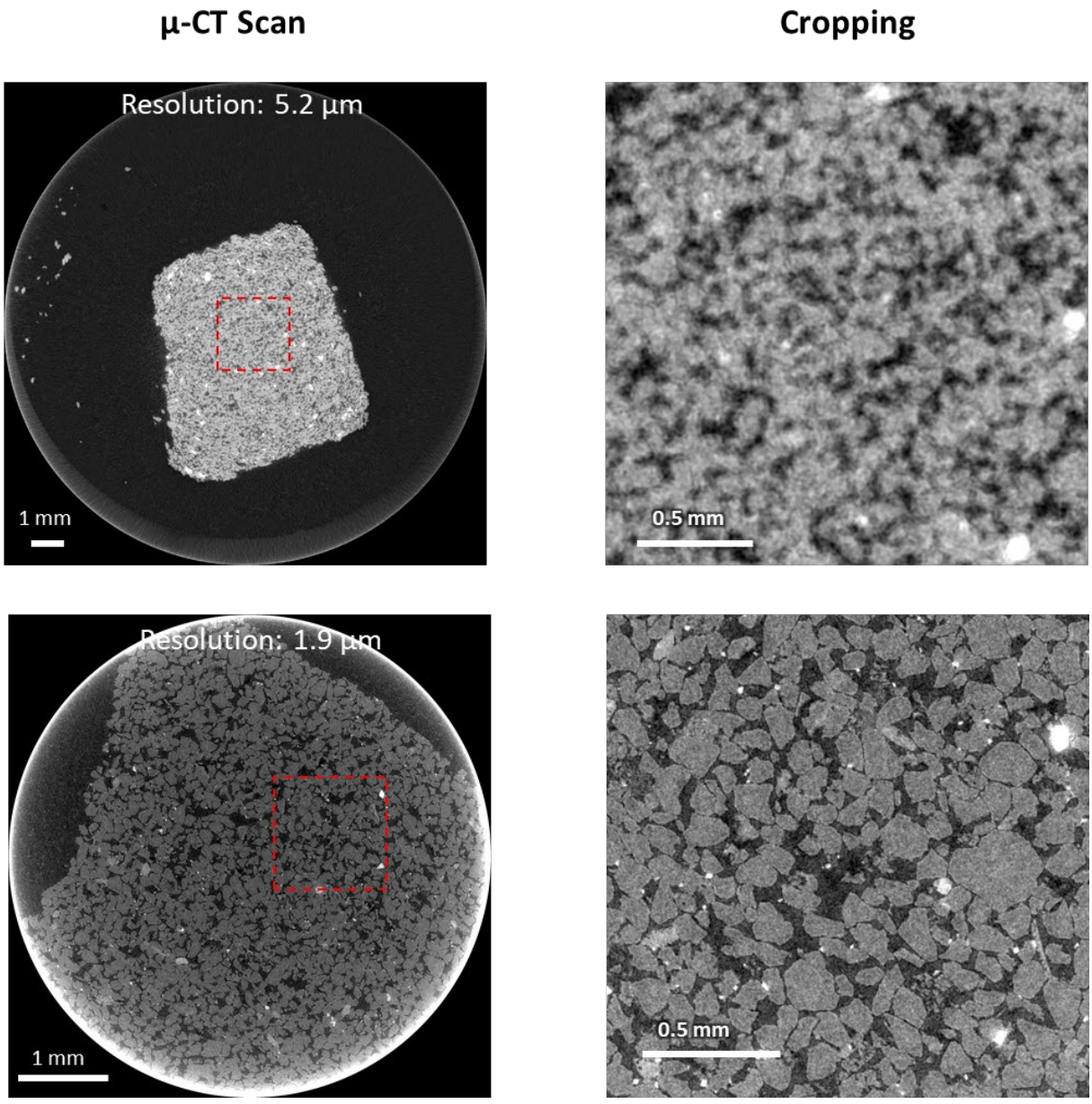

**Appendix F** 3D volume from µ-CT at 1.9 µm of resolution.

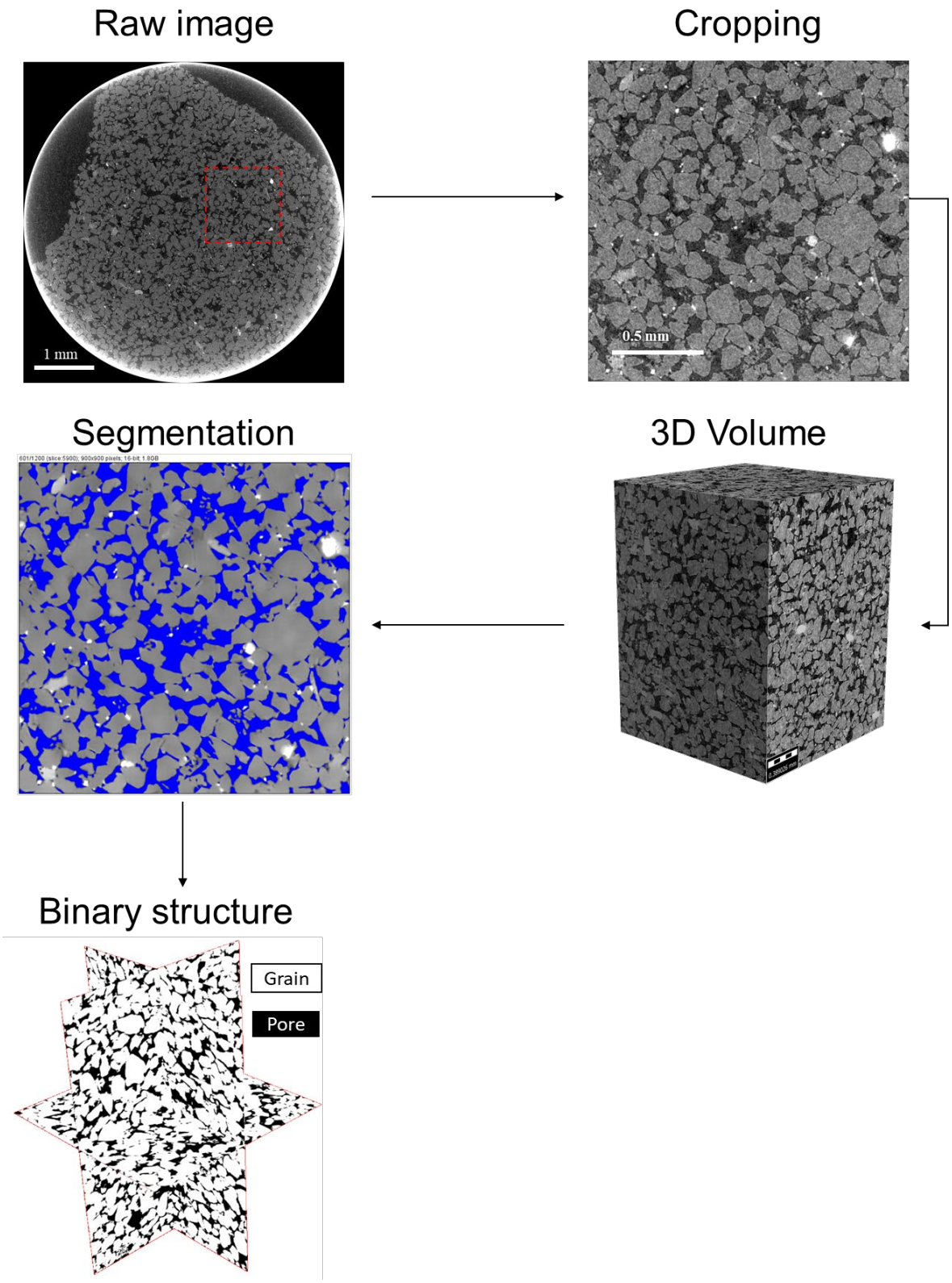

**Appendix G** Flow velocity from digital rock analysis.

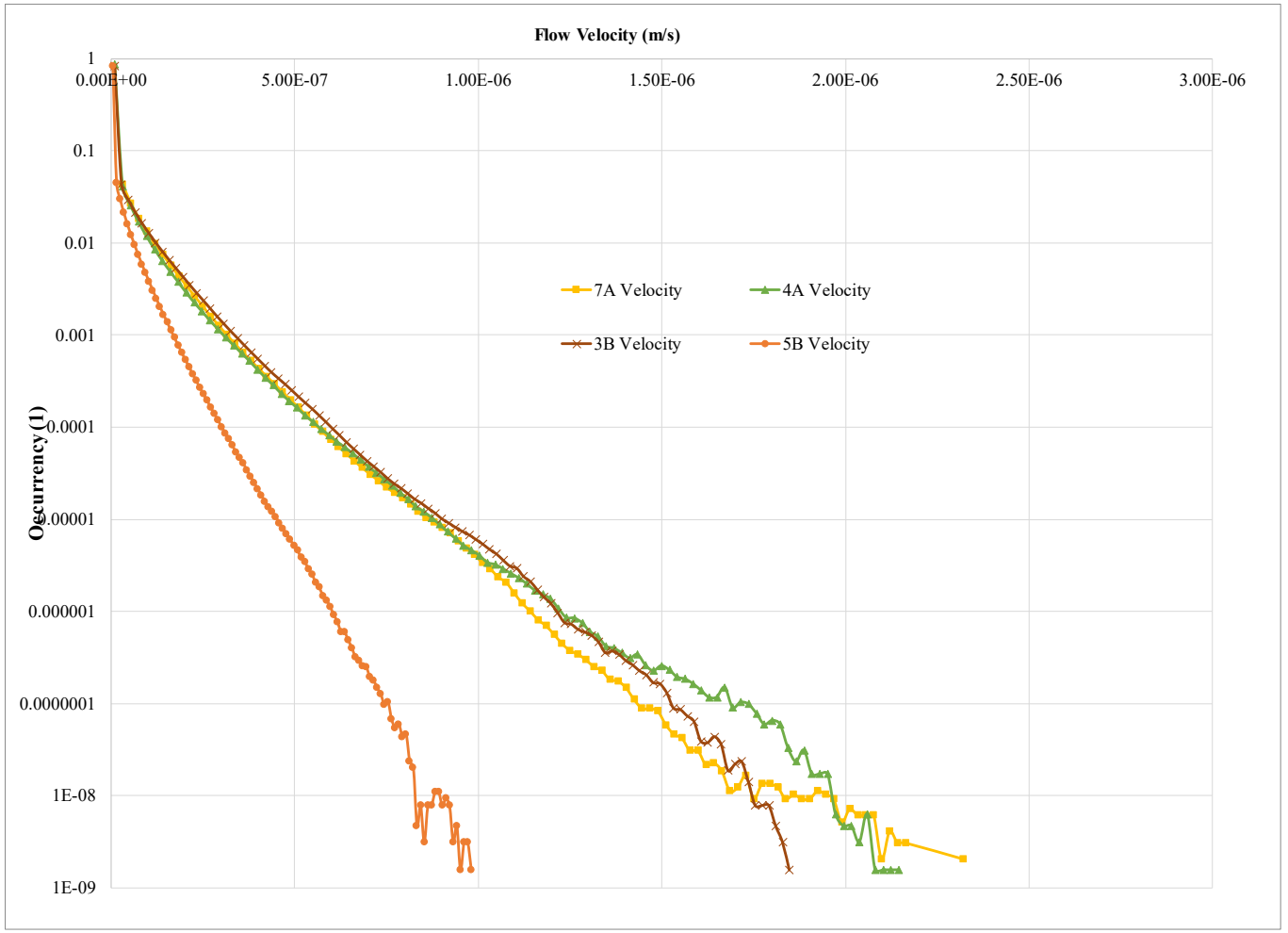

**Appendix H** Absolute brine permeability from previous core analysis (Nicoud, 2000)

**Table 6-1. Summary of Porosities, Permeabilities, and Saturations of Core Plugs Used in USBM Wettability Tests**

| Field | Hebron | Hebron | Hebron | Hebron |
|---|---|---|---|---|
| Well | D-94 | D-94 | D-94 | D-94 |
| Formation | Ben Nevis | Ben Nevis | Ben Nevis | Ben Nevis |
| Depth (m) | 1839.19 | 1839.27 | 1896.59 | 1896.65 |
| Net overburden pressure, NOBP (psi) | 3000 | 3000 | 3000 | 3000 |
| Length, L (cm) | 5.080 | 5.060 | 5.080 | 5.070 |
| Pore volume, $V_p$ ($cm^3$) | 11.91 | 11.66 | 16.52 | 16.36 |
| Grain volume, $V_{ma}$ ($cm^3$) | 43.68 | 43.54 | 38.64 | 38.85 |
| Bulk volume, $V_b$ ($cm^3$) | 55.58 | 55.20 | 55.16 | 55.21 |
| Cross-sectional area, A ($cm^2$) | 10.94 | 10.91 | 10.86 | 10.89 |
| Porosity, $\phi$ (frac. BV) | 0.214 | 0.211 | 0.300 | 0.296 |
| Grain density, $\rho_{ma}$ ($g/cm^3$) | 2.670 | 2.665 | 2.654 | 2.646 |
| Absolute brine permeability (md) | NA | 6.68 | NA | 1427 |
| Effective oil permeability at $S_{wi}$, $K_{o,iw}$ (md) | 9.21 | 7.48 | 909 | 908 |